Changes of inhibitory micronetworks in the epileptic hippocampus and their response to anticonvulsant drugs

Dissertation
zur
Erlangung des Doktorgrades (Dr. rer. nat.)
der
Mathematisch-Naturwissenschaftlichen Fakultät
der
Rheinischen Friedrich-Wilhelms-Universität Bonn

vorgelegt von

Leonie Pothmann

aus

Geldern

Bonn, 2015

Angefertigt mit Genehmigung der Mathematisch-Naturwissenschaftlichen Fakultät der Rheinischen Friedrich-Wilhelms-Universität Bonn

1. Gutachter: Prof. Dr. Heinz Beck
2. Gutachter: Prof. Dr. Horst Bleckmann

Tag der Promotion: 12.10.2015
Erscheinungsjahr: 2015

Teile dieser Arbeit wurden in Form eines wissenschaftlichen Artikels veröffentlicht:
Pothmann, L., Müller, C., Averkin, R. G., Bellistri, E., Miklitz, C., Uebachs, M., Remy, S., de la Prida, L. M., Beck, H., 2014. Function of inhibitory micronetworks is spared by Na^+ channel-acting anticonvulsant drugs. *J Neurosci 34, 9720-9735.*

Abstract

With around 50 million people worldwide suffering from chronic epilepsy, it is one of the most common neurological disorders. However, despite extensive research in this area, the actual network mechanisms involved in the generation of seizures are still not fully understood. This lack of insight is especially important given that 30 % of patients still cannot be treated sufficiently with the available antiepileptic drugs. Outstanding alterations in the epileptic brain are the loss of inhibitory interneuron subtypes and a reduction in GABAergic responses. They suggest that the pathological hyperexcitability characteristic of epilepsy is related to a reduction in GABAergic inhibition. However, the role of GABAergic inhibition is far from limited to reducing neuronal excitability: inhibitory interneurons control spike timing of pyramidal cells, synchronize large populations of neurons and play a role in network oscillations that occur during different states of the brain. These different tasks of interneurons suggest that changes in the spatial and temporal profile of surviving interneurons will also strongly influence network. In the first part of my PhD thesis I therefore investigated whether the spatiotemporal profile of feed-back inhibition is changed in chronically epileptic rats using the pilocarpine model of epilepsy. I focused on the CA1 area of the hippocampus because this brain region is strongly affected in temporal lobe epilepsy, a subform of epilepsy with a high incidence of pharmacoresistance. Using electrical activation of inhibitory feed-back microcircuits in acute hippocampal slices, I could show that the spatiotemporal profile of inhibition provided by the surviving interneurons is altered in experimental epilepsy. As a result, the usually strong initial feed-back inhibition onto CA1 pyramidal cells was reduced. These data suggest marked changes in the dynamics of feed-back inhibition in chronic epilepsy that may be relevant for the initiation of seizure activity in the CA1 ensemble.

In the second part of my thesis I investigated the effects of commonly used sodium channel blocking anticonvulsants on inhibitory microcircuits. GABAergic interneurons are able to fire at very high rates and should consequently be affected by these drugs. This however would cause a further reduction of GABAergic inhibition and thus increase excitability. My experiments revealed that, based on intrinsic and circuit properties, under these experimental conditions, both feed-forward and feed-back inhibition are not affected by these drugs, enabling them to fulfill their function. Furthermore, this study shows that the net effect of CNS drugs on the complex neuronal circuitry within the brain cannot be predicted by their action on individual cell types but also critically depends on the interplay of neuronal subtypes within this network.

Contents

1 Introduction

1.1 Epilepsy

Epilepsy is a family of neurological disorders characterized by an increased propensity of the brain to generate recurrent epileptic seizures (Fisher et al., 2005; Engel, 2006). Epileptic seizures are caused by an abnormal excessive or synchronous neuronal activity in the brain (Fisher et al., 2005; Engel and Pedley, 2008). The clinical manifestation of this pathological network activity depends on the brain area where it originates, as well as speed and pattern of its spread. Epileptic seizures can affect sensory, motor, and autonomic functions, they can alter behavior, change the emotional state and interfere with mnemonic and cognitive processes (Fisher et al., 2005). With around 50 million people worldwide suffering from chronic epilepsy, it is one of the most common neurological disorders (World Health Organization, 2012. Epilepsy Fact sheet N°999.). In addition to the seizures, epilepsy patients also suffer from a wide range of comorbidities like depression, psychosis or cognitive deficits (Sillanpää, 2004; Whatley et al., 2010; Kerr, 2012). Furthermore, the unpredictability of seizures leads to an increased risk of injury as well as social complications, i.e. driving restrictions, limitations in the choice of occupations and social isolation (Sillanpää, 2004; Whatley et al., 2010).

Upon stimulation even normal brain tissue may generate epileptic seizures. However, in chronic epilepsy the brain shows pathological alterations that increase the propensity to generate unprovoked spontaneous seizures. These pathological changes can be caused by brain lesions, structural disorders or metabolic abnormalities (Engel, 2001b; Shneker and Fountain, 2003). Other epilepsy syndromes have a genetic origin and are caused by mutations in ion channels, neurotransmitter receptors or associated proteins (Engel, 1996a; Johnson and Sander, 2001; Beck and Elger, 2008). There are also forms of epilepsy in which the etiology is still unknown (Engel, 2001b; Engel and Pedley, 2008).

Depending on location and spread of the abnormal brain activity, seizures can be categorized into partial and generalized seizures. During generalized seizures, abnormal activity is present in both hemispheres, whereas partial seizures are restricted to a limited area of the brain (Engel et al., 2008). Partial seizures can be further divided into simple and complex partial seizures, depending on whether consciousness is preserved or impaired (Shneker and Fountain, 2003; Engel et al., 2008).

In epilepsy, the main therapeutic approach is to reach a seizure free state by appli-

cation of antiepileptic drugs (AEDs, see Section 1.4). However, these drugs mainly treat the symptoms (the seizures) but do not target the underlying cause (Shneker and Fountain, 2003; Kwan and Sander, 2004; Picot et al., 2008; Sisdosiya et al., 2008; Kwan et al., 2010; Pitkänen and Lukasiuk, 2011). In approximately 70 % of the cases, seizures are successfully suppressed by the applied AEDs (Kwan and Brodie, 2000; Brodie et al., 2012). Unfortunately, in the remaining 30 % of patients, seizures cannot be sufficiently controlled. Clinical studies suggest that after failure of two to three AEDs appropriate for the specific case of epilepsy, the success rate of trying additional AEDs is moderate (Aso and Watanabe, 2000; Kwan and Brodie, 2000; Mohanraj and Brodie, 2006). In refractory epilepsy, surgical removal of the epileptic focus can be an alternative strategy (Engel, 1996b). To categorize patients in everyday clinical work, the Task Force of the ILAE[1] Commission on Therapeutic Strategies proposed the following definition: Patients that do not respond to two tolerated and appropriate AEDs are operationally defined as 'pharmacoresistant' (Kwan et al., 2010). This definition mainly aims to reduce delays before specialists are consulted and alternative strategies are considered (Engel, 2004).

1.1.1 Temporal lobe epilepsy

One subform of epilepsy with a high incidence of pharmacoresistance is mesial temporal lobe epilepsy (mTLE). In mTLE, seizures originate from the hippocampus and adjacent structures within the mesial temporal lobe (Engel, 2001a; Schmidt and Löscher, 2005; Sendrowski and Sobaniec, 2013). Patients diagnosed with mTLE mainly suffer from simple or complex partial seizure that rarely generalize (Engel, 1996a; Sendrowski and Sobaniec, 2013). Additionally, they often experience depression and memory deficits (Engel, 1996a; Elger et al., 2004). As many as 75 % of these patients are refractory to AED treatment. However, for 60-80 % of patients with medically refractory mTLE, seizure control can be achieved by surgical resection within the mesial temporal lobe (Engel, 1996b; Blümcke et al., 2002; Jeong et al., 2005).

mTLE is one of the most common and well defined symptomatic and localization-related epilepsies (Engel, 2001a). It represents approximately 60 % of all partial epilepsies (Walker et al., 2007). Patients suffering from mTLE often show structural changes inside the brain. The most common of these neuropathological lesions in mTLE patients is hippocampal sclerosis (60-65 % of surgical cases; Margerison and Corsellis, 1966; Blümcke et al., 2002; Blümcke et al., 2013). This sclerosis is mainly characterized by loss of pyramidal cells within CA1 and the subiculum, both subregions of the hippocampal formation (for an anatomical description of the hippocampus see Section 1.2). Additional features of hippocampal sclerosis are gliosis, i.e. a proliferation or hypertrophy of glial cells, loss of inhibitory interneurons, mossy fiber sprouting and dentate granule cell dispersion. The hippocampal sclerosis results in hippocampal atrophy that can be detected

[1] International League Against Epilepsy

with magnetic resonance imaging (Engel, 1996a; Blümcke et al., 2013). Around 50 % of mTLE patients have a history of a brain insult early in life (Blümcke et al., 2002). Possible injuries are prolonged febrile seizures, status epilepticus, birth trauma, head injuries and CNS infections. These 'initial precipitating insults' are followed by a latent period of several years before spontaneous seizures occur (Mathern et al., 1995; Wieser, 2004). Together with a genetic predisposition, the initial precipitating insult is thought to induce multiple changes that convert a normal into a chronic epileptic brain (Wieser, 2004; Beck and Elger, 2008; Kasperaviciute et al., 2013; Cendes et al., 2014). This process is referred to as 'epileptogenesis'. Since seizures are absent during this period, the development often remains unnoticed. Furthermore, human brain tissue from epilepsy surgery is only available at later stages of the disease. Therefore, most research has been conducted in animal models, in which the brain insult is triggered artificially. In most of these models, pharmacological induction of a single status epilepticus (SE) serves as initial precipitating insult (Kandratavicius et al., 2014). The status epilepticus is followed by a latent period before animals develop spontaneous chronic seizures. Usually, during the latent period seizures are absent. Both, studies from patients and animal models have shown that the initial precipitating insult can induce alterations in expression and distribution of neurotransmitter receptors and ion channels in hippocampal neurons (Blümcke et al., 2000; Pathak et al., 2007; Bernard et al., 2004; Becker et al., 2008; Cendes et al., 2014). Additionally, during the chronic epileptic phase recurrent seizures can induce further changes that lead to a secondary epileptogenesis (Sendrowski and Sobaniec, 2013). Often, however, it is not evident whether the observed changes are pro-epileptic or might even be compensatory (Walker et al., 2002).

1.2 Anatomy of the hippocampus

The hippocampal formation is located within the medial temporal lobe of mammals (Squire et al., 2004) and is critical for the formation of declarative memory (Bunsey and Eichenbaum, 1996; Squire, 1992, 2004), as well as for spatial navigation (O'Keefe and Dostrovsky, 1971; O'Keefe, 1976; Moser et al., 2008). It consists of the dentate gyrus, the hippocampus proper, the subiculum, the presubiculum, the parasubiculum and the entorhinal cortex. The hippocampus proper can be further divided into three subregions: cornu ammonis 1 to 3 (CA1-CA3) (Amaral, 1993; Amaral and Lavenex, 2007). The most compelling feature of the hippocampal formation is the largely unidirectional flow of excitatory information from one region to the next. The phylogenetically younger neocortex on the other hand consists of strongly reciprocally connected subregions (Amaral and Lavenex, 2007). Information from the neocortex reaches the three-layered hippocampus via the six-layered entorhinal cortex. The first station inside the hippocampal formation is the dentate gyrus (DG, **Fig. 1.1**). Excitatory pyramidal cells in layer II of the entorhinal cortex (EC) tar-

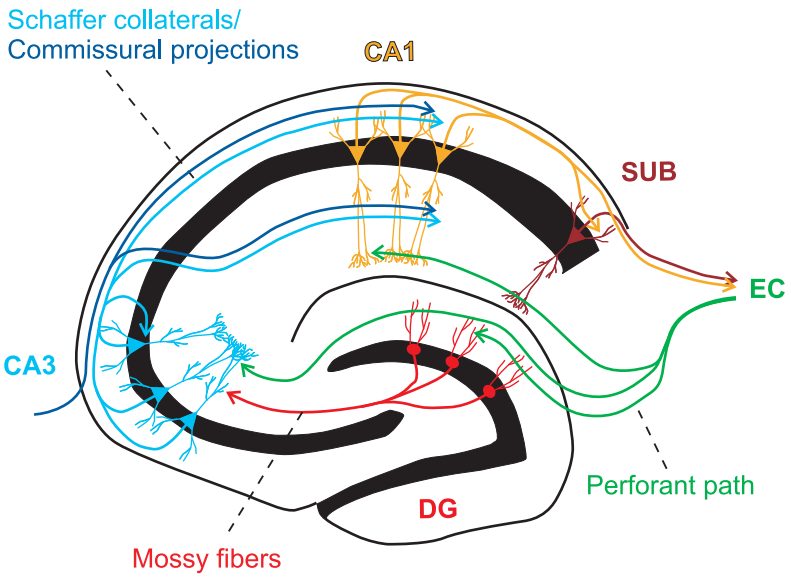

Figure 1.1: Scheme of the intrahippocampal circuitry. Information from the entorhinal cortex (EC) reaches the hippocampus via the perforant path. Granule cells (red) of the dentate gyrus (DG) target CA3 pyramidal neurons (blue) via the mossy fibers. From CA3 information is conveyed to CA1 (orange) via the Schaffer collaterals. Both CA1 and the subiculum (SUB) project to the entorhinal cortex. Pyramidal and granule cell layers are indicated in black. Adapted from Amaral and Witter (1989) and Amaral and Lavenex (2007).

get dentate granule cells via the perforant path (Steward and Scoville, 1976; Witter et al., 1989; Witter, 1993). After processing, information is passed from the dentate gyrus to CA3 via axonal projections of dentate granule cells, the mossy fibers. CA3 pyramidal cells possess highly ramifying axons with additional axon collaterals that target CA3 pyramidal cells themselves. This innervation pattern leads to a strong recurrent excitation within CA3. Outside of CA3, the main target of CA3 pyramidal cells are CA1 pyramidal cells on both sides of the brain. Fibers that target the ipsilateral CA1 region are termed 'Schaffer collaterals', those that terminate on the contralateral hemisphere are named 'commissural projection'. Within CA1, both Schaffer collaterals and commissural projections innervate pyramidal cell dendrites in stratum oriens and radiatum (**Fig. 1.1** and **1.2**). From CA1 information is then conveyed to both the subiculum and to layer V of the entorhinal cortex (Witter et al., 1989; Witter, 1993).

In addition to this classical intrahippocampal loop, CA3, CA1 and the subiculum receive direct monosynaptic input from the entorhinal cortex via the temporo-ammonic pathway (Steward, 1976; Witter et al., 1989, **Fig. 1.1**). The entorhinal fibers terminate in stratum lacunosum moleculare of CA1 and CA3 and the molecular layer of the subiculum. Furthermore, information from the entorhinal cortex to CA1 is also conveyed via the temporo-alvear pathway (Stanfield and Cowan, 1979; Witter et al., 1989). In contrast to entorhinal input to the dentate gyrus and CA3, these fibers originate in layer III of the

entorhinal cortex (Amaral, 1993).

In summary, information from the neocortex reaches hippocampal subregions both directly and indirectly. Information is sent either through the direct pathway from the entorhinal cortex to CA1 and CA3, or through the indirect pathway by passing through the dentate gyrus and CA3 before arriving in CA1.

1.2.1 Anatomical organization of CA1 and its role in temporal lobe epilepsy

Similar to the dentate gyrus, CA3 and the subiculum, the CA1 region is a three layered structure. Pyramidal cell somata are located in the pyramidal cell layer (stratum pyramidale, SP, **Fig. 1.2**). Their basal dendrites extend into stratum oriens (SO) and their strongly ramifying apical dendritic tree reaches into stratum radiatum (SR) and stratum lacunosum moleculare (SLM). The dendrites in strata oriens and radiatum are therefore mainly innervated by excitatory inputs from CA3, whereas the distal apical tuft in stratum lacunosum moleculare receives excitatory input from the entorhinal cortex (**Fig. 1.2**). In addition to the excitatory inputs from CA3 and the entorhinal cortex, the CA1 region receives excitatory inputs from the nucleus reuniens of the thalamus and the basolateral nucleus of the amygdala. These projections terminate in SLM (Wouterlood et al., 1990), or SLM, SR and SO, respectively (Amaral and Lavenex, 2007; Pikkarainen et al., 1999; Kemppainen et al., 2002). The myelinated axons of CA1 pyramidal cells either originate at the soma or a basal dendrite (Thome et al., 2014), pass through stratum oriens and travel in a fiber bundle, the alveus, to innervate targets in the subiculum and the entorhinal cortex .

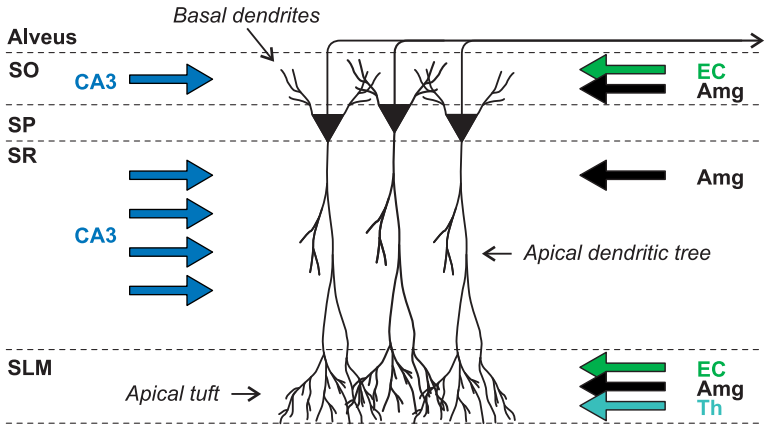

Figure 1.2: Excitatory inputs to CA1 pyramidal cells. Somata of CA1 pyramidal cells (black) are located in stratum pyramidale (SP), their dendrites extend into stratum oriens (SO), stratum radiatum (SR) and stratum lacunosum moleculare (SLM). Excitatory inputs from CA3 pyramidal cells (blue) terminate in SO and SR of CA1. The entorhinal cortex (EC) targets pyramidal cell dendrites within SO and SLM, whereas the amygdala (Amg) additionally innervates SR. The thalamus (Th) sends fibers only to SLM. Adapted from Amaral and Lavenex (2007), Pikkarainen et al. (1999) and Wouterlood et al. (1990).

In contrast to the CA3 region where recurrent interconnectivity is high, CA1 pyramidal cells have only few axon collaterals that remain in CA1. These local axon collaterals mainly terminate inside the alveus and stratum oriens, and rarely enter stratum radiatum (Knowles and Schwartzkroin, 1981; Amaral et al., 1991). Paired recordings in hippocampal slices suggest that the connectivity between pyramidal cells is low, with one pair out of 100 being synaptically connected (Deuchars and Thomson, 1996). By comparison, the probability of finding a synaptic connection between a presynaptic pyramidal cell and a postsynaptic interneuron ranges from 4.5 to 33.3 %, depending on the interneuron subtype (Ali and Thomson, 1998; Ali et al., 1998). These physiological studies were later confirmed anatomically (Takacs et al., 2012): electron micrographs of *in vivo* labeled pyramidal cells have shown that 39.2 % of their synapses target pyramidal cells, whereas interneurons receive 53.8% of the labeled synaptic boutons.

In TLE, CA1 plays an important role in restricting seizure spread from CA3 to the subiculum and further to the entorhinal cortex. *In vitro* models of TLE suggest that functional inhibitory microcircuits inside of CA1 play an important role in this restriction of seizure spread (Benini and Avoli, 2005; Orman et al., 2008). Additionally, there is evidence that alterations in the circuitry enable the entorhinal cortex to directly recruit CA1 into the epileptic network, via the temporo-ammonic pathway (Sari and Kerr, 2001; Barbarosie et al., 2000; Wozny et al., 2005; Ang et al., 2006).

1.2.2 CA1 inhibitory microcircuits

CA1 pyramidal cells are controlled by a large number of different inhibitory interneurons. Most of these interneurons have local projections and act via the neurotransmitter γ-amminobutyric acid (GABA), the main inhibitory neurotransmitter in the CNS. In the brain, three different GABA receptors, $GABA_{A\text{-}C}$, are present. $GABA_A$ receptors are ligand gated ion-channels that are situated intra- as well as extrasynaptically on both excitatory and inhibitory cells. They are heteropentameric receptors which can be formed by 19 potential subunits. This diversity leads to a large heterogeneity in receptor expression (Olsen and Sieghart, 2008). The subunit composition influences both functional as well as pharmacological properties of the receptors.

Synaptic $GABA_A$receptors mediate fast phasic GABAergic currents, whereas extrasynaptic receptors are responsible for slow, tonic inhibition (Brickley et al., 2001; Hamann et al., 2002; Brickley and Mody, 2012). These ligand gated ion-channels are permeable for both chloride and bicarbonate ions. Current flow through the receptor depends on both the electrical and chemical driving forces on these ions. At the GABA reversal potential, electrical and chemical driving forces are in an equilibrium and no net current flow takes place. As the permeability for chloride is five times higher than for bicarbonate (Bormann et al., 1987), the GABA reversal potential is dominated by the equilibrium potential for chloride.

Opening of $GABA_A$ receptors inhibits the postsynaptic cell via hyperpolarization and/or shunting. Usually, the GABA reversal potential is below the resting membrane potential, and activation of $GABA_A$ receptors leads to a hyperpolarizing influx of chloride. This hyperpolarization drives the cell further away from action potential threshold and therefore reduces cell excitability. Shunting inhibition on the other hand is independent of the driving force and depends only on the opening of the receptor. This opening leads to an increase in membrane conductance and concomitantly to a shunt of excitatory inputs. It thereby reduces the depolarizing effects of excitatory inputs (Koch et al., 1983; Staley and Mody, 1992). Usually, opening of $GABA_A$receptors induces both shunting and hyperpolarizing inhibition. At the GABA reversal potential however, only shunting inhibition is effective and no hyperpolarizing potential will be induced. In contrast to hyperpolarizing inhibition, shunting inhibition is temporally restricted to the opening period of the receptor. Therefore, it is temporally more precise.

$GABA_B$ receptors are $G_{i/o}$-protein coupled receptors, that are expressed pre- as well as postsynaptically. On the postsynaptic side they cause slow, long lasting hyperpolarizations by increasing the potassium conductance through opening of GIRK-type K^+-channels[2] (Bettler et al. 2004). Presynaptically, they inhibit high-voltage activated Ca^{2+}-channels (P/Q- and N-type channels), thereby modulating transmitter release from both glutamatergic as well as GABAergic terminals.

Similar to $GABA_A$receptors, $GABA_C$ receptors are ligand gated ion channels. Compared to $GABA_A$ receptors, they exhibit a higher sensitivity for GABA, a lower conductance, a longer mean opening time and a lower rate of desensitization (Martínez-Delgado et al., 2010).

Compared to pyramidal cells, inhibitory interneurons form a much more diverse neuronal population, with approximately 21 different subtypes in the hippocampus having been described (Freund and Buzsaki, 1996). Interneuron subtypes differ in their axonal and dendritic morphology, their molecular expression profile and their physiological properties (Freund and Buzsaki, 1996; McBain and Fisahn, 2001; Maccaferri and Lacaille, 2003; Ascoli et al., 2008). This diversity enables interneuron subtypes to perform different functional roles inside the hippocampal network.

One feature commonly used to classify interneurons is the spatial distribution of their axons (McBain and Fisahn, 2001; Ascoli et al., 2008; DeFelipe et al., 2013, **Fig. 1.3**). The axon morphology determines which compartment of a pyramidal cell is innervated by the interneuron. A first differentiation is made between perisomatic and dendritic targeting interneurons (Han et al., 1993; Buhl et al., 1994a). In the hippocampus, perisomatic interneurons are further divided into two main groups, the axo-axonic (or chandelier) cells and the basket cells (Somogyi et al., 1983; Buhl et al., 1994b; Freund and Buzsaki, 1996; Halasy et al., 1996, **Fig. 1.3**). Axo-axonic interneurons innervate the axon initial segment,

[2]GIRK channels: G protein-coupled inwardly-rectifying potassium channels

whereas basket cells target the somata of pyramidal cells. Basket cells are further differentiated into fast spiking -parvalbumin (PV) positive- and regular spiking -cholecystokinin (CCK) positive- basket cells (Kosaka et al., 1987; Nunzi et al., 1985; Freund and Buzsaki, 1996; Pawelzik et al., 2002). Axo-axonic cells also express PV and additionally have a similar firing pattern to PV positive basket cells. These two cell types can therefore only be differentiated by electron microscopy.

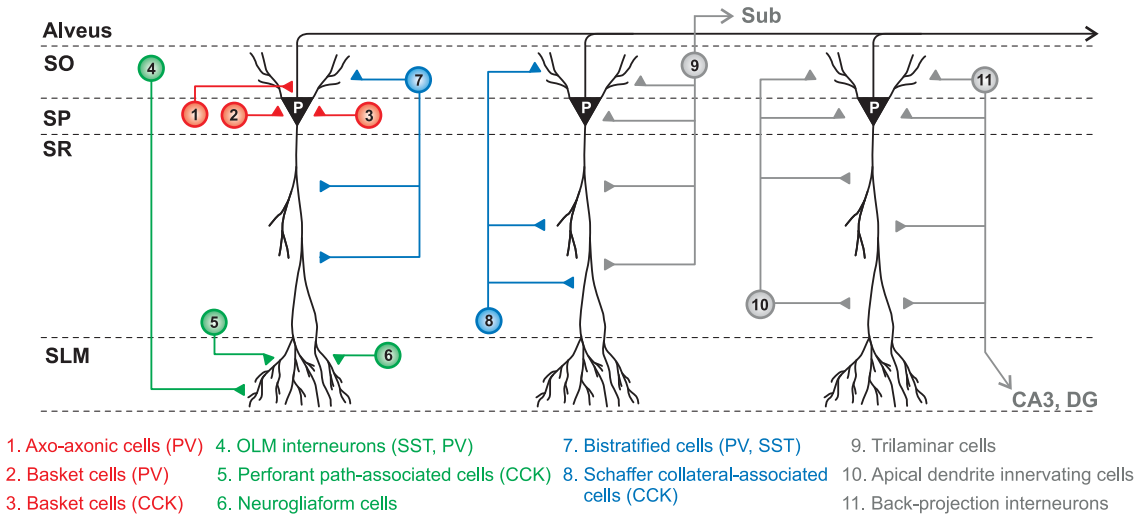

Figure 1.3: Morphological classification of interneurons in CA1. Interneuron subtypes differ in regard of the pyramidal cell compartment they innervate. Perisomatic interneurons (1-3, red) target the soma and axon initial segment of pyramidal neurons (P, black). Distal dendritic interneurons (4-6, green) target the apical tuft in stratum lacunosum moleculare (SLM). Proximal dendritic interneurons (7-11) target the proximal dendrites in stratum oriens (SO) and radiatum (SR). Some of these cells (gray) additionally innervate the somatic compartment. Cell type specific expression of parvalbumin (PV), somatostatin (SST) and cholecystokinin (CCK) is indicated. DG: dentate gyrus, SP: stratum pyramidale, Sub: Subiculum. Note, that this figure displayes only a fraction of interneuron subtypes. Adapted from Klausberger et al. (2003) and Somogyi and Klausberger (2005).

At the soma, all synaptic inputs are integrated and the decision of action potential generation is made (Stuart et al., 1997). Therefore, perisomatic interneurons are ideally located to control action potential output of their target cells (Buzsáki and Chrobak, 1995; Miles et al., 1996). Indeed, it has been shown that PV^+ interneurons control spike timing of principal cells (Pouille and Scanziani, 2001; Losonczy et al., 2010; Royer et al., 2012). Additionally, perisomatic cells are involved in the synchronization of large numbers of pyramidal cells and play a role in network oscillations that occur during different states of the brain (Cobb et al., 1995; Tamás et al., 2000; Mann and Paulsen, 2007; Mann and Mody, 2008; Ellender et al., 2010; Chen et al., 2012, but see Freund and Katona, 2007). This function is supported by the interconnectivity of basket cells, both via chemical and electrical synapses (Cobb et al., 1997; Tamás et al., 2000; Meyer et al., 2002).

The group of dendritic targeting interneurons is even more diverse compared to the

somatic targeting interneurons (Klausberger, 2009, **Fig. 1.3**). The subtypes of dendrite targeting interneurons mainly differ in regard of the dendritic compartment of pyramidal cells they innervate. Interestingly, the axonal projections of these neuron subtypes often match the layers of the different excitatory inputs (compare **Fig. 1.2** and **1.3**). Thereby, excitatory inputs from different sources can be modulated by different subtypes of local inhibitory interneurons. Bistratified cells and Schaffer collateral-associated cells target proximal dendrites in strata oriens and radiatum, thus modulating excitatory inputs from the Schaffer collaterals that terminate in these layers (Buhl et al., 1994a; Cossart et al., 1998). Oriens-lacunosum moleculare (OLM) interneurons, on the other hand, have their somata located in stratum oriens and innervate the distal apical tuft of pyramidal cells in stratum lacunosum moleculare, the region that receives excitatory inputs from the thalamus and the entorhinal cortex (McBain et al., 1994; Sik et al., 1995). OLM cells express both the neuropeptide somatostatin (SST) and low levels of PV (Maccaferri et al., 2000; Klausberger et al., 2003). The distal apical tuft is also covered by perforant path-associated and neurogliaform cells that have somata in stratum radiatum and stratum lacunosum moleculare (Hájos and Mody, 1997; Cossart et al., 1998; Vida et al., 1998). Other interneurons like trilaminar and apical dendrite innervating cells are not restricted to one compartment but innervate both the somatic and dendritic regions of pyramidal cells (Sik et al., 1995; Klausberger et al., 2005). Some interneuron classes also have axon collaterals leaving CA1 to target CA3/the dentate gyrus (back-projection interneurons) and/or the subiculum (Buhl et al., 1994a; Freund and Buzsaki, 1996; Somogyi and Klausberger, 2005; Klausberger and Somogyi, 2008). Additionally, long range GABAergic projection neurons target cells in subcortical and cortical areas outside the hippocampal formation (Jinno et al., 2007).

The different dendrite targeting interneurons are involved in processing and controlling excitatory inputs that impinge on these dendrites. Due to their dendrite targeting synapses, these interneurons can locally shunt excitatory inputs and influence the opening of voltage-gated ion channels (McBain and Fisahn, 2001). This enables them to control the generation of dendritic (d-) spikes and, consequently, of d-spike driven action potentials (Lovett-Barron et al., 2012). Thereby, they can also influence spiking behavior of pyramidal cells. Accordingly, *in vivo* experiments revealed that SST^+ interneurons are able to control bursting behavior of pyramidal cells during exploratory behavior (Losonczy et al., 2010; Royer et al., 2012; Stark et al., 2014). Furthermore, fear conditioning experiments have shown that the perturbation of SST^+ interneurons directly influences behavior (Lovett-Barron et al., 2014).

In addition to the innervation of different pyramidal cell compartments, interneurons also target other inhibitory cells and/or form autaptic connections with themselves (Cobb et al., 1997; Hájos and Mody, 1997). Some interneurons, like basket cells, innervate both principal cells and interneurons (Harris et al., 1985; Cobb et al., 1997; Pawelzik et al., 2003),

whereas other interneurons are specialized to target only interneurons (Acsády et al., 1996; Gulyás et al., 1996, 2003). The latter class is usually referred to as interneuron specific cells and can further be divided based on projection patterns and moleculare profiles (Somogyi and Klausberger, 2005).

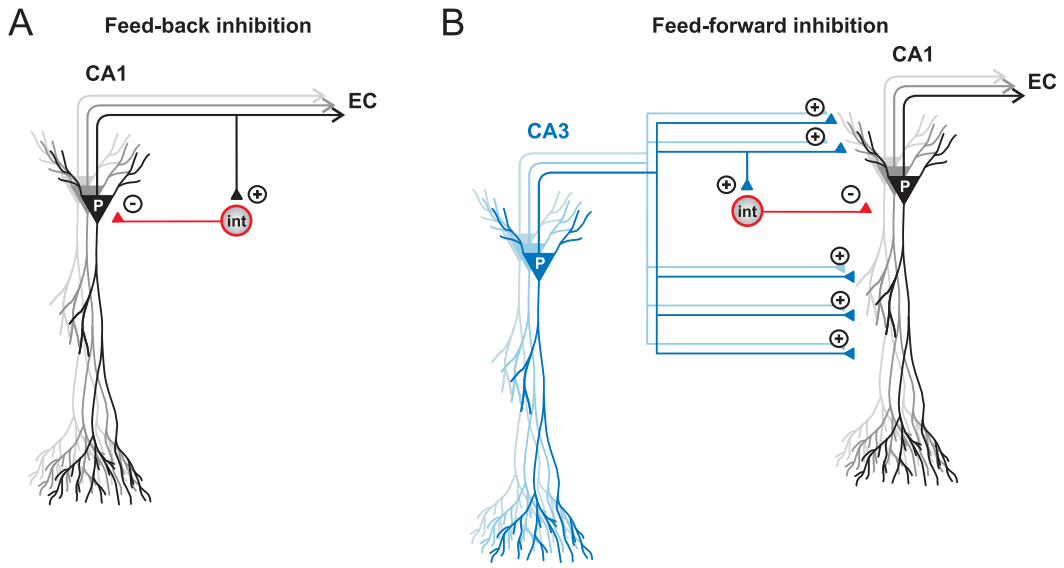

Figure 1.4: Inhibitory microcircuits in CA1. Interneurons in CA1 receive two major of excitatory inputs. **(A)** Feed-back inhibition: CA1 inhibitory interneurons (int, red) are innervated by recurrent axon collaterals of local CA1 pyramidal neurons (P, black). **(B)** Feed-forward inhibition: CA1 interneurons receive additional excitatory input from CA3 pyramidal neurons (P, blue) that also excite CA1 pyramidal neurons. EC: entorhinal cortex.

For inhibition to properly fulfill its function, not only the spatial but also the temporal pattern of inhibition is important. The temporal activity pattern of interneuron subtypes is modulated differently during the diverse oscillatory rhythms of the brain (Klausberger and Somogyi, 2008). Together with the differences in axonal projection patterns of interneuron subtypes, a complex spatio-temporal pattern of inhibition is generated.

The temporal pattern of activity of interneurons is shaped by the excitatory inputs which they receive (**Fig. 1.4**). Interneurons in CA1 are strongly innervated by the local excitatory axon collaterals of CA1 pyramidal cells. As the interneurons then project back to and inhibit CA1 pyramidal cells, an inhibitory feed-back circuit is created (**Fig. 1.4A**). Since feed-back interneurons are activated by their target cells, the resulting feed-back inhibition is proportional to the target (pyramidal) cell activity (Bartos et al., 2011; Mittmann et al., 2004). The second major excitatory input to CA1 interneurons are the Schaffer collaterals from CA3, that innervate both CA1 pyramidal cell and CA1 interneurons in stratum oriens and stratum radiatum. Because of this, excitatory inputs to CA1 pyramidal cells also directly activate interneurons, that inhibit the pyramidal cells with a small delay. This way of inhibitory microcircuit is called 'feed-forward inhibition' (**Fig.**

1.4B). Unlike feed-back inhibition, feed-forward inhibition is scaled to the strength of excitatory input to pyramidal cells. Thereby, it terminates the temporal window for excitation and increases the temporal precision of firing in their principal cell targets (Pouille and Scanziani, 2001; Bartos et al., 2011).

Further sources of input to CA1 interneurons are the subiculum and the septum. The subicular projection is both excitatory and inhibitory, whereas the septal projection is mainly inhibitory and plays an important role in the generation of the theta rhythm (Sun et al., 2014; Vandecasteele et al., 2014).

1.3 Interneurons and epilepsy

Epilepsy is a disorder of increased neuronal excitability and synchronization. Accordingly, both the inhibition of target cells and their ability to synchronize neuronal populations place interneurons into the focus of epilepsy research. GABAergic inhibition is generally thought to be anticonvulsant and a loss of interneurons could therefore contribute to an increased excitability of the brain. A pathological alteration of interneuron activity on the other hand could induce hypersynchronization and thus promote epileptiform activity.

The increase observed in excitability in epilepsy suggests a decreased inhibitory control over the neuronal network. A number of studies seem to support this hypothesis. For instance, substances blocking GABAergic inhibition like bicuculline or picrotoxin can synchronize populations of cells (Miles and Wong, 1983) and induce epileptic activity both *in vitro* (Brady and Swann, 1984; Swartzwelder et al., 1988) and *in vivo* (Meldrum and Horton, 1971; Meldrum, 1975). Similarly, substances strengthening the GABAergic response, for example GABA receptor agonists or drugs increasing the GABA concentration inside the synaptic cleft, are potent anticonvulsants (Treiman, 2001; Rogawski and Löscher, 2004). In addition, GABAergic interneurons appear to contribute to the control of seizure propagation (i.e. Trevelyan et al., 2006, 2007; Schevon et al., 2012) and to counteract the progressive synchronization of larger cell ensembles (Liotta et al., 2011). These studies emphasize the potential impact a failure of inhibition might have.

Indeed, a large number of studies from both animal models and epilepsy patients reveal multiple changes in the GABAergic system. These changes include alterations in receptor expression levels, changes in the chloride reversal potential and alterations in morphology as well as selective cell death. Studies from both animal models (Brooks-Kayal et al., 1998; Fritschy et al., 1999) and TLE patients (Loup et al., 2000) report cell type and region specific changes in receptor number and subunit expression. As a consequence, inhibitory postsynaptic responses and receptor pharmacology (e.g. response to benzodiazepines) are changed (Brooks-Kayal et al., 1998; Nusser et al., 1998; Gibbs et al., 1997). These alterations are region specific and dynamically modulated during epileptogenesis, with increases of GABAergic currents in dentate granule cells (Nusser et al., 1998) and

decreased responses in CA1 pyramidal cells (Gibbs et al., 1997; González et al., 2013). Additionally, impaired receptor functions due to epilepsy associated mutations have been reported (Baulac et al., 2001; Wallace et al., 2001).

The magnitude of the postsynaptic GABAergic current does not only depend on the receptor but also on the driving force for chloride. Both, studies on animal models and human tissue have shown that in a subset of cells the GABA reversal potential is shifted to a more depolarized potential (Cohen et al., 2002). This shift is caused by a reduced expression of the chloride transporter KCC2 which results in an intracellular accumulation of chloride (Huberfeld et al., 2007). The resulting alteration in driving force further reduces the strength of the inhibitory response and can even cause a depolarizing GABAergic potential.

The TLE associated changes described so far influence the postsynaptic response to GABA. However, the most prominent alteration in the GABAergic system is the specific loss of interneuron subtypes (Cossart et al., 2001, 2005). A highly vulnerable population of interneurons are the dendritically targeting, SST expressing interneurons in both CA1 (Cossart et al., 2001; Dinocourt et al., 2003) and the hilus (Buckmaster and Jongen-Rêlo, 1999; de Lanerolle et al., 1989). Structural as well as electrophysiological experiments further revealed that the decrease in SST positive cells is accompanied by a decrease in distal dendritic inhibition (Cossart et al., 2001). The number of axo-axonic cells decreases as well (Dinocourt et al., 2003), indicating that perisomatic inhibition is also partially disturbed. However, both parvalbumin expressing basket cells and dendritically projecting bistratified cells seem to be preserved in both experimental and human epilepsy (Cossart et al., 2001; Dinocourt et al., 2003; Maglóczky and Freund, 2005; Wittner et al., 2005). Note that these studies have to be interpreted carefully, as the loss of a marker protein might not be caused by loss of a cell type, but a decrease in expression of the same marker protein (Maglóczky and Freund, 2005).

In addition to cell loss, axonal projections of surviving interneurons are changed. In the pilocarpine model of epilepsy, surviving SST^+ cells in the hilus show an increased axon length, accompanied by an increase in granule cell innervation (Zhang et al., 2009). In CA1, sprouting axons of SST^+ OLM cells leave the SLM to target granule cells in the dentate gyrus (Peng et al., 2013). Conversely, innervation of pyramidal cells by CCK^+ basket cells is reduced (Wyeth et al., 2010). In addition, excitatory inputs to interneurons are changed as well, with increased excitatory inputs to hilar SST^+ cells in experimental epilepsy (Halabisky et al., 2010). These changes, however, remain controversial and do not necessarily overlap between animal models and human hippocampus (de Lanerolle et al., 1989; Maglóczky and Freund, 2005).

The studies mentioned so far show that inhibition is disturbed in epilepsy in a complex way. Cell loss and reduction of receptor expression suggest that decreased inhibition is at least partly responsible for hyperexcitability. Axonal sprouting of interneurons, increased

excitatory inputs to interneurons or increases in the number of GABA receptors are usually interpreted as compensatory mechanisms to regain control over the epileptic network. However, the role of inhibitory interneurons goes beyond the control of neuronal excitability and involves synchronization of large populations of pyramidal cells (Cobb et al., 1995). Changes in the spatio-temporal pattern of inhibition might further disturb the neuronal balance. Indeed, in some forms of epilepsy, pathologically increased inhibition has been suggested to support the generation of seizures (Mann and Mody, 2008). Proconvulsive effects of interneuron activity can be mediated by pathological increases in synchronization, depolarizing effects of GABA (Staley et al., 1995; Cohen et al., 2002; Ben-Ari and Holmes, 2005; Huberfeld et al., 2007) or by an increased rebound excitation (Chen et al., 2001; Mann and Mody, 2008). Furthermore, interneurons are under inhibitory control as well. Increased inhibition of interneurons can cause a disinhibition of pyramidal cells and thus increase the excitability of a neuronal network (Lee and Maguire, 2013). These studies clearly show that GABAergic interneurons and their changes in epilepsy cannot be classified as simply pro- or anticonvulsant. To gain a better understanding of the relation of inhibition and epilepsy, the spatio-temporal activity pattern of GABAergic interneurons within the brain needs to be investigated.

1.4 Antiepileptic drugs

One key goal for anticonvulsant drugs is to prevent seizures without disturbing normal ongoing brain activity. To reduce seizure susceptibility, AEDs may target the intrinsic excitability of cells, increase synaptic inhibition or decrease synaptic excitation. Usually, an AED acts on more than one target protein. Potential target molecules include voltage-gated ion channels, neurotransmitter receptors or molecules that modulate neurotransmitter concentrations in the synaptic cleft. Voltage-gated ion channels control cell excitability, dendritic integration as well as action potential firing and are therefore key players in the control of excitability.

1.4.1 Sodium channels as targets for antiepileptic drugs

A prominent target for AEDs are voltage-gated sodium channels (VGSCs). VGSCs control cell excitability and are responsible for action potential generation (Ragsdale and Avoli, 1998). They are therefore directly involved in the generation of sustained and synchronized firing of action potentials during seizure activity. VGSCs give rise to the fast inactivating, transient sodium current responsible for action potential generation as well as the non-inactivating, persistent sodium current. The transient sodium current (I_{NaT}) shows a fast submillisecond activation that is followed by fast channel inactivation (Catterall, 2000).

Channel activation is voltage dependent. At resting membrane potential most sodium channels are in a closed, resting state. Upon membrane depolarization, channels change

their conformation into the open, conducting state. From this activated state, channels rapidly convert into the non-conducting, inactivated state within milliseconds (Catterall, 2000). The recovery from inactivation into the resting, activatable state requires repolarization of the membrane. The rapid cycling through these states is necessary to enable neurons to fire rapid trains of action potentials. During prolonged depolarizations and high frequency repetitive firing, a second process of slow inactivation takes place. In contrast to fast inactivation, onset and recovery of slow inactivation is in the order of seconds and contributes to the termination of action potential bursts and slow spike-frequency adaptation (Goldin, 2003; Ulbricht, 2005; Oliva et al., 2012).

Voltage-gated sodium channels consist of the main α subunit, a 260 kDa transmembrane protein that forms the ion conducting pore (Catterall, 2000). It is associated with two of four potential auxiliary subunits, β1 to β4, that are not required for expression of functional sodium channels, but modulate their expression pattern, the kinetics and voltage dependence of channel gating as well as their pharmacology (Catterall, 2000; Brackenbury and Isom, 2011; Uebachs et al., 2010). In mammals, there are nine different sodium channel isoforms, $Na_v1.1$ to $Na_v1.9$ (Goldin et al., 2000; Catterall et al., 2005). However, only four of these isoforms are expressed in the adult CNS ($Na_v1.1$ - 1.3 and $Na_v1.6$). Their expression differs in regard of development, cell type and cell compartment (Trimmer and Rhodes, 2004). The main sodium channel isoforms expressed in excitatory cells are $Na_v1.2$ and $Na_v1.6$, whereas $Na_v1.1$ seems to be mainly expressed in (parvalbumin expressing) GABAergic interneurons (Yu et al., 2006; Ogiwara et al., 2007).

The α subunit consists of four homologous domains (I-IV) that are composed of six transmembrane α helices, S1-S6. The pore loops between S5 and S6 serve as ion selective filter at the entrance of the channel. A short intracellular loop located between domain III and IV serves as inactivation gate, blocking the pore during fast inactivation. Slow inactivation does not depend on this inactivation gate, but is thought to result from structural rearrangements of the channel pore (Goldin, 2003).

One prototypical AED acting on voltage gated sodium channel is carbamazepine (CBZ), a dibenzazepine that is effective in treatment of partial and generalized tonic clonic seizures (Ragsdale and Avoli, 1998; Brodie, 2010). The binding site of CBZ lies within the sodium channel pore and is formed by amino acid residues of the S6 segments of domains I, III and IV (Ragsdale et al., 1994, 1996; Yarov-Yarovoy et al., 2001, 2002). Binding of CBZ to the receptor blocks the channel pore and thereby prevents ion permeation. Additionally, CBZ stabilizes the inactivated state and thus delays recovery from inactivation into the activatable state (Schwarz and Grigat, 1989; Ragsdale and Avoli, 1998; Kuo, 1998; Lipkind and Fozzard, 2010). The position of the drug binding site within the sodium channel pore requires the opening of the pore to allow CBZ to bind (Payandeh et al., 2011). As the proportion of sodium channels in the open/inactivated state increases with depolarization and during prolonged high frequency firing, CBZ blocks sodium chan-

nels in a use- and voltage-dependent manner (Willow et al., 1985; McLean and Macdonald, 1986; Schwarz and Grigat, 1989; Kuo et al., 1997). As seizures are characterized by sustained depolarizations as well as by prolonged high frequency firing, CBZ preferentially interferes with pathological high frequency activity, while leaving normal ongoing activity intact.

So far, similar to other CNS drugs, the mechanism of action of sodium channel blockers have mainly been studied on the level of potential target proteins in isolated preparations. Little is known about their action on the many different neuron types as well as on their behavior on complex micronetworks. There are few studies investigating sodium channel blocker effects on a network level. These studies were conducted using field potential recordings and/or single unit recordings of pyramidal cells (Hershkowitz and Ayala, 1981; Hood et al., 1983; Olpe et al., 1985; Ashton et al., 1988). However, these studies do not clearly identify the cell types directly modulated by the drug. The importance of a more differentiated network approach becomes apparent when taking GABAergic interneurons into account. Some of these interneuron subtypes are able to fire at very high rates (Freund and Buzsaki, 1996; Ascoli et al., 2008). The use-dependent action of CBZ and similar anticonvulsants would suggest that firing of these interneurons is strongly affected by these compounds. Reduced firing of interneurons would lead to a decreased synaptic inhibition. A block of inhibitory interneurons by anticonvulsants seems to be contradictory to their strongly antiexcitatory effect. However, interneuron subtypes differ in their physiological properties, serve different functions and show different activity patterns during network oscillations. The network effect of a use-dependent interneuron blockade therefore cannot be predicted by studying isolated cell types.

1.5 Key questions

Loss of interneuron subtypes and a reduction in GABAergic responses are outstanding alterations in the epileptic brain. However, the different tasks of interneurons suggest that morphological and behavioral alterations of surviving cells will also strongly influence network activity. To exert its multiple functions correctly, inhibition has to occur both at the right time and in the appropriate location. The temporal activity pattern of a given interneuron is shaped by its synaptic inputs as well as its intrinsic properties. The spatial component is given by the difference in axon morphology of interneuron classes. In the first part of this thesis, I therefore investigated whether the spatio-temporal role of feed-back inhibition is changed in chronic epilepsy. Due to its upstream position to the subiculum and the entorhinal cortex and its potential role in controlling seizure spread, I focused on the CA1 area of the hippocampus. In the second part of this thesis, I studied the effects of CBZ and similar anticonvulsants on inhibitory microcircuits in both control and epileptic animals.

2 Material & Methods

2.1 Pilocarpine model of epilepsy

All slice experiments in chronically epileptic animals were performed in the pilocarpine model of epilepsy that mimics key features of human temporal lobe epilepsy (Turski et al., 1983; Cavalheiro, 1995; Toyoda et al., 2013). In this model a status epilepticus is induced by a single systemic injection of the muscarinic acetylcholine agonist pilocarpine. After a latent period this leads to the subsequent development of chronic epileptic seizures.

Male Wistar rats were ordered with a body weight of 150-180 g (Charles River, Sulzfeld, Germany) 2-3 days prior to injections to allow acclimatization in the animal facility. Pilocarpine hydrochloride (340 mg/kg body weight, Sigma Aldrich, Hamburg, Germany) was diluted in aqua ad injectabilia and injected intraperitoneally. 30 min prior to the pilocarpine treatment, animals were injected subcutaneously with scopolamine methyl nitrate (1 mg/kg body weight, Sigma Aldrich, Hamburg, Germany), diluted in ringer (in mM: 143.1 NaCl, 4.02 KCl, 2.24 CaCL $\cdot$ 2 H_20; Fresenius Kabi, Bad Homburg, Germany). This competitive muscarinic acetylcholine antagonist does not cross the blood brain barrier and therefore reduces the peripheral side effects of pilocarpine (Peroutka and Snyder, 1982; Turski et al., 1983; Brown, 1990). Within 60 min after injection of pilocarpine, 30-50 % of the animals developed a status epilepticus. The status was terminated after 40 min with an intraperitoneal injection of 1 ml diazepam (0.5 %, Ratiopharm, Ulm, Germany). Additionally, animals received subcutaneous injections of 1 ml ringer and 1 ml glucose (5 %, Fresenius Kabi, Bad Homburg, Germany) to compensate for the loss of energy and fluid. Animals that did not develop a status epilepticus within the first 60 min post injection received a second dose of pilocarpine.

The pilocarpine-induced status epilepticus is usually followed by a latent period of 7-14 days, during which epileptogenesis is taking place (Turski et al., 1983). This latent period is followed by the chronic phase in which animals start to generate spontaneous generalized seizures. To ensure that only chronically epileptic animals were used, animals were video-monitored for 7 days starting on day 17 post injection. Only animals displaying at least one spontaneous seizure in this monitoring were included in the study. Experiments were then conducted in a time window of 4-8 weeks post injection. Pilocarpine-treated epileptic rats were compared to age matched, sham-injected control rats. These control animals were injected with identical doses of scopolamine methyl nitrate, diazepam, glucose and

ringer. For the study on the anticonvulsant drug action (Section **3.2**), sham-control and normal age-matched Wistar rats were pooled. All animal experiments were conducted in accordance with the guidelines of the Animal Care and Use Committee of the University of Bonn.

2.2 Slice preparation

Rats were deeply anesthetized with a subcutaneous injection of 1.5 ml xylacine hydrochloride (2 %, Bayer, Leverkusen, Germany) and 0.5 ml ketamin hydrochloride (10 %, Pfizer, Berlin, Germany). Before decapitation, animals were transcardially perfused with 15-20 ml of ice-cold preparation solution containing (in mM): 60 NaCl, 100 sucrose, 2.5 KCl, 1.25 NaH_2PO_4, 26 $NaHCO_3$, 1 $CaCl_2$, 5 $MgCl_2$ and 20 D-glucose (equilibrated with 95 % O_2 and 5 % CO_2). Subsequently, the brain was quickly removed, glued with the ventral surface onto the stage of a vibratome (Microm HM 650 V, Thermo Fisher Scientific, Walldorf, Germany) and transverse 300 µM-thick hippocampal slices were prepared. After equilibration for 30 minutes at 35°C in the preparation solution, slices were transferred to artificial cerebrospinal fluid (ACSF) containing (in mM): 125 NaCl, 3 KCl, 1.25 NaH_2PO_4, 26 $NaHCO_3$, 2.6 $CaCl_2$, 1.3 $MgCl_2$ and 15 D-glucose (equilibrated with 95 % O_2 and 5 % CO_2) and stored at room temperature. During all experiments $GABA_B$ receptors were blocked with CGP 52432 (500 nM, Tocris Bioscience, Bristol, UK).

2.3 Electrophysiological recordings

For electrophysiological recordings, slices were transferred to a submerged chamber mounted on the stage of an upright microscope (Axioscope 2 FS, Zeiss) and continuously perfused with ACSF (equilibrated with 95 % O_2 and 5 % CO_2). All experiments were performed at 31-32°C either via an inline solution heater (TC324B, Warner instruments, Hamdon, USA) or a temperature controllable bath chamber (Temperaturcontroller III, Luigs and Neumann, Ratingen, Germany). Cells were visualized with infrared oblique illumination optics (TILL Photonics, Gräfelfing, Germany), a water immersion objective (Olympus 60x/NA 0.9, Tokyo, Japan) and a TILL-IMAGO camera (TILL Photonics, Gräfelfing, Germany) .

Somatic whole-cell recordings of interneurons or pyramidal neurons in the CA1 region were obtained with an Axopatch 200B amplifier (Molecular Devices, Biberach an der Riss, Germany), a BVC-700A amplifier (Dagan Corporation, Minneapolis, Minnesota, USA) or a Multiclamp 700B amplifier (Molecular Devices, Biberach an der Riss, Germany). Data were filtered at 10 kHz and sampled at 100 kHz with a Digidata 1440 interface, controlled by pClamp Software (Molecular Devices, Biberach an der Riss, Germany). Recording pipettes were made from thick walled borosilicate glass capillaries (GB 150F 8P, Science

Products, Hofheim, Germany) on a vertical puller (PP-830, Narishige, Tokyo, Japan). Recording pipettes for whole-cell recordings had a resistance of 3-6 MΩ and were filled with (in mM): 140 K-gluconate, 5 HEPES, 0.16 EGTA, 0.5 $MgCl_2$, 5 phosphocreatine and 0.3 % biocytin. The pH was adjusted with KOH (1 mol/l) and the osmolarity set to 280-290 mOsm by addition of sucrose. Series resistance ranged from 10 to 25 MΩ. The calculated liquid junction potential was -15 mV, and membrane potential values were corrected accordingly. In experiments investigating the effects of phenytoin and lamotrigine on firing rates, a different intracellular solution was used, containing (in mM): 130 K-gluconate, 20 KCl, 10 4-(2-hydroxyethyl)-1-piperazineethanesulfonic acid (HEPES), 0.16 ethylene glycol tetraacetic acid (EGTA), 2 Mg-ATP, 2 Na_2-ATP and 15 D-glucose. Pipettes for loose patch recordings had a resistance of 7-10 MΩ and were filled with ACSF.

Interneurons and pyramidal cells were visually identified under infrared difference interference contrast optics, and further characterized functionally as well as morphologically by biocytin labeling and reconstruction.

2.4 Morphological reconstructions

Slices containing biocytin filled cells were incubated at 4°C in paraformaldehyd (4 %) dissolved in 0.1 phosphate buffer (PB, pH 7.4) for at least 24 h. For biocytin staining slices were washed in 0.15 M phosphate buffer saline (PBS) and permeabilized for 30 minutes with Triton X 100 (0.4 % in PBS). Slices were then incubated for two hours in strepavidin alexa fluor 488 (Life Technologies, Carlsbad, USA, 1:500 in PBS and 0.5 % Triton X 100). Subsequently, sections were washed in 0.1 M PB three times for 5 minutes, and mounted with Aqua-Poly/Mount (Polyscience Inc., Warrington, USA). Filled neurons were scanned with a confocal microscope (TriM Scope Confocal, LaVision BioTec, 20 fold magnification) and reconstructed from z-stacks (step size: 2 µM) using Corel DRAW Graphics Suite 12.

2.5 Analysis of synaptic excitation of CA1 pyramidal cells

Stimulation was carried out with bipolar steel electrodes (FHC, Bowdoin, Maine, USA). Biphasic charge neutral pulses with a duration of 50-100 µs were generated with a stimulus isolator (A-M Systems Model 2100, Carlsborg, WA, USA). For monosynaptic activation of CA1 pyramidal cells I stimulated Schaffer collaterals by placing a stimulation electrode into the stratum radiatum. During this stimulation, either cell-attached recordings (**Fig. 3.22**) or whole-cell recordings (**Fig. 3.23**) were obtained to assess CBZ effects on synaptically induced firing and excitatory postsynaptic currents (EPSCs), respectively. Both experiments were conducted in presence of the $GABA_A$ antagonist gabazine (SR 95531 hydrobromide, 10 µM, Tocris). Additionally, a cut was made between CA1 and CA3, to avoid network events due to the disinhibition of the recurrent CA3 network. In

cell-attached recordings, stimulation strength was adjusted to elicit the maximal firing probability over the duration of the stimulus train (0.2-0.4 mA). During long stimulus protocols of 25 stimuli at 50 Hz stimulation was repeated every 30s.

2.6 Analysis of feed-back activation of CA1 interneurons

For synaptic feed-back activation of CA1 interneurons, I stimulated CA1 axons by placing the stimulation electrode into the alveus adjacent to the subiculum (**Fig. 2.1**). This stimulation leads to the antidromic activation of CA1 pyramidal cell axons. Recurrent axon collaterals of the stimulated fibers then activate CA1 interneurons synaptically. To prevent feed-forward activation of interneurons via stimulation of Schaffer collaterals as well as a direct electrical stimulation of interneurons, a cut was made at the CA1-subiculum border through strata lacunosum-moleculare, radiatum, pyramidale and oriens with only the alveus left intact (Pouille and Scanziani, 2004, see **Fig. 2.1A,B**, Cut 1). A second cut was made at the CA1/CA3 border to limit spontaneous activity in CA1 neurons (**Fig. 2.1B**, Cut 2). Synaptic activation of feed-back interneurons (e.g. **Fig. 3.4**) was examined with whole-cell recordings of excitatory postsynaptic potentials (EPSPs). Afterwards the $GABA_A$ antagonist gabazine (SR 95531 hydrobromide, 10 µM, Tocris Bioscience, Bristol, UK) was applied to estimate whether, in addition to excitatory input, feed-back dynamics are shaped by inhibitory inputs onto interneurons (see Section **3.1.3**).

CBZ effects on synaptically induced firing of interneurons was monitored with cell attached recordings and subsequent repatching in whole-cell mode to allow biocytin staining and morphological identification. In case of the cell-attached recordings, stimulation strength was adjusted at a stimulation frequency of 50 Hz to elicit a firing probability of $\geq$ 90 % in response to at least one of the first four stimuli. Stimulation paradigms were applied at 0.1 Hz. In the absence of any drug application, the firing probability of all classes of interneurons was stable over at least 15 minutes (basket cells: n=5, p=0.96; proximal dendritic cells: n=5, p=0.28; OLM cells: n=4, p=0.54, paired t-test). To prevent contamination by reciprocal inhibition between interneurons, gabazine (10 µM) was present during the whole experiment.

2.7 Analysis of feed-back and feed-forward inhibition of CA1 pyramidal cells

To analyze feed-back inhibition onto CA1 pyramidal cells, feed-back interneurons were activated analogous to Section **2.6** and resulting inhibitory postsynaptic currents (IPSCs) or potentials (IPSPs) in pyramidal cells were recorded in the whole-cell mode. To confirm the GABAergic nature of synaptic events, the $GABA_A$ receptor antagonist gabazine (SR 95531 hydrobromide, 10 µM, Tocris, Bristol, UK) was applied at the end of all stimulation

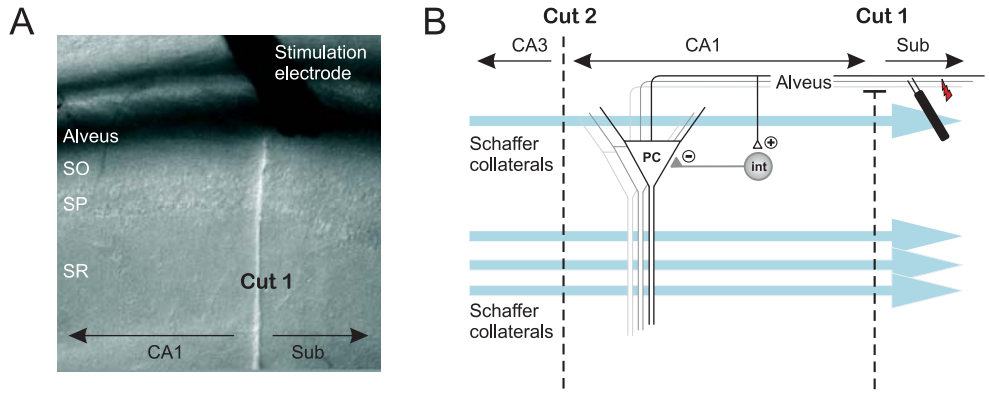

Figure 2.1: Stimulation configuration to activate feed-back microcircuits in CA1. **(A)** Photograph of the experimental setup showing the stimulus electrode placed into the alveus and the cut separating CA1 and subiculum (Sub). **(B)** Schematic drawing of the stimulus configuration. CA1 pyramidal cell (PC) axons are stimulated with a bipolar electrode placed into the alveus. This stimulation will also activate local CA1 axon collaterals that target feed-back interneurons (Int). Cut 1: Cut at the border between CA1 and subiculum preventing stimulation of Schaffer collaterals as well as direct stimulation of CA1 interneurons. Note that Schaffer collaterals are disrupted while only the alveus is left intact. A second cut was made between CA3 and CA1 to prevent recurrent excitation and network events. SR: stratum radiatum, SP: stratum pyramidale, SO: stratum oriens.

experiments. In voltage clamp recordings the IPSC component was subsequently isolated by subtraction. In these recordings, pyramidal neurons were clamped at -65 mV. This procedure usually revealed no or only a minor excitatory component, indicating that contamination by Schaffer collateral or recurrent excitatory CA1 input is negligible in this paradigm (see **Fig. 3.17**).

For activation of feed-forward inhibition within the CA1 subfield, a stimulation electrode was placed into the pyramidal cell layer of CA3, thereby inducing feed-forward activation of CA1 interneurons. The resulting IPSCs in CA1 pyramidal cells were recorded in the whole-cell configuration (see **Fig. 3.30**). In these recordings, I frequently noted the appearance of stimulation-evoked compound EPSCs in CA1 neurons following application of gabazine. These were probably due to stimulation-evoked recurrent activity in the CA3 network. To exclude that potential CBZ effects on this EPSC component might contaminate the assessment of effects on IPSCs, I examined the effect of CBZ on Schaffer collateral EPSCs in separate recordings (see **Fig. 3.23**). In these experiments, no effects on EPSCs were observed. In these recordings, the CA3 subfield was separated from CA1 with a cut in order to prevent propagation of spontaneous activity in the CA3 region during gabazine application to the CA1 subfield.

2.8 Pharmacology

Anticonvulsants were obtained from Sigma Aldrich (CBZ and phenytoin, Hamburg, Germany) or Tocris (lamotrigine, Bristol, UK) and used in concentrations in a range that is

found in brain tissue from epilepsy patients (Rambeck et al., 2006). CBZ (final concentration 30 µM) was dissolved in ethanol, whereas lamotrigine (LTG, final concentration 25 µM) and phenytoin (PHT, final concentration 50 µM) were directly dissolved in ACSF. Control ACSF therefore either contained equivalent concentrations of ethanol compared to the CBZ-containing solution (0.05 %), or no solvent. Drug effects were analyzed 15 minutes after initiating the drug application. A washout was conducted for at least 15 minutes. The analysis of the effects of CBZ on maximal firing rates was done by identifying the current injection at which maximal firing rates were obtained under control conditions. Effects of CBZ and washout were quantified using this current injection magnitude. The baseline membrane potential was adjusted to 75 mV by current injection for all measurements. To compensate for changes in intrinsic cell properties over recording duration (e.g. Xu et al., 2005) mean values of control recordings before drug application and after 15 min washout were compared to recordings 15 min after drug application in all experiments. For analysis of CBZ effects on action potential (AP) properties, traces with two action potentials in the first 50 ms of current injection were selected, and the first AP was analyzed. In addition, I also examined APs occurring later during the current injection (300–500 ms after onset). Since both the AP properties themselves and the effects of CBZ will be influenced by the number of preceding action potentials, I selected traces with 10 APs in the first 500 ms of current injection (average time of peak of the analyzed AP, 427.4 ± 12.1 ms; average number of preceding APs, 10.8 ± 0.6). In individual cells, the current injection steps were selected such that the number of APs within the first 500 ms of the current injection in ACSF, in CBZ, and after washout was identical.

2.9 Data analysis and statistics

Average values in the text and figures are expressed as mean ± standard error of the mean (SEM). For statistical analysis Wilcoxon signed-rank test, Student's t-test, Kruskal Wallis test or ANOVA were used as appropriate and as indicated in the text. In some cases, a Tukey's post-hoc test or Dunn's multiple comparison test for parametric and nonparametric data, respectively, were employed to determine individual group differences. The properties of PSCs/PSPs were usually analyzed from an average of 10 sweeps. Firing probabilities during the cell attached recordings were calculated from 10 repetitions. In case of the long trains with 25 stimuli average firing frequencies were binned over 5 stimuli (100 ms). For analysis of AP properties, traces with two action potentials in the first 50 ms of current injection were selected and the first AP analyzed. Fast after hyperpolarizing potentials (fAHPs) were measured relative to the threshold of the analyzed AP. Broadening of APs over a 1s current injection was analyzed in traces of maximal firing rate. The input resistance R_{in} was calculated from voltage deflections over current injections ranging from -50 to +50 pA with a linear fit (IGOR PRO Wavemetrics, Lake Oswego, OR). The

membrane time constant τ was estimated using negative current injections and a standard exponential fit (Clampfit 10.2, Molecular Devices, Union City, CA).

3 Results

3.1 Alterations of inhibitory microcircuits in the epileptic hippocampus

3.1.1 Identification and classification of inhibitory interneurons in CA1

Interneurons can be classified based on the morphology of their axonal arbor (Somogyi and Klausberger, 2005). Using post hoc biocytin stainings, recorded interneurons were divided into three categories covering different areas of the pyramidal cell (PC) dendritic tree (see **Fig. 3.1**, upper panel, for representative reconstructions of the axonal arbor). The first category consisted of basket cells (BCs) that innervate pyramidal cell somata in stratum pyramidale (**Fig. 3.1 A**). A second, more heterogeneous group included cells that target the proximal dendrites of pyramidal cells in stratum radiatum and oriens (e.g. bistratified cells), as well as interneurons that additionally innervate stratum pyramidale (e.g. trilaminar cells). This group was termed proximal dendritic cells (PD, **Fig. 3.1 B**). The third category contained oriens-lacunosum moleculare (OLM) interneurons that are characterized by somata located in stratum oriens and axonal arbors that innervate the distal apical tuft in stratum lacunosum moleculare (**Fig. 3.1 C**).

Interneuron subtypes were then further characterized physiologically (**Fig. 3.2** and **3.3**). During long 1s current injections basket cells and proximal dendritic cells had significantly higher average maximal firing rates in comparison to pyramidal cells (101.9 ± 18.5 Hz, n=11 and 129.4 ± 1.4 Hz, n=13, for BCs and PDs respectively, compared to 22.3 ± 1.3 Hz in pyramidal cells, n=13, see **Fig. 3.2 A**). In contrast, with a maximal firing rate of 60.9 ± 5.1 Hz, firing rates of OLM interneurons were significantly lower than in PD interneurons (n=12. ANOVA, $F_{(3,44)}=11.94$, $p < 0.0001$. See **Fig. 3.2 A** for individual p values between groups, as given by a Tukey's post-hoc test).

When analyzing action potential properties, no additional differences between the interneuron subtypes were revealed (**Fig. 3.2 B-F**, ANOVA and a Tukey's post-hoc test). However, when comparing interneurons to pyramidal cells, minor differences were revealed. Action potentials of pyramidal cells had a larger amplitude compared to OLM cells and PD cells (80.2 ± 3.9 mV vs. 68.7 ± 3.0 and 68.2 ± 3.7mV for PC, PD and OLM cells, respectively, ANOVA and Tukey's post-hoc test, see asterisks in **Fig. 3.2 D**). Additionally, they were broader (**Fig. 3.2 E**) and had a smaller fast after hyperpolarizing potential (fAHP) compared to all interneuronal subtypes (**Fig. 3.2 F**).

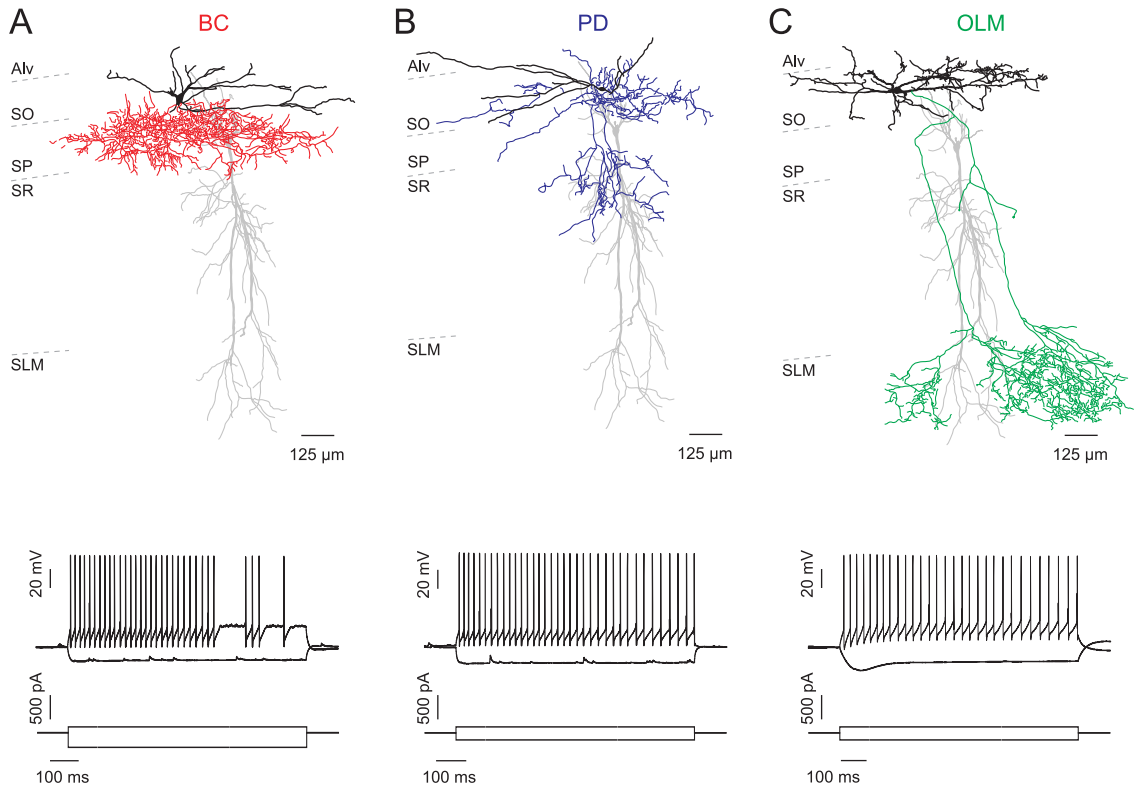

Figure 3.1: Classification of interneuron subtypes in CA1 based on axon morphology. (A) Upper panel: Reconstruction of a representative basket cell (BC) innervating pyramidal cell somata in stratum pyramidale (SP). Lower panel: Response to a hyperpolarizing and a depolarizing current step (duration: 1s) of the cell depicted above. **(B)** Reconstruction and example recordings of a bistratified cell innervating proximal dendrites of pyramidal cells in stratum oriens (SO) and radiatum (SR). **(C)** Oriens-lacunosum moleculare (OLM) interneuron targeting the distal apical tuft in stratum lacunosum moleculare (SLM). Axons of interneurons are depicted in red, blue or green, respectively and dendrites are shown in black. To indicate interneuron position relative to the pyramidal cell dendritic tree a separately recorded and reconstructed pyramidal cell is indicated in gray. Alv: Alveus, PD: Proximal dendritic targeting cell, OLM: OLM interneuron.

A comparison of passive cell properties revealed that interneurons had a threefold higher input resistance (**Fig. 3.3 A**) and a smaller cell capacitance (**Fig. 3.3 C**, n=11, n=13, n=12 and n=13 for BC, PD, OLM and PCs respectively. ANOVA and Tukey's post-hoc test, see asterisks in **A** and **C**) than pyramidal cells. Additionally, the time constant of OLM interneurons was significantly larger than in BCs and PDs (29.1 ± 4.7 for OLM interneurons, compared to 14.9 ± 3.0 and 13.9 ± 2.3 for BCs and PD cells respectively, ANOVA and Tukey's post-hoc test, **Fig. 3.3 B**).

3.1.2 Short-term dynamics of feed-back activation of CA1 interneurons

Next, I investigated the spatio-temporal pattern of synaptic feed-back activation of interneurons in CA1 (**Fig. 3.4**). To activate the presynaptic CA1 pyramidal cell axons, a stimulus electrode was placed into the alveus and excitatory postsynaptic potentials

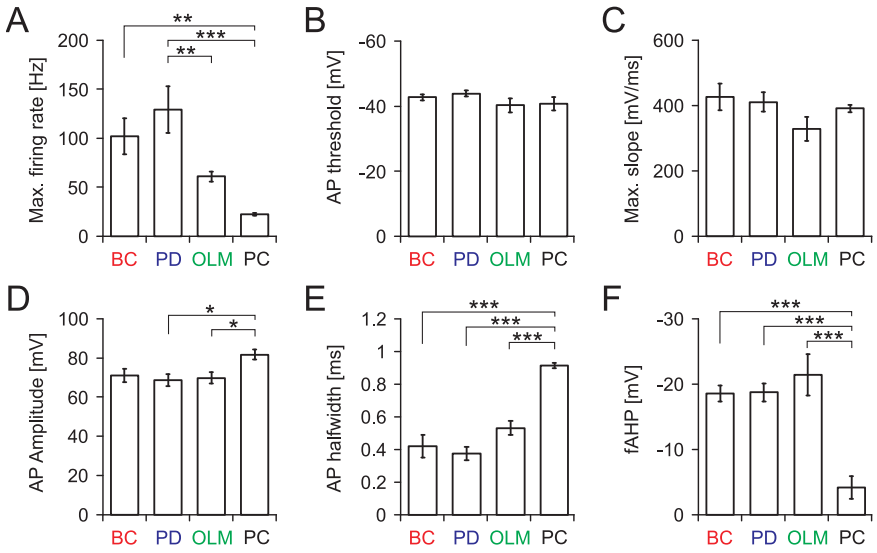

Figure 3.2: Active properties of identified CA1 interneurons and pyramidal cells. (A) Average maximal firing rate during long 1s current injections of interneurons and pyramidal cells. For every cell the current injection with the maximal number of action potentials was selected and the average firing rate calculated. **(B-F)** For analysis of action potential (AP) properties current injections inducing two APs inside the first 50 ms were selected and the first AP analyzed. Fast after hyperpolarizing potentials (fAHPs) in **(F)** were measured relative to action potential threshold. Bargraphs in A-F show average ± SEM. *, ** and *** depict $p < 0.05$, 0.01 and 0.001, respectively (Tukey's post-hoc test). BC: basket cells, PD: proximal dendritic interneurons, OLM: OLM interneurons, PC: pyramidal cells.

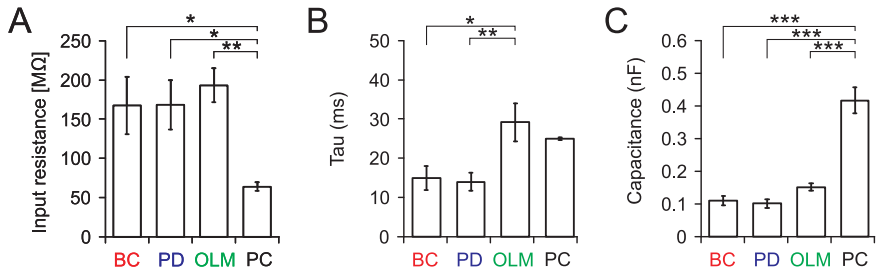

Figure 3.3: Passive properties of interneurons and pyramidal cells in CA1. (A) Input resistance was estimated from voltage deflections induced by current injections ranging from -50 to +50 pA. **(B)** Time constant was estimated from negative current injections and a standard exponential fit. **(C)** Cell capacity was calculated from R_{in} and τ. Bargraphs in A-C show mean ± SEM. *, ** and *** indicate p values < 0.05, 0.01 and 0.001, respectively as given by a Tukey's post-hoc test. BC: basket cells, PD: proximal dendritic interneurons, OLM: OLM interneurons, PC: pyramidal cells.

(EPSPs) were recorded in post hoc identified interneurons (**Fig. 3.4 A**). During a high frequency stimulus train (10 stimuli at 50 Hz), interneuron subtypes revealed opposite forms of short-term plasticity. Both, basket and PD cells received large amplitude excitatory inputs at the beginning of a stimulus train that were followed by strong synaptic depression (**Fig. 3.4 B,C**). In contrast, OLM interneurons showed the opposite input pattern with small EPSPs in response to the first stimulus and a subsequent strong facilitation. To compare the short-term dynamics between interneuron classes, the percent

change in EPSP amplitude over the stimulus train (1st EPSP vs. mean of the last three EPSPs, see blue boxes in **B**, upper panel) was calculated (**Fig. 3.4 D**). Basket and proximal dendritic cells showed an average decrease in EPSP amplitude of -48.2 ± 6.9% (n=9) and -27.7 ± 16.9 % (n=12) respectively. EPSP dynamics in OLM cells were significantly different from BCs and PDs, with an increase in EPSP amplitude of 71.9 ± 6.9 % over the stimulus train (n=12; Kruskal-Wallis test, $p < 0.0001$; Dunn's multiple comparison test, see asterisks in **Fig. 3.4 D**).

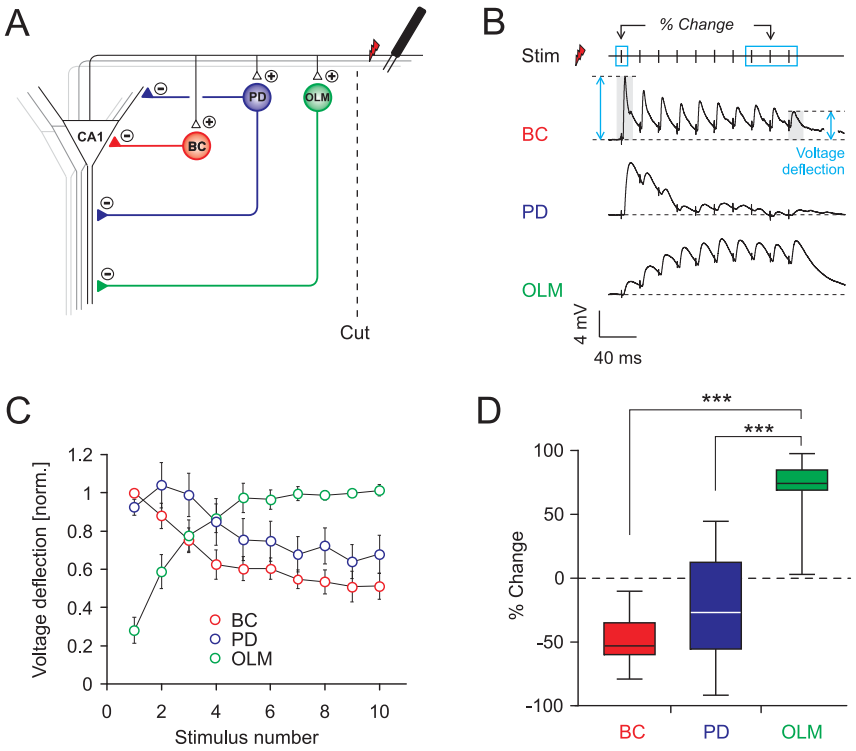

Figure 3.4: Short-term dynamics of feed-back activation of CA1 interneurons. **(A)** Experimental set up to elicit feed-back EPSPs in interneurons via antidromic activation of CA1 pyramidal cell axons. The stimulus electrode was placed in the Alveus and EPSPs in interneurons were recorded in the whole-cell mode. Interneurons were identified with post hoc biocytin stainings of axon morphology. **(B)** Representative recordings of a basket cell (BC), a proximal dendritic cell (PD) and an OLM interneuron (OLM). Traces depict averages of 10 consecutive recordings and stimulus artifacts are truncated. 'Stim' indicates time points of alveus stimulation. **(C)** Normalized and averaged EPSP peak amplitudes over the stimulus train. EPSP amplitude was measured as the peak voltage deflection (see blue arrows in **B**). **(D)** % Change of EPSP amplitude over the stimulus train. The mean amplitude of the last three EPSPs was compared to the amplitude of the first EPSP. Negative values indicate a decrease in EPSP amplitude, a positive value indicates facilitation. Boxplots in D show median, standard deviation, maximum and minimum. *** indicates $p < 0.001$ (Kruskal Wallis and Dunn's multiple comparison test).

The firing of CA1 pyramidal neurons is modulated by different oscillatory rhythms of the brain. During exploratory behavior and REM sleep, firing of pyramidal cells is phase locked to the theta rhythm, a field potential oscillation of 5-10 Hz (Ylinen et al., 1995; Csicsvari et al., 1999). To further explore the short-term properties of feed-back

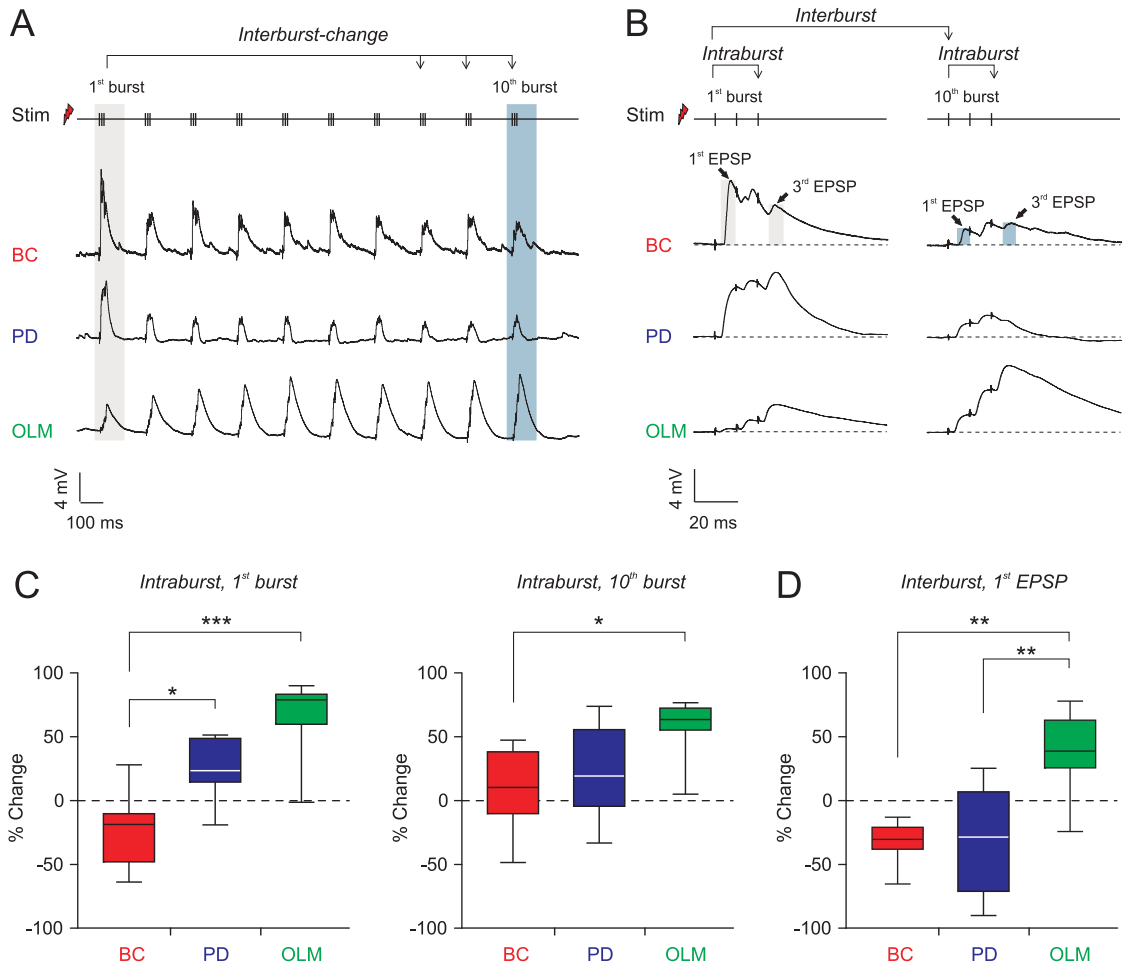

Figure 3.5: Spatio-temporal profile of theta patterned feed-back activation of CA1 interneurons. Recording configuration as in Fig. 3.4 A. **(A)** Representative whole-cell recordings of different interneuron subtypes during theta burst stimulation of pyramidal cell axons. Responses to the first and last burst in the train are enlarged in **(B). (C)** Comparison of the 1st and 3rd EPSP inside a burst (*intraburst change*, see panel **B**). Left panel: 1st burst, right panel: 10th burst. **(D)** Change in EPSP amplitude over the stimulus train (*interburst change*). The 1st EPSP inside the 1st burst was compared to the 1st EPSP of the last three bursts (see panel **A**). Boxplots in C and D show median, standard deviation, maximum and minimum. *, ** and *** indicate $p < 0.05$, 0.01 and 0.001, respectively.

interneurons in CA1, stimulation experiments were repeated with a theta burst protocol consisting of a high frequency component (three stimuli at 100 Hz) repeated ten times at a frequency of 5 Hz (see upper panel in **Fig. 3.5 A**). This protocol enabled me to look at both the dynamics during a short high frequency burst and during rhythmic ongoing activity. Therefore, the change in EPSP amplitude inside the bursts (*intraburst change*, see **Fig. 3.5 B**) as well as the change over the burst train (*interburst change*, **Fig. 3.5 A,B**) was analyzed. Within the first, burst EPSP amplitude in basket cells decreased on average -24.3 ± 8.4 % (n=10, 1st vs. 3rd EPSP) whereas PD and OLM cells received significantly different input with an increase in EPSP amplitude of 23.0 ± 7.1 (n=11) and

66.7 ± 10.4 % (n=8), respectively (**Fig. 3.5 C**, left panel, representative recordings in **A** and **B**. Kruskal-Wallis test, $p < 0.0001$; Dunn's multiple comparison test, $p < 0.001$ for BCs vs. OLM cells and $p < 0.05$ for BCs vs. PD cells). In contrast, EPSPs inside the 10^{th} burst of the train were facilitating in all three classes of interneurons, albeit with OLM cells showing a significantly stronger facilitation than basket cells (**Fig. 3.5 C,** right panel. Kruskal-Wallis test, $p < 0.014$; Dunn's multiple comparison test, $p < 0.05$ for BCs vs. OLM cells).

When now comparing the first EPSP inside the first burst relative to the first EPSP inside the last three bursts of the theta train (*interburst change*, **Fig. 3.5 D**, example recordings in **A** and **B**) basket and PD cells both showed strongly depressing EPSPs. OLM interneurons displayed the opposite behavior with a strong facilitation over the burst train, similar to the behavior during the 50 Hz stimulation. These experiments show that over a prolonged input period EPSP amplitude of both basket and PD cells decreases, thereby opposing input properties of OLM cells, whereas during short high frequency activity PD interneurons do facilitate as well.

3.1.3 Modulation of feed-back recruitment by disynaptic inhibition

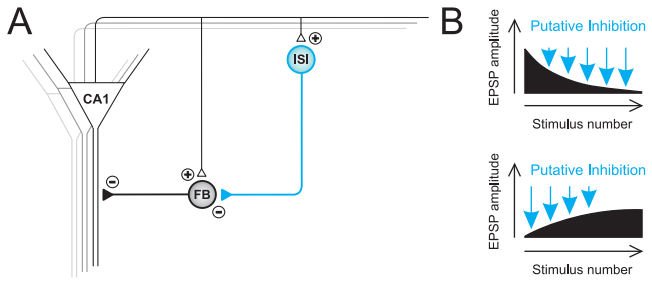

Figure 3.6: Putative disynaptic inhibition onto interneurons during CA1 pyramidal cell activity. (A) Schematic drawing of disynaptic inhibition. Both interneurons (FB, ISI) receive excitatory input of CA1 pyramidal cell axons. The feed-back interneuron (FB, black) projects to CA1 pyramidal cells, providing feed-back inhibition whereas the interneuron selective interneuron (ISI) innervates the feed-back interneuron. Therefore during alveus stimulation the FB interneuron receives both monosynaptic excitation from pyramidal cells as well as disynaptic inhibition from ISIs. **(B)** Depression in EPSP amplitude could be caused by an increase in inhibition over the train (upper panel), whereas facilitation could be emphasized by initially strong inhibition ceasing over the stimulus train (lower panel).

Cells with strongly depressing synapses are generally thought to have high release probability synapses, whereas OLM cells are described to have a low initial release probability that increases over the stimulus train (Zucker and Regehr, 2002; Sylwestrak and Ghosh, 2012). However, interneurons in CA1 receive also inhibitory input from other interneurons. Therefore, the temporal pattern of excitatory inputs might further be shaped by disynaptic inhibition that is recruited by CA1 pyramidal cells as well (Freund and Buzsaki, 1996, Pouille and Scanziani, 2004 see scheme in **Fig. 3.6 A**).

To investigate the role of disynaptic inhibition during feed-back activation, stimulation experiments were repeated in presence of the $GABA_A$ antagonist gabazine (SR 95531 hydrobromide, 10 µM, **Fig. 3.7** and **3.8** for 50 Hz and theta burst stimulation, respectively). During 50 Hz stimulation, neither the absolute EPSP amplitude (**Fig. 3.7 A-C**, middle panels, paired t-test, n=5, n=8 and n=7 for BCs **(A)**, PD **(B)** and OLM cells **(C)**, respectively) nor the dynamic over the stimulus train (**Fig. 3.7**, right panels, Wilcoxon signed-rank test. Example recordings in left panels) were significantly affected by gabazine in any of the interneuron subgroups. These data indicate that depression in BCs and PDs and facilitation in OLM interneurons is not caused by disynaptic inhibition. During theta patterned feed-back activation, absolute EPSP amplitudes were also not altered by application of gabazine (**Fig. 3.8 A-C**, left and middle panels, n=6, n=9 and n=7 for BC, PD and OLM cells respectively, paired t-test). As expected from this result, neither the interburst change over the stimulus train (**Fig. 3.8 A-C**, right panels, Wilcoxon signed-rank test) nor the intraburst change were significantly affected by gabazine.

3.1.4 Recruitment of interneurons in the epileptic hippocampus

The temporal pattern of interneuron firing is shaped by the synaptic input they receive. To check whether this input is changed in epilepsy, I repeated the stimulation experiments in slices of chronically epileptic rats (see Section 2.1 for details on the pilocarpine model of epilepsy; **Fig. 3.9**). During a 50 Hz stimulus train, behavior of both basket and PD cells was significantly altered. In contrast to the depressing synapses in control rats, short-term dynamics of both types of interneurons were shifted to a facilitating phenotype (**Fig. 3.9 A,B**, summary in **Fig. 3.9 D,** left and middle panel. Mann Whitney U-test, p=0.008, n(Sham)=9, n(Post SE)=12 and p=0.03, n(Sham)=12, n(Post SE)=7 for basket and PD cells, respectively). The behavior of OLM interneurons however, was unchanged (**Fig. 3.9 C,D**, right panel. Mann Whitney U-test, p=0.84, n(Sham)=12, n(Post SE)=13). Similarly, during theta patterned burst stimulation (**Fig. 3.10**) both PD and basket cells showed a significant shift to facilitating behavior over the whole stimulus train (*interburst change*, **Fig. 3.10 A,B**, summary in **D**, left and middle panel, Mann Whitney U-test, p=0.01, n(Sham)=10, n(Post SE)=12 and p=0.01, n(Sham)=11, n(Post SE)=7 for basket and PD cells, respectively). However, when looking at the dynamics within the first burst (*intraburst dynamic*s, **Fig. 3.10 E**, left and middle panel) only basket cell behavior was also shifted to facilitation. By contrast, PD cells in both control and Post SE animals showed an increase in amplitude from the first to the third EPSP (Mann Whitney U-test, p=0.002, n(Sham)=10, n(Post SE)=12 and p=0.59, n(Sham)=11, n(Post SE)=7 for basket and PD cells, respectively). Within the 10^{th} stimulus burst, both BC and PD cell dynamics were unchanged in epileptic animals (**Fig. 3.10 F**, left and middle panel, p=0.53 and p=0.65 for BC and PD). Again, behavior of OLM cells was unchanged both over the stimulus train as well as inside the first and last burst (**Fig. 3.10 C**

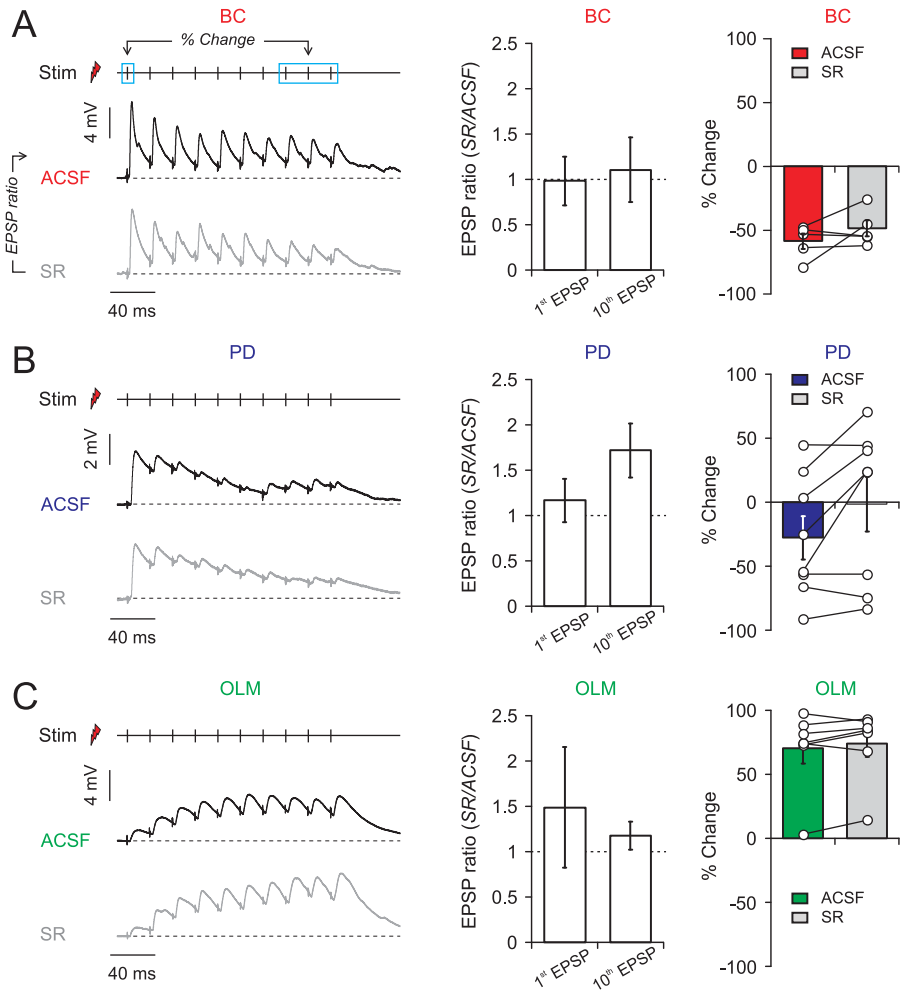

Figure 3.7: Short-term dynamics during 50 Hz alveus stimulation are not caused by polysynaptic inhibition. Left panels: Representative recordings of a basket cell **(A)**, a PD interneuron **(B)** and an OLM cell **(C)** before (ACSF, black trace) and after application of gabazine (SR, gray trace). Middle panels: Comparison of EPSP amplitude in ACSF and after washin (EPSP ratio, as indicated in **A**, left panel). 1st EPSP: p=0.94, p=0.92 and p=0.32; 10th EPSP: p=0.61, p=0.064 and p=0.36 for BC, PD and OLM cells, respectively (paired t-test). Right panel: % Change in EPSP amplitude from the 1st to the mean of the last three EPSPs. p=0.625, p=0.11 and p=0.30 for BC, PD and OLM cells respectively (Wilcoxon signed-rank test). Bargraphs show average ± SEM.

and **D-F**, right panels, n(Sham)=8, n(Post SE)=10 and p=0.26, 0.86 and 0.06 for **D-F,** respectively). These experiments show that in epilepsy excitatory inputs onto basket and PD interneurons are shifted to facilitation, whereas behavior of OLM interneurons remains unchanged.

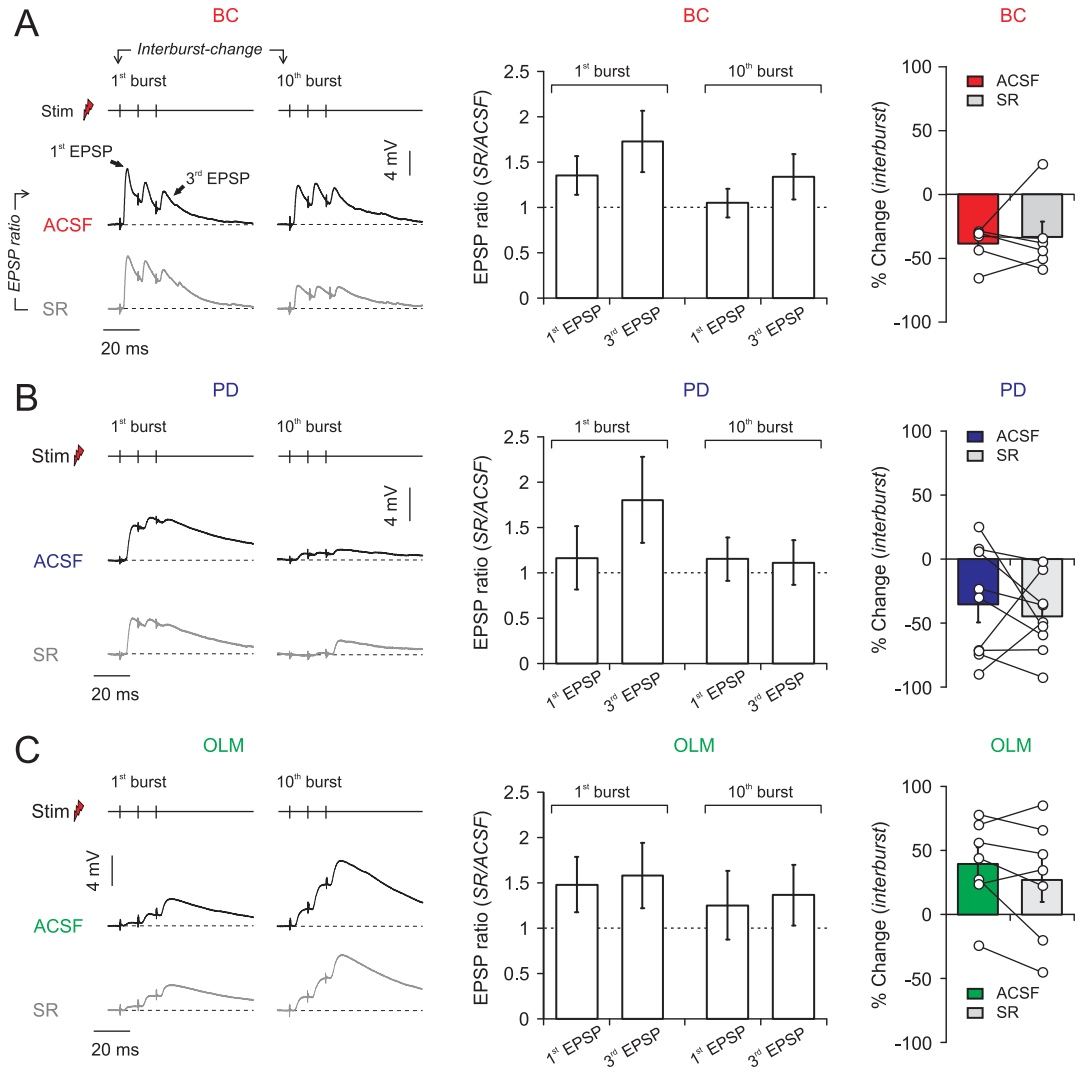

Figure 3.8: Impact of disynaptic inhibition on theta patterned feed-back activation. Left panels: Example recordings show the response to the 1st and 10th burst of the theta train before (ACSF, black trace) and after application of gabazine (SR, gray trace) of a Basket cell **(A)**, PD interneuron **(B)** and an OLM cell **(C)**. Middle panels: Comparison of EPSP amplitudes in ACSF and after washin inside the first and the last burst. Statistics: paired t-test. Right panels: % Change in EPSP amplitude from the 1st to the last three burst (Amplitude of the first EPSP inside the bursts was analyzed). Statistics: Wilcoxon signed-rank test. Bargraphs show average ± SEM.

3.1.5 Mechanisms underlying changes of feed-back recruitment in the epileptic hippocampus

a) Changes in disynaptic inhibition

The alterations in input dynamics of basket and proximal dendritic cells could be caused by an increase in initial disynaptic inhibition onto those cells (see **Fig. 3.6 B**). To test this hypothesis, I repeated the stimulation experiments in presence of gabazine for both 50 Hz and theta burst stimulation (**Fig. 3.11** and **3.12**). In basket cells, block of GABAergic

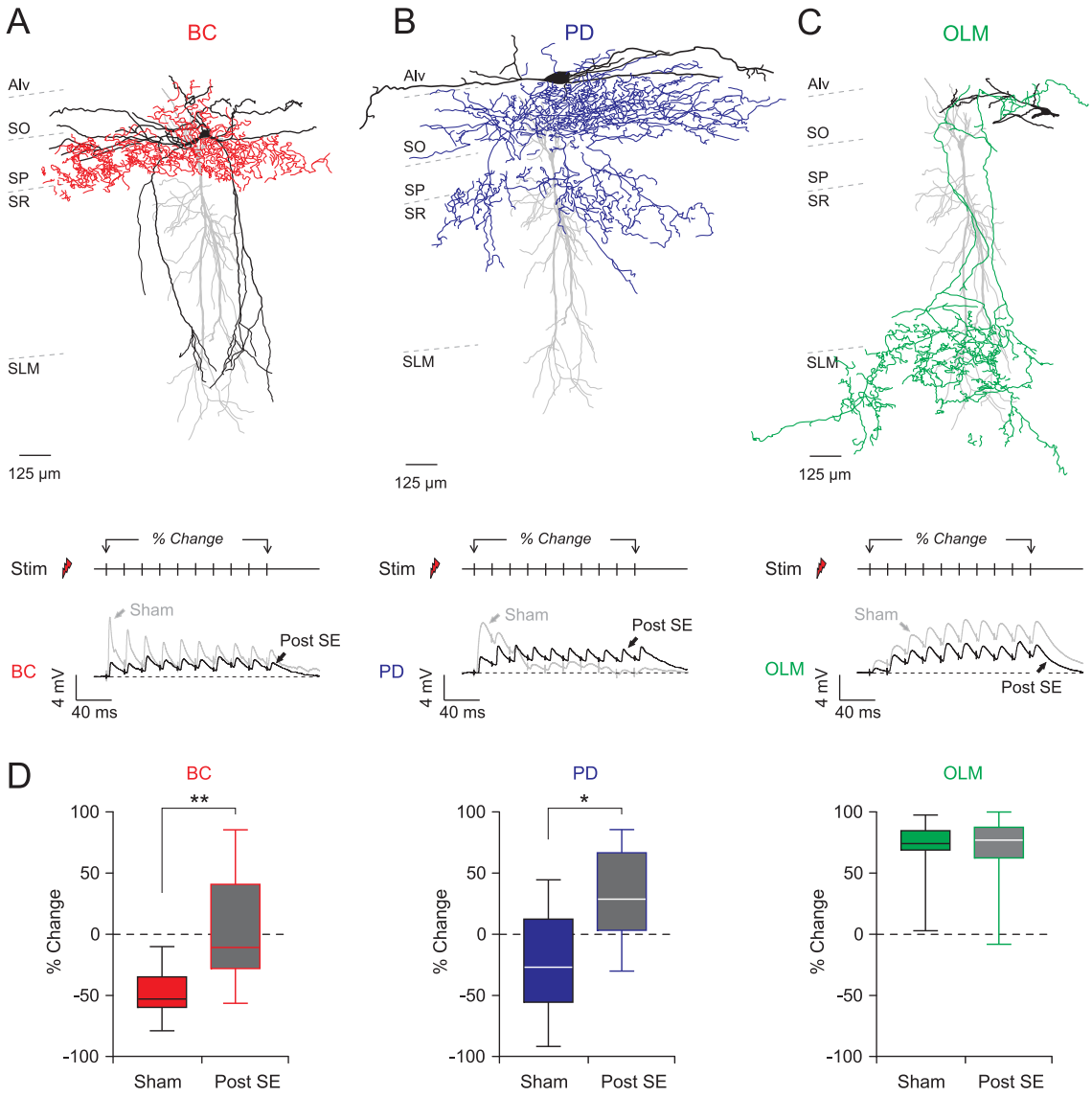

Figure 3.9: Epilepsy-associated changes in feed-back recruitment during a 50 Hz stimulus train. (A-C) Upper panels: Morphological reconstructions of a basket cell **(A)**, a PD interneuron **(B)** and and OLM cell **(C)** recorded in tissue from epileptic animals (Post SE). Lower panels: Response to a 50 Hz stimulus train (black trace) of the cells depicted above. For comparison, recordings conducted in sham-injected animals are indicated in gray. **(D)** Comparison of the % change in EPSP amplitude over the stimulus train between control and epileptic animals for basket (BC, left panel), proximal dendritic (PD, middle panel) and OLM cells (right panel). Control data are taken from Fig. 3.4. Boxplots show median, standard deviation, maximum and minimum. ** and * depict $p < 0.01$ and 0.05, respectively (Mann Whitney U-test).

inputs had no effect on the amplitude of the first EPSP during a 50 Hz stimulus train (**Fig. 3.11 A**, left and middle panel. Paired t-test, n=7, p=0.13). However, the response to the 10^{th} stimulus was significantly increased (1.9 ± 0.5 mV vs. 2.8 ± 0.5 mV in ACSF and gabazine, respectively; n=7, p=0.03, paired t-test), indicating that basket cells receive facilitating disynaptic inhibition during CA1 pyramidal cell activity. The increased

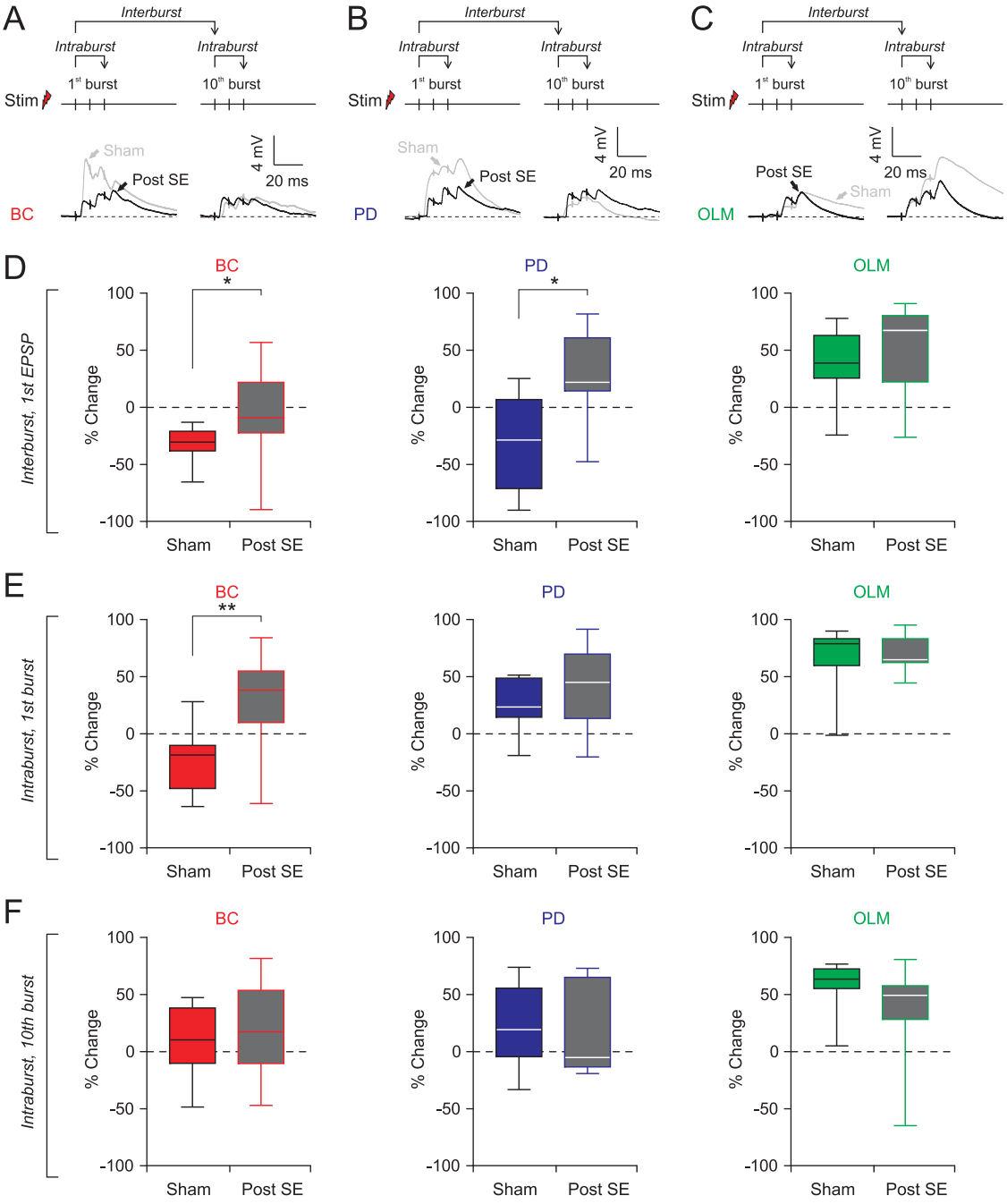

Figure 3.10: Epilepsy-associated changes in feed-back recruitment during theta patterned burst stimulation. **(A-C)** Example recordings of a basket cell **(A)**, a PD interneuron **(B)** and an OLM cell **(C)** during theta burst stimulation. Only responses to the first and the 10^{th} burst in the stimulus train are shown. For comparison the responses of control recordings in sham-injected animals are indicated in gray. **(D-F)** Comparison of short-term dynamics between control and epileptic animals. **(D)** For interburst comparison, the amplitude of the first EPSP inside the bursts was analyzed. Inside bursts **(E, F)**, EPSP amplitudes of the first and third EPSP were compared. Control data are taken from Fig. 3.5. Boxplots in D-F show median, standard deviation, maximum and minimum. ** and * depict $p < 0.01$ and 0.05, respectively (Mann Whitney U-test).

inhibition at the end of the 50 Hz train might restrict the observed shift of basket cells to facilitation of EPSPs. I therefore tested whether blocking GABAergic inhibition amplifies the facilitating phenotype observed in epilepsy. Application of gabazine however did not lead to a further increase of facilitation in basket cells (**Fig. 3.11 A**, right panel. Wilcoxon signed-rank test p=0.15, n=7).

In PD interneurons, the amplitude of the first EPSP largely increased upon application of gabazine, with an EPSP ratio of 3.7 ± 1.6 (1.03 ± 0.4 mV vs. 2.3 ± 0.6 mV in ACSF and gabazine, respectively, **Fig. 3.11 B**, left and middle panel, paired t-test, p=0.0062, n=5). In contrast, amplitude of the last EPSP was not changed. These data would suggest that the altered short-term plasticity in epileptic animals found in this cell class (compare **Fig. 3.9 D**, middle panel) is caused by an increased initial inhibition. However, short-term dynamics were not rescued by application of gabazine (**Fig. 3.11 B**, right panel, Wilcoxon signed-rank test, p=0.06, n=5). Consistent with the above results, interburst dynamics during theta patterned burst stimulation were also unaffected by application of gabazine in all three classes of interneurons (**Fig. 3.12** left and right panels, n=8, 6 and 12 and p=0.10, 0.84 and 0.11 for basket, PD and OLM cells respectively, Wilcoxon signed-rank test). In contrast to the 50 Hz stimulation, significant changes in the EPSP amplitudes were observed only in OLM cells (**Fig. 3.12 C**, middle panel, n=12, p=0.029, paired t-test).

These data show that inhibition of interneurons is increased in epileptic animals. However, they do not explain the changed short-term plasticity of excitatory inputs onto those interneurons. In basket cells, inhibitory inputs rather contradict the observed changes in short-term plasticity whereas in PD neurons and OLM cells dynamics of disynaptic inhibition is rather suited to even further emphasize facilitation at the pyramidal cell-to-interneuron synapse.

b) Changes in presynaptic release probability

Changes in the short-term plasticity of a synaptic connection can also be caused by pre- or postsynaptic alterations. One important characteristic of a synaptic connection is the basal probability of the presynapse to release neurotransmitter (Atwood and Karunanithi, 2002; Burnashev and Rozov, 2005). Synapses showing short-term depression often have a high initial probability of transmitter release. Upon single action potentials, their vesicles readily fuse with the membrane. During repetitive activity, however, this strong initial transmitter release causes a rapid depletion of the vesicle pool. Thus, the release probability decreases during the train. Conversely, facilitation can be caused by a low initial probability of transmitter release. In these synapse, a single action potential is unlikely to elicit transmitter release and vesicles are spared. However, during trains of action potentials, the accumulation of intracellular Ca^{2+} leads to an increase in release probability and consequently, facilitation. Therefore, one hypothesis explaining the observed changes

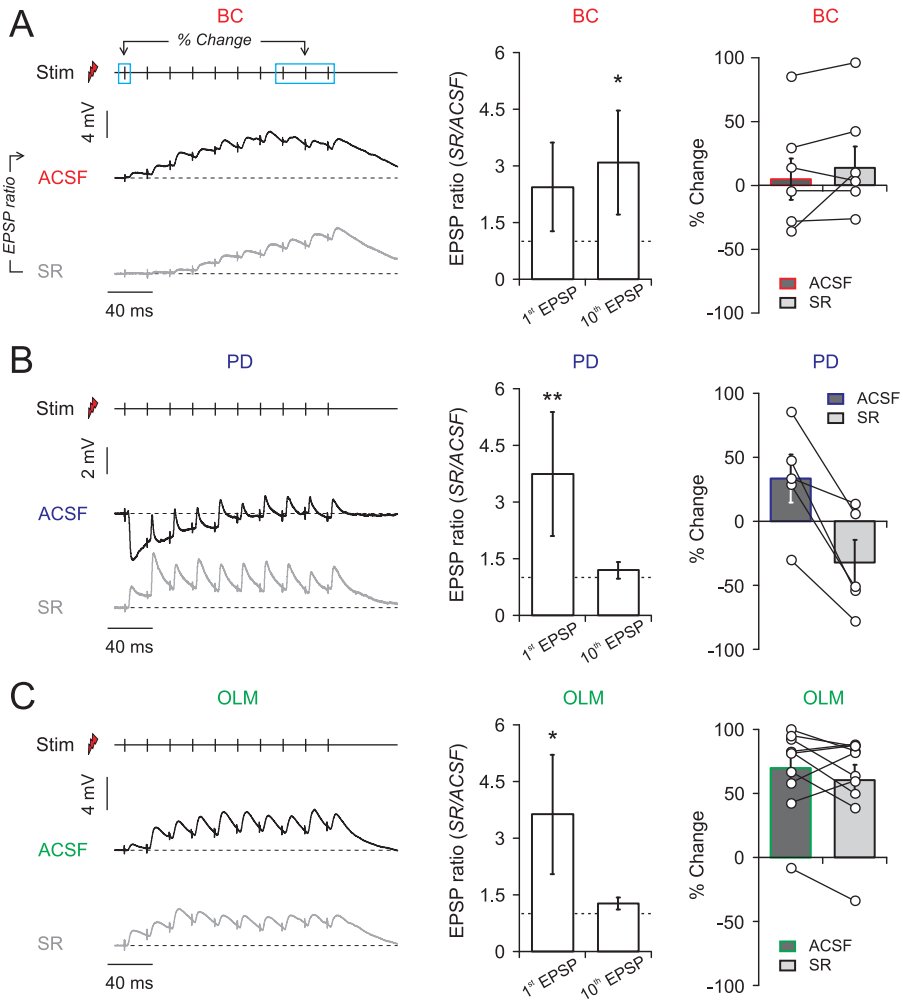

Figure 3.11: Impact of disynaptic inhibition on short-term dynamics in epileptic animals. Left panels: Representative recordings of a basket cell **(A)**, a PD interneuron **(B)** and an OLM cell **(C)** before (ACSF, black traces) and after application of gabazine (SR, gray traces). CA1 pyramidal cells were stimulated with a 50 Hz stimulus train of 10 stimuli. Middle panels: Comparison of EPSP amplitude in ACSF and after washin (EPSP ratio, as indicated in **A**, left panel). Right panels: % Change in EPSP amplitude from the 1st to the last three EPSPs (see blue boxes in **A**, left panel). Bargraphs show average ± SEM. * and ** indicate $p < 0.05$ and 0.01, respectively. Middle panels: Paired t-test, right panels: Wilcoxon signed-rank test.

in basket and proximal dendritic cells is a change in the basal release probability of those synapses.

One common indicator for a change in the presynaptic release probability is the paired pulse ratio (PPR). In this experimental approach, two consecutive stimuli are given in a short time interval and the amplitude ratio of the postsynaptic responses is calculated. An increase in amplitude from the first to the second pulse (PPR > 1) indicates a low release probability, whereas a decrease (PPR < 1) suggests a high release probability synapse. To test this hypothesis, I repeated the alveus stimulation experiments with two stimuli given

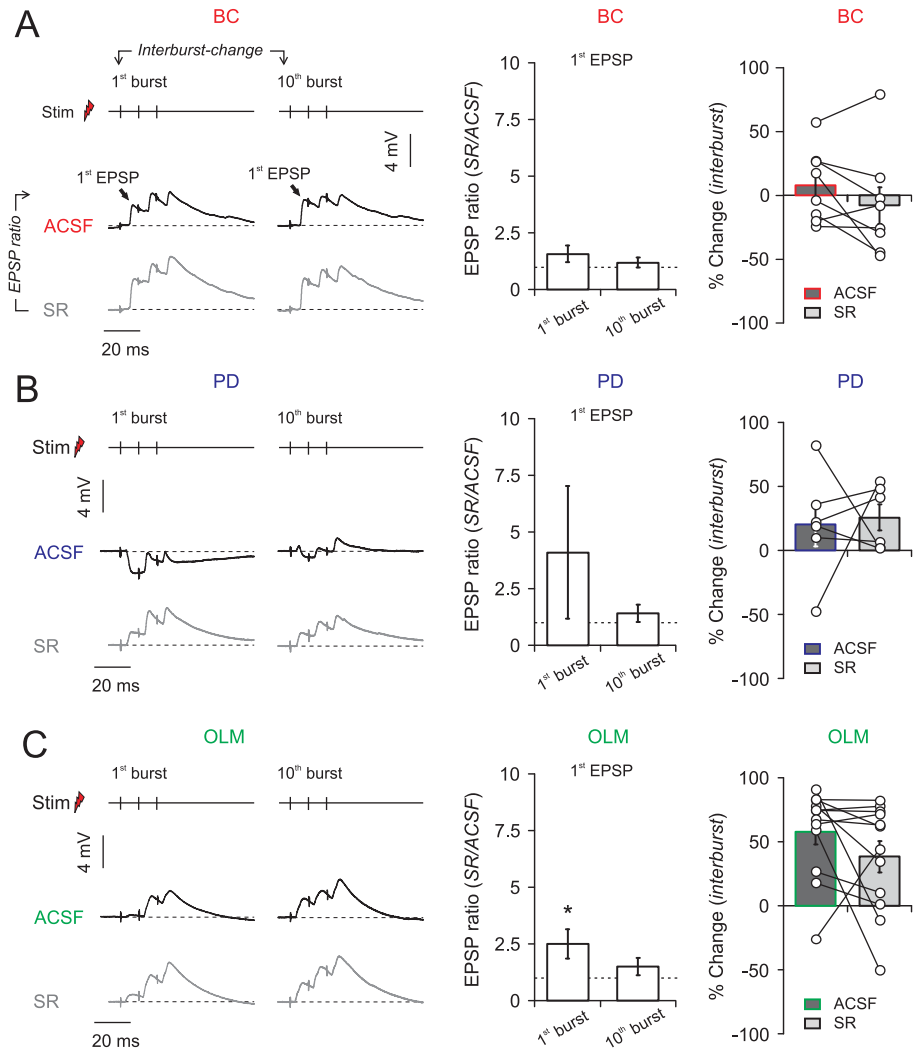

Figure 3.12: Impact of disynaptic inhibition in epileptic animals during theta patterned feedback stimulation. Left panels: Representative recordings of a basket cell **(A)**, a PD interneuron **(B)** and an OLM cell **(C)** before (ACSF, black traces) and after application of gabazine (SR, gray traces). Middle panels: Comparison of EPSP amplitude in ACSF and after washin (EPSP ratio, as indicated in **A**, left panel). EPSP amplitude of the first and third EPSP inside the first and 10$^{\text{th}}$ burst are analyzed. Right panels: Interburst change in EPSP amplitude from the 1$^{\text{st}}$ to the 10$^{\text{th}}$ burst. Bargraphs show average ± SEM. * indicates $p < 0.05$. Middle panels: Paired t-test, right panels: Wilcoxon signed-rank test.

at 50 Hz while recording EPSPs in morphologically identified interneurons. To isolate the monosynaptic excitatory component, experiments were conducted in presence of 10 µM gabazine. In this stimulus paradigm, the response to the individual pulses rather than the absolute voltage deflection is of interest. In these experiments I thus measured the relative EPSP amplitude of both peaks (see **Fig. 3.13 A**, left panel).

In basket cells of control animals, the relative EPSP amplitude decreased strongly from the first to the second pulse (**Fig. 3.13 A,** left and middle panel, n=9), with an average paired pulse ratio of 0.61 ± 0.07 (**Fig. 3.13 A,** right panel). In pilocarpine-

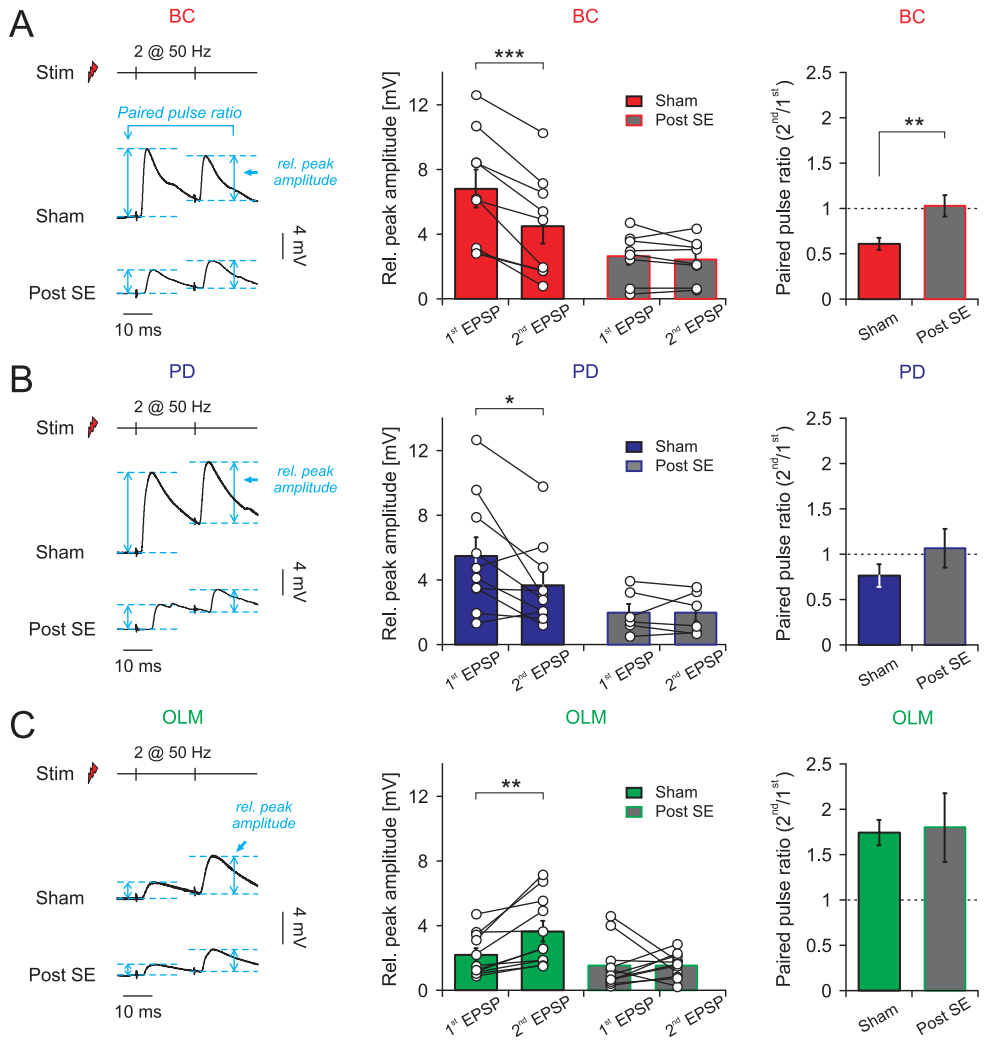

Figure 3.13: Alterations in the paired pulse ratio as possible mechanism of change. (A) Left panel: representative recordings of two basket cells recorded in a sham control (upper panel) and an epileptic animal (Post SE, lower panel). Middle panel: Relative peak amplitude was measured as indicated in left panel (dashed blue lines). Statistics: paired t-test. Right panel: Paired pulse ratio was calculated as indicated in left panel. Statistics: Mann Whitney U test. **(B,C)** Paired pulse analysis of proximal dendritic **(B)** and OLM interneurons **(C)**. Experiments were conducted in presence of gabazine. *, ** and *** indicate $p < 0.05$, $p < 0.01$ and $p < 0.001$, respectively. Bargraphs show average ± SEM.

treated animals, the relative peak amplitude did not differ significantly between the first and second pulse (**Fig.3.13 A,** left and middle panel, n=8). Correspondingly, the paired pulse ratio of 1.03 ± 0.12 was significantly different from control animals (**Fig. 3.13 A**, right panel). In PD cells, EPSP amplitude of control animals also decreased from the first to the second stimulus, with a paired pulse ratio of 0.76 ± 0.13 **(Fig. 3.13 B,** left and middle panel, n=10). However, in contrast to basket cells, the PPR in PD cells was not significantly changed in epileptic animals (**Fig. 3.13 B**, right panel, n=6). In control animals, OLM cells showed a significant increase in EPSP size from the first to the second

pulse (**Fig. 3.13 C**, left and middle panel, n=11). The resulting paired pulse ratio of 1.74 ± 0.14 was significantly different from basket and PD cells, as expected (Kruskal Wallis test, p=0.0001; Dunn's multiple comparison test, BC vs. PD: $p > 0.05$, BC vs. OLM: $p < 0.001$ and PD vs. OLM: $p < 0.01$), compare left bars in **Fig. 3.13 A, B** and **C**, right panels). In accordance with the absence of any change in short-term dynamics, the paired pulse ratio of OLM cells was not altered in epileptic animals (**Fig. 3.13 C**, right panels 1.8 ± 0.4, n=11).

3.1.6 Changes in intrinsic cell properties

The activity pattern of interneurons within a network will be determined by both their synaptic inputs and their intrinsic properties. To assess whether cell excitability is changed in chronic epilepsy, I injected long (1s) square pulses of current through the patch pipette and monitored the relation of current amplitude and firing frequency (**Fig. 3.14**). In both basket and OLM cells this input-output relation was shifted to higher current injection magnitudes in epileptic animals (**Fig. 3.14 A,C**. Summary in **D**, left and right panel). This shift was probably caused by the strongly reduced input resistance found in epileptic animals (**Fig. 3.14 E**, left and right panel. Basket cells: n=11 and n=6 for both sham and epileptic animals, p=0.04; OLM cells: n=12 and n=13 for sham and epileptic animals, $p < 0.0001$, Student's t-test). PD cells also showed a decrease in input resistance (**Fig. 3.14 E**, middle panel), however this did not lead to a shift in the input-output relation (**Fig. 3.14 D**, middle panel). In contrast, in pyramidal cells, the firing behavior at lower current injection magnitudes did not differ in epileptic animals. However the maximal average firing rate that could be elicited was significantly increased (**Fig. 3.15 A-C**). Additionally, the input resistance was also reduced in epileptic animals, albeit to lower degree than in interneurons (**Fig. 3.15 D**, n(post SE)= 14, p=0.04, Student's t-test). These results suggest that in epileptic animals pyramidal cells are able to fire at higher frequencies, whereas a reduced input resistance makes BC and PD cells less excitable.

When looking at action potential properties only minor changes were observed in epileptic animals (**Fig. 3.16**). Relative to control animals, OLM cells had a significantly increased action potential amplitude, whereas in PD cells action potential slope was increased. This was accompanied by a reduction in action potential half width (**Fig. 3.16 B-D**). In pyramidal cells only the action potential half width was reduced, whereas action potential properties in basket cells were unchanged.

3.1.7 Impact of changes on feed-back inhibition of pyramidal cells

The observed changes in synaptic and intrinsic properties of interneurons will influence feed-back inhibition onto CA1 pyramidal cells. I therefore conducted experiments to analyze whether feed-back inhibition is changed in epileptic animals. To characterize the

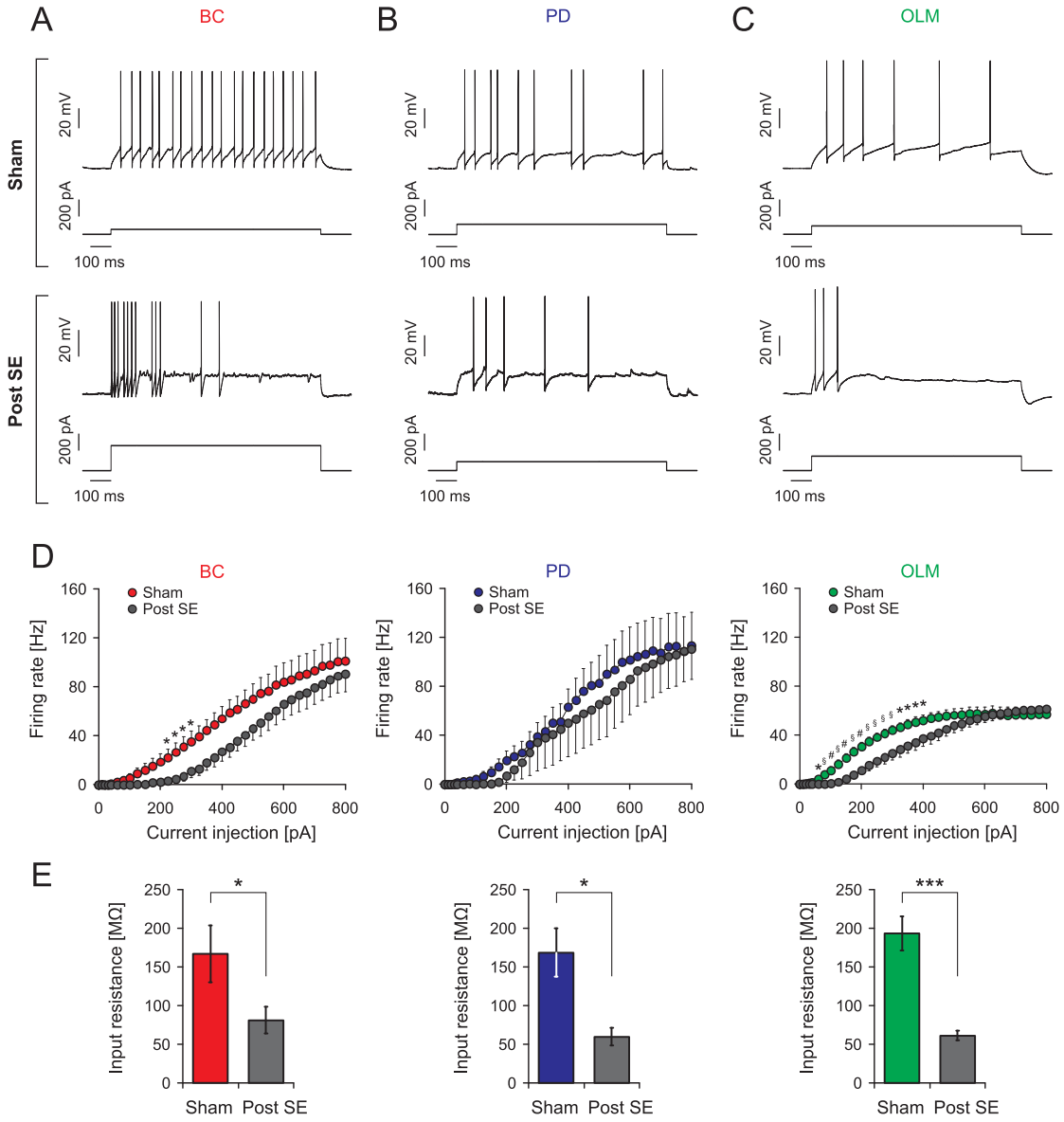

Figure 3.14: Excitability of interneurons in epileptic animals is decreased. **(A-C)** Example recordings of basket **(A)**, PD **(B)** and OLM interneurons **(C)** recorded in sham-injected (upper panels) and epileptic (Post SE, lower panels) animals during long, one second current injections. In all cases the current amplitude that elicited more than one action potential was displayed. **(D)** Input-output relation of basket (left), PD (middle) and OLM cells (right). Current injections had a duration of 1s and the average firing rate per current injection was calculated. *, § and # depict $p < 0.05$, 0.01 and 0.001, respectively. **(E)** Input resistance was estimated from voltage deflections induced by current injections ranging from -50 to +50 pA. Left: basket cells, middle: PD cells, right: OLM cells. Bargraphs show average ± SEM. * and *** indicate $p < 0.05$ and 0.001, respectively (Student's t-test).

inhibitory input pyramidal cells receive I started with recordings of isolated GABAergic currents (IPSCs) in pyramidal cells, while activating the feed-back microcircuit with a stimulus electrode in the alveus (**Fig. 3.17** and **3.18**).

During 50 Hz stimulation, the amplitude of IPSCs in control animals decreased strongly

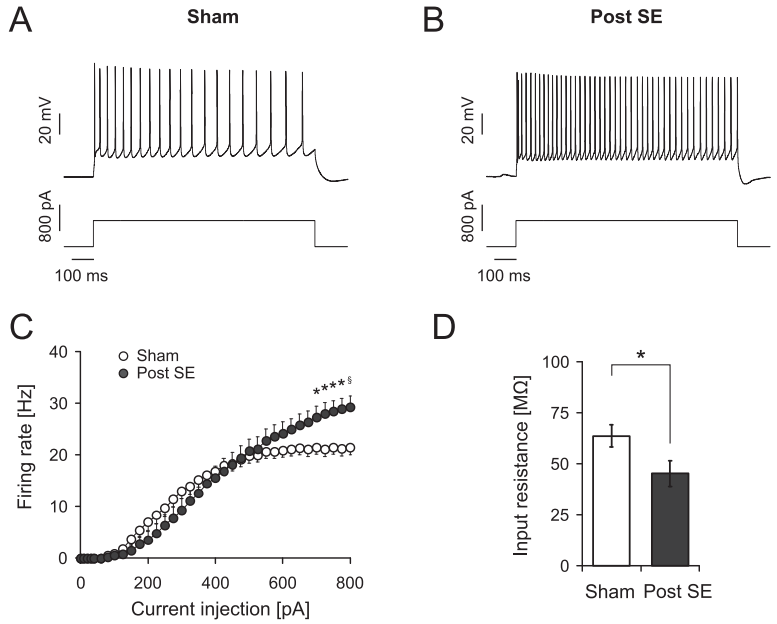

Figure 3.15: In experimental epilepsy, the potential maximal firing rate of pyramidal cells is increased. (A,B) Representative recordings of pyramidal cells recorded in a sham-injected **(A)** and an epileptic **(B)** animal during a one second current injection of 800 pA. **(C)** Corresponding input-output relation of the average firing rate during the 1 s current injection vs. the magnitude of the current injection. **(D)** Input resistance was estimated as in Fig. 3.14 E. Bargraphs show average ± SEM. * and § depict p < 0.05 and 0.01, respectively (Student's t-test).

from the first to the 10^{th} stimulus, with an average decrease of -77.75 ± 1.67% (**Fig. 3.17 A**, and **C**, open bar, n=25). In pilocarpine-treated animals, the depression in amplitude was significantly diminished (average decrease: -44.9±7.6 % , n=15, **Fig. 3.17 B**, and **C**, gray bar. Mann Whitney U test, p=0.0002). The paired pulse experiments suggest that in epileptic animals the release probability of synapses onto basket cells is reduced. Hence, they should be recruited less efficiently at the beginning of a stimulus train (see Section 3.1.5). If this hypothesis holds true, than also the absolute amplitude of the IPSCs at the beginning of a stimulus train should also reduced. To examine this, IPSC amplitudes of the first and 10^{th} IPSC were compared between control and epileptic rats **(Fig. 3.17 D)**. In control animals, the first IPSC had an average amplitude of 197.47 ± 23.73 pA (**Fig. 3.17 D**) whereas in epileptic animals, IPSC amplitude was significantly reduced (85.04 ± 17.12 pA, Student's t-test, p=0.0018). In contrast, amplitude of the 10^{th} IPSC was not significantly changed in epileptic animals (p=0.67).

To further assess whether the changes above lead to an overall reduction in inhibitory input, the charge transfer over the whole stimulus train was analyzed (**Fig. 3.17 E**), revealing a significant reduction in epileptic animals (11.4 nA*ms compared to 7.3 nA*ms for control and epileptic animals, respectively. Student's t-test, p=0.04).

During theta patterned feed-back stimulation, the differences in interburst dynam-

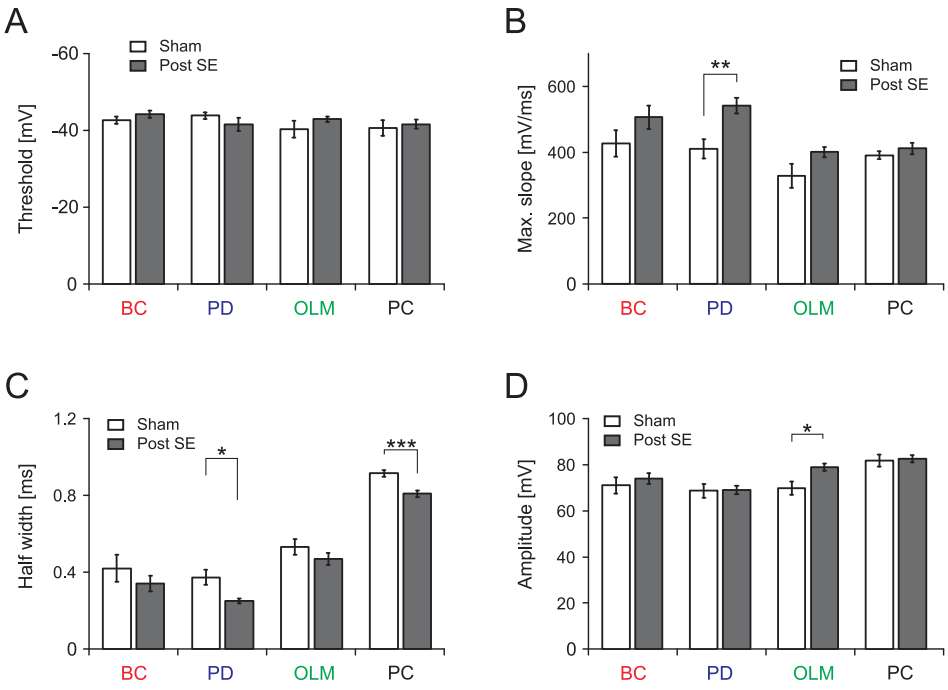

Figure 3.16: Changes of action potential properties in epileptic animals. For measurement of action potential (AP) threshold **(A)**, maximal slope **(B)**, half width **(C)** and AP amplitude **(D)** current injections inducing two APs inside the first 50 ms were selected and the first AP analyzed. Bargraphs show average ± SEM. *, ** and *** depict $p < 0.05$, 0.01 and 0.001, respectively (Tukey's post-hoc test). BC: Basket cells, PD: PD cells, OLM: OLM cells, PC: Pyramidal cells.

ics between control and epileptic animals were even more pronounced than during 50 Hz stimulation (**Fig. 3.18 C**, example recordings in panel **A** and **B**). Under control conditions, IPSC amplitude decreased -51.44 ± 3.80 % from the first to the 10th burst (**Fig. 3.18 A**,**C**, n=9). In epileptic animals, this interburst depression was strongly reduced, with an average reduction of only -10.56 ± 11.49 % (**Fig. 3.18 B,C**, n=9. Mann Whitney U test, p=0.004).

When looking at the intraburst dynamics (**Fig. 3.18 D**), in all cases IPSC amplitude decreased from the first the third stimulus with only dynamics inside the first burst being significantly changed under epileptic conditions (left panel: first burst, p=0.02; right panel: 10th burst, p=0.44, Mann Whitney U-test). This shift, however, was less pronounced than during the interburst dynamics. When comparing the absolute IPSC amplitudes in control and epileptic animals, the first IPSC inside the first burst decreased from 93.76 ± 11.49 pA to 44.37 ± 6.7 pA **(Fig. 3.18 E,** Student's t-test, p=0.0019). In contrast, the first IPSC inside the 10th burst was not significantly different from control animals (p=0.39, Student's t-test). In this stimulus protocol, the charge transfer during the first and the 10th stimulus burst were analyzed separately. In accordance to the alteration seen in the absolute IPSC amplitude, only the charge transfer inside the first burst was significantly reduced in epileptic animals, while the charge transfer inside the last burst remained

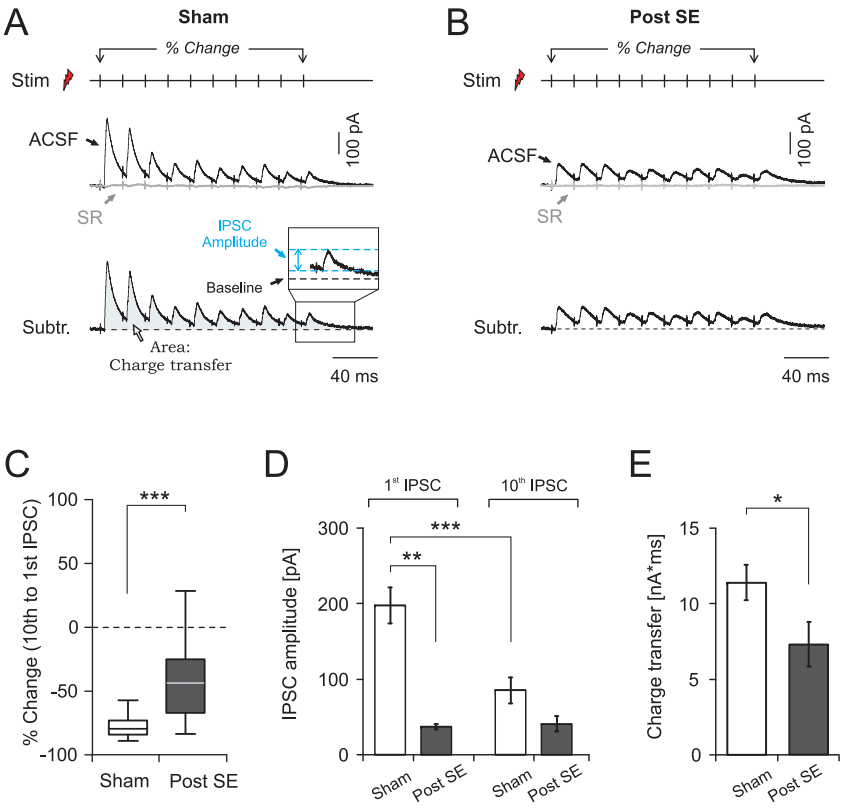

Figure 3.17: Changes in inhibitory input onto CA1 pyramidal cells in epileptic animals. **(A)** Upper traces: representative recordings of feed-back IPSCs in a sham-injected animal before (ACSF) and after application of gabazine (SR). Lower trace: the gabazine sensitive component was isolated by subtraction. Feed-back IPSCs were elicited with alveus stimulation and PSCs recorded in pyramidal cells clamped at -65 mV. **(B)** Representative recordings in an epileptic animal. **(C)** % Change in IPSC amplitude from the first to the 10^{th} stimulus. IPSC amplitude was measured as indicated in A (see dashed blue lines). **(D)** Comparison of absolute IPSC amplitude between control and epileptic animals. **(E)** The charge transfer was calculated over the whole stimulus train, as indicated in A. Boxplots in C show median, standard deviation, maximum and minimum; bargraphs in D and E show average ± SEM. *, ** and *** indicate p <0.05, 0.01 and 0.001, respectively.

unchanged. These data further suggest that during repetitive activity initial feed-back inhibition is reduced in epileptic animals.

The recorded IPSCs mainly reflect the inhibitory input pyramidal cells receive, while the actual inhibitory effect of this input can better be estimated by means of the deflection in the membrane potential. To further evaluate feed-back inhibition in epileptic animals, I therefore repeated the stimulation experiments while recording postsynaptic inhibitory potentials (IPSPs) in pyramidal cells (**Fig. 3.19**). In control animals, IPSP dynamics during 50 Hz stimulation mirrored behavior of inhibitory currents with large amplitude IPSPs at the beginning of a stimulus train, that decreased strongly upon repetitive stimulation (Average change: -57.5 ± 3.6 %, **Fig. 3.19 A**, upper panel, **B**. n=20). In epileptic animals the IPSP amplitude decreased on average -34.0 ± 9.5 % (**Fig. 3.19 A**, lower panel, **B**. n=21). This reduction in IPSP depression however was not significantly different from

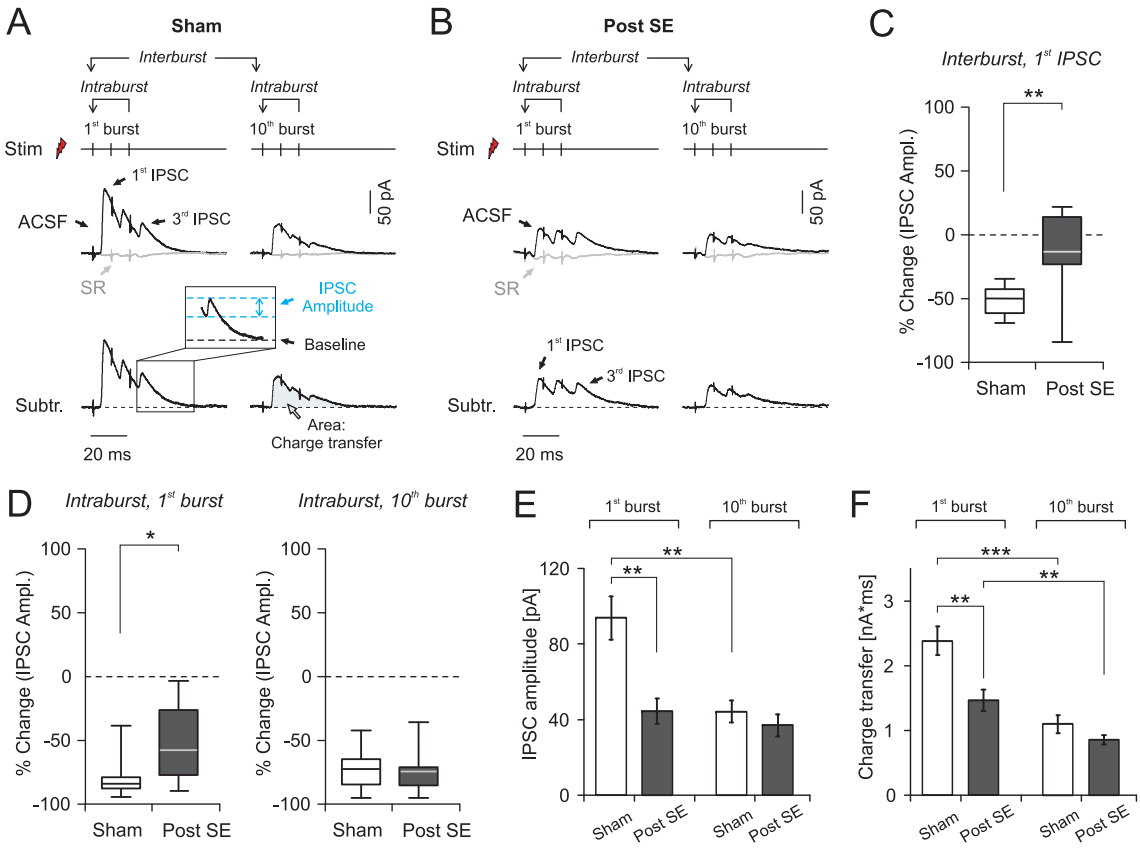

Figure 3.18: Changes in inhibitory input during theta patterned feed-back activity. (A) Upper traces: representative recordings of feed-back IPSCs in a sham-injected animal before (ACSF) and after application of gabazine (SR). Lower trace: the gabazine sensitive component was isolated by subtraction. Stimulation was carried out analogous to Fig. 3.17 and only the response to the first and the 10^{th} burst are shown. **(B)** Representative recordings in an epileptic animal, analogous to A. **(C)** % Change in IPSC amplitude over the burst train. The first IPSC of the first burst was compared to the first IPSC of the last three bursts. IPSC amplitudes were measured as indicated in A (see dashed blue lines). **(D)** Intraburst dynamics inside the first (left panel) and the last burst (right panel). In both cases the first IPSC was compared to the third. **(E)** Comparison of the absolute IPSC amplitude between control and epileptic animals. Only the first IPSC inside the first and 10^{th} bursts was analyzed. **(E)** The charge transfer during the first and the last burst were analyzed separately. Boxplots in C and D show median, standard deviation, maximum and minimum; bargraphs in E and F show average ± SEM.*, ** and *** indicate p < 0.05, 0.01 and 0.001, respectively.

control data (**Fig. 3.19 B**, Mann Whitney U test, p=0.07).

During theta patterned feed-back stimulation, initial stimulation elicited large IPSP bursts that decreased strongly over the train with an average change in IPSP amplitude of -54.9 ± 3.7 (**Fig. 3.20 A,C**, open bar, n=22). In epileptic animals, the first stimulus in the train elicited only small IPSPs that changed only little over the stimulus train (average decrease: -16.0 ± 10.4 %, n=21, **Fig. 3.20 A,C**, filled bar). This shift in interburst dynamics was highly significant from control data (p=0.0001, Mann Whitney U-test). In contrast, the dynamics inside the bursts were not changed in epileptic animals. In both groups, IPSP amplitude increased from the first to the third EPSP, in both, the

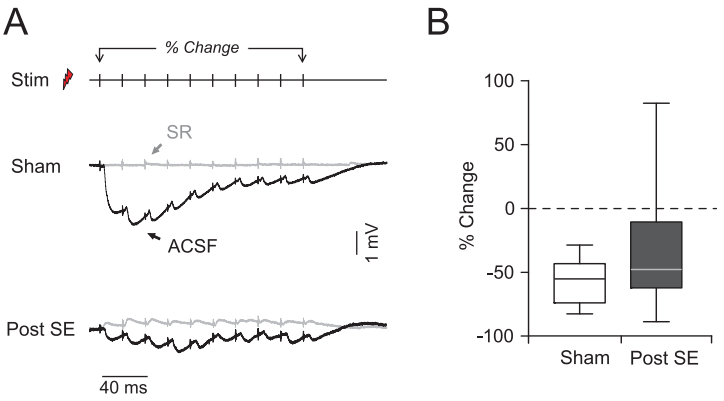

Figure 3.19: IPSP dynamics during 50 Hz stimulation are not changed in epileptic animals. **(A)** Upper traces: representative recordings of feed-back IPSPs in a sham-injected animal before (ACSF, black trace) and after application of gabazine (SR, gray trace). Lower traces: Corresponding recordings in an epileptic animal. **(B)** % Change in IPSP amplitude from the first to the 10^{th} stimulus. IPSP amplitude was measured as peak voltage deflection relative to baseline. Boxplots show median, standard deviation, maximum and minimum.

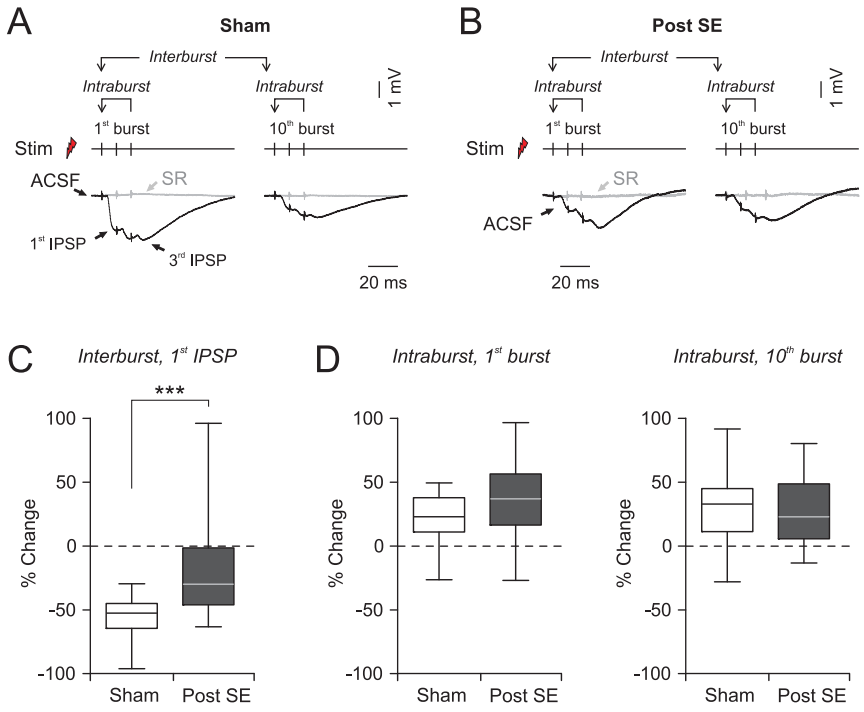

Figure 3.20: Changes in IPSP dynamics during theta burst stimulation mirror changes observed in inhibitory currents. **(A)** Example recordings in a control animal before (ACSF, black trace) and after application of gabazine (SR, gray trace). Only responses to the first (left) and 10^{th} burst (right) are shown. **(B)** Corresponding recordings in an epileptic animal. **(C)** Interburst change from the first IPSP in the first burst relative to the first IPSP in the last three bursts. **(D)** IPSP dynamics inside the first (left panel) and the last burst (right panel). The third intraburst IPSP was compared to the first. IPSP amplitudes were measured as peak voltage deflection relative to baseline. Boxplots show median, standard deviation, maximum and minimum. *** depicts $p < 0.001$ (Mann Whitney U-test).

first and the 10^{th} burst.

Changes in the absolute amplitude of IPSCs and IPSPs are also influenced by additional factors, such as the number of stimulated axons or changes in intrinsic cell properties. Hence, they are difficult to interpret. However, both IPSC and IPSP data taken together suggest that in addition to changes in short term dynamics, the initial inhibition is reduced in epileptic animals.

3.2 Anticonvulsant drug action on inhibitory microcircuits

In the second part of this thesis, I analyzed the effects of the sodium channel blocking anticonvulsant drugs on the different components of CA1 inhibitory microcircuits. Initially, AED effects were tested in healthy control animals.

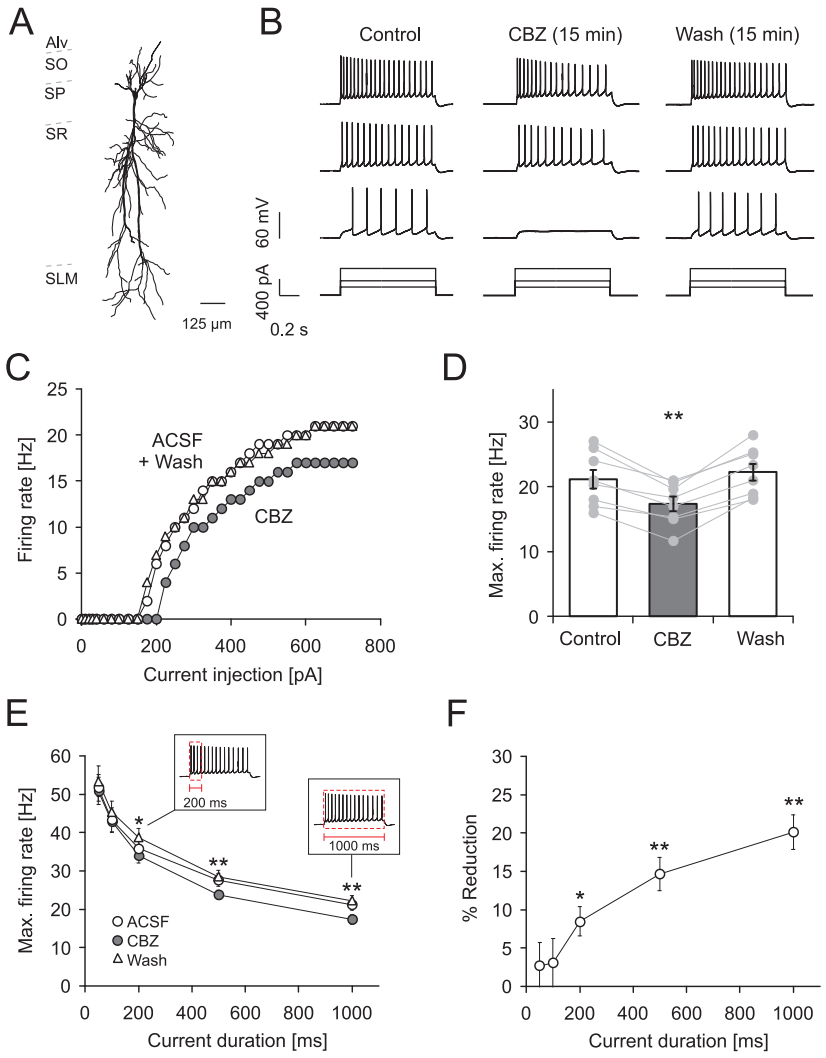

Figure 3.21: Carbamazepine effects on firing properties of principal neurons. (A) Morphological reconstruction of a representative pyramidal neuron. **(B)** Effects of 30 µM CBZ on intrinsic firing induced by current injection (lowermost traces 225, 400 and 700 pA, 1000 ms) in the cell shown in panel A. **(C)** Corresponding input-output relation of the average firing rate during the 1 s current injection vs. the magnitude of the current injection. **(D)** Effects of CBZ on the maximal discharge frequency measured during the 1s current injection. Bargraphs show average ± SEM (** denotes $p < 0.01$). **(E)** CBZ effects on the maximal firing rate measured during the first 50, 100, 200, 500 and 1000 ms of current duration (see insets. * $p < 0.05$, ** $p < 0.01$, Wilcoxon signed-rank test). **(F)** Percent reduction in firing frequency by CBZ within the different time intervals shown in E.

3.2.1 CBZ effects on CA1 pyramidal neurons in control animals

One important unit within the CA1 micronetwork are the excitatory pyramidal neurons, as they are both, source of input and primary target of local interneurons. Additionally, the sensitivity of hippocampal pyramidal cells to carbamazepine and other sodium channel blockers is one important feature of their anticonvulsant drug action. Therefore, drug effects on CA1 pyramidal cells can serve as reference frame to evaluate CBZ action on GABAergic interneurons. First, the impact of CBZ (30 µM) on CA1 pyramidal cell firing was tested with long, one second current injections of different magnitude (**Fig. 3.21 A-C**). This approach ensured that CBZ effects on pyramidal cells were analyzed isolated from any network effect. Additionally, the long current injections mimic periods of strong depolarizations and firing that occur during seizure activity. To analyze CBZ effects, the current injection magnitude inducing the maximal firing rate under control condition was selected. CBZ effects on the firing rate were analyzed during the same current injection magnitude (see **Fig. 3.21 C**). CBZ reliably reduced the maximal firing rate on average by 20.1 ± 2.3 % (**Fig. 3.21**, n=9, p=0.008, Wilcoxon signed-rank test, **Fig. 3.21 D**).

To further assess how the reduction of firing rates develops over the action potential train, the maximal firing rates obtained for different time intervals from onset of the current injection (**Fig. 3.21 E**) were examined, and the % reduction in firing rate for these time intervals (**Fig. 3.21 F**) calculated. This analysis shows that, in a concentration of 30 µM, CBZ reduces firing significantly after a current duration of $\geq$ 200 ms (see asterisks in **Fig. 3.21 E, F**, Wilcoxon signed-rank test).

To complement the results based on current injections, I additionally analyzed the sensitivity of CA1 pyramidal cell firing to CBZ when driven by synaptic inputs. Therefore, I activated CA1 pyramidal neurons synaptically with electrical stimulation of Schaffer collaterals while recording the elicited action potentials in the cell-attached configuration (25 stimuli at 50 Hz, **Fig. 3.22 A,B**). Since CA3 neurons are highly interconnected, stimulation of Schaffer collaterals might induce network events. Therefore, recurrent activity was prevented with a cut between CA1 and CA3. As for somatic current injections, a significant block by CBZ was observed only late in the stimulus train after a period of 400 ms (**Fig. 3.22 C,D**, n=9, asterisks indicate significant differences, Wilcoxon signed-rank test, p=0.004 for both the 400 and 500 ms time interval).

Previous studies suggest, that CBZ might have additional effects on glutamate release (Hood et al., 1983; Sitges et al., 2007). Although these results are controversial (Olpe et al., 1985), I excluded that effects on synaptically induced firing were due to direct effects on excitatory transmission driving the action potentials. I repeated the stimulation protocol used in the previous experiment and recorded Schaffer collateral EPSCs in CA1 pyramidal cells in the whole-cell configuration. Under these conditions, no CBZ effects on EPSCs were observed (**Fig. 3.23**, n=5, Wilcoxon signed rank test).

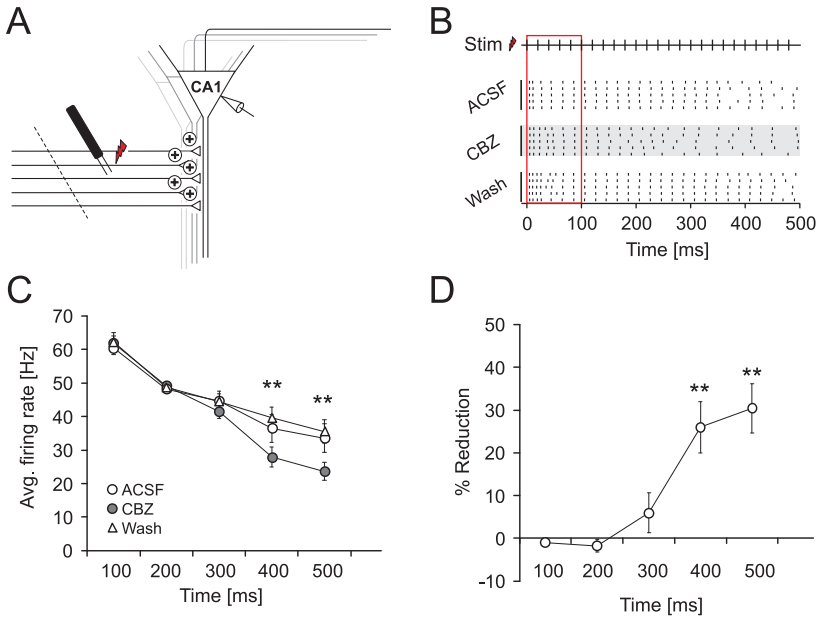

Figure 3.22: Carbamazepine effects on synaptically induced firing of principal neurons. (A) Recording configuration to examine CBZ effects on synaptically induced firing. Schaffer collaterals were stimulated with a bipolar steel electrode placed in the radiatum while firing was monitored with cell-attached recordings. To prevent recurrent excitation a cut was made between CA1 and CA3. **(B)** Raster plot of action potential firing during a 50 Hz stimulus train of 500 ms duration. All three conditions (control, application and washout) were conducted in the presence of the $GABA_A$ blocker gabazine (10 µM). **(C, D)** CBZ effects on the average firing frequency during consecutive 100 ms intervals **(C)** and the corresponding magnitude of reduction in synaptically driven firing frequency in % **(D)**.

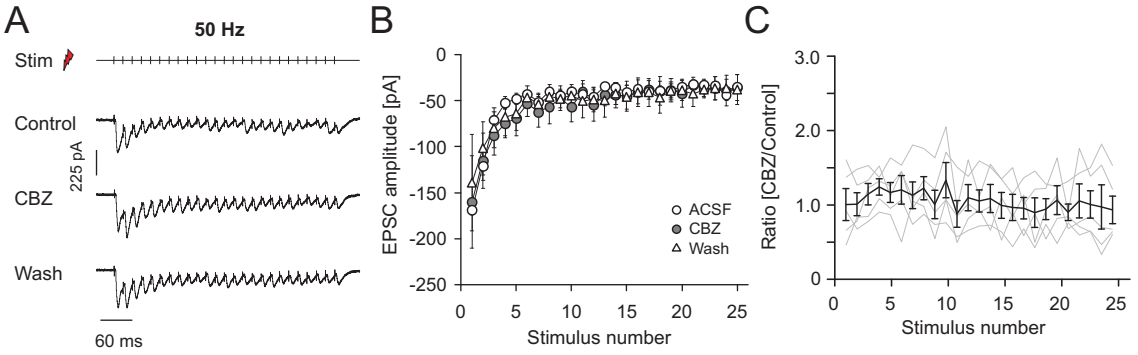

Figure 3.23: Effects of CBZ on Schaffer collateral EPSCs. (A-C) Effects of CBZ on Schaffer collateral EPSCs (25 stimuli @ 50 Hz) recorded in the presence of 10 µM gabazine. Stimulation was carried out as in Fig. 3.22 A and EPSCs were recorded in the whole-cell configuration. **(A)** Representative recordings under control conditions (upper trace), in 30 µM CBZ (middle trace) and after washout (lower trace). Traces show averages from 10 consecutive sweeps and stimulus artifacts were truncated. **(B)** Quantification of peak EPSC amplitude showed no effect of CBZ on excitatory Schaffer collateral inputs. **(C)** Peak EPSCs after CBZ application normalized to the mean of control and washout. Gray traces correspond to individual cells, black trace shows average ± SEM.

3.2.2 CBZ effect on CA1 interneurons

Next, I investigated CBZ effects on the firing behavior of basket cells, proximal dendritic interneurons and OLM interneurons. During long 1s current injections, firing of all three categories was significantly reduced, albeit to a different degree. The maximal average firing rate of perisomatically targeting basket cells and distal dendritic targeting OLM interneurons was reduced by 23.6 ± 7.6 % and 27.2 ± 6.7 %, respectively (**Fig. 3.24 A-B**. Left panel: BCs, n=7, p=0.015. Right panel: OLM cells, n=7, p=0.015, Wilcoxon signed-rank test). In contrast, firing of PD interneurons was strongly affected (reduction of maximal average firing rate by 55.2 ± 7.6 %, n=7, p=0.015, Wilcoxon signed-rank test, **Fig. 3.24 A-B**, middle panel). When comparing the effects of CBZ between pyramidal neurons and the different interneuron types, a stronger inhibition of proximal dendritic cells vs. all other cell types was observed (ANOVA ($F(3,25)=6.543$, $p=0.002$, post-hoc Tukey test: $p=0.008$, $p=0.022$ and $p=0.002$ vs. basket cells, OLM cells and pyramidal neurons, respectively; **Fig. 3.25**).

Following this, I examined how the CBZ effects on interneuron subtypes evolve with increasing current injection duration (**Fig. 3.24 C,D**). Similar to pyramidal cells, all interneuron subtypes showed an increase in blocking effects with increasing current durations. In all three subtypes, significant effects of CBZ were observed for current injection durations $\geq$ 200 ms (**Fig. 3.24 C,D**, asterisks indicate $p<0.05$, Wilcoxon signed rank tests). Additionally, I examined the effects of CBZ on further passive and active cell properties in all four neuron types (see summary of results in **Table 3.1** and **Table 3.2**). There were significant effects of CBZ on action potential properties of pyramidal neurons, basket cells and OLM cells. However, in interneurons these effects were invariably quite small (~10%).

As a next step within this microcircuit I examined how CBZ affects interneuron firing when induced by synaptic activation. I therefore stimulated CA1 pyramidal cell axons with a stimulation electrode placed into the alveus (see Section 2.6 for stimulation configuration). Firing of different interneuron subtypes was monitored with cell-attached recordings (see **Fig. 3.26 A** for representative cell-attached recordings). Following these recordings, cells were repatched in the whole-cell patch-clamp configuration, to allow for biocytin filling and post hoc morphological identification. Due to the synaptic delay, spike latency of synaptically elicited firing in interneurons was significantly larger than that of antidromically elicited spikes recorded in CA1 pyramidal cells (see insets in **Fig. 3.26 A**, **Fig. 3.26 B**, n=6, 5, 5, and 4 for pyramidal neurons, BCs, PD cells and OLM cells respectively).

During stimulation trains of 10 stimuli at 50 Hz, OLM interneurons showed a progressive increase in discharge probability during the trains, whereas basket- and PD cells displayed a high initial firing probability that decreased sharply after the first 50 ms of the stimulus train (**Fig. 3.26 C**, upper panels show representative raster plots from individual

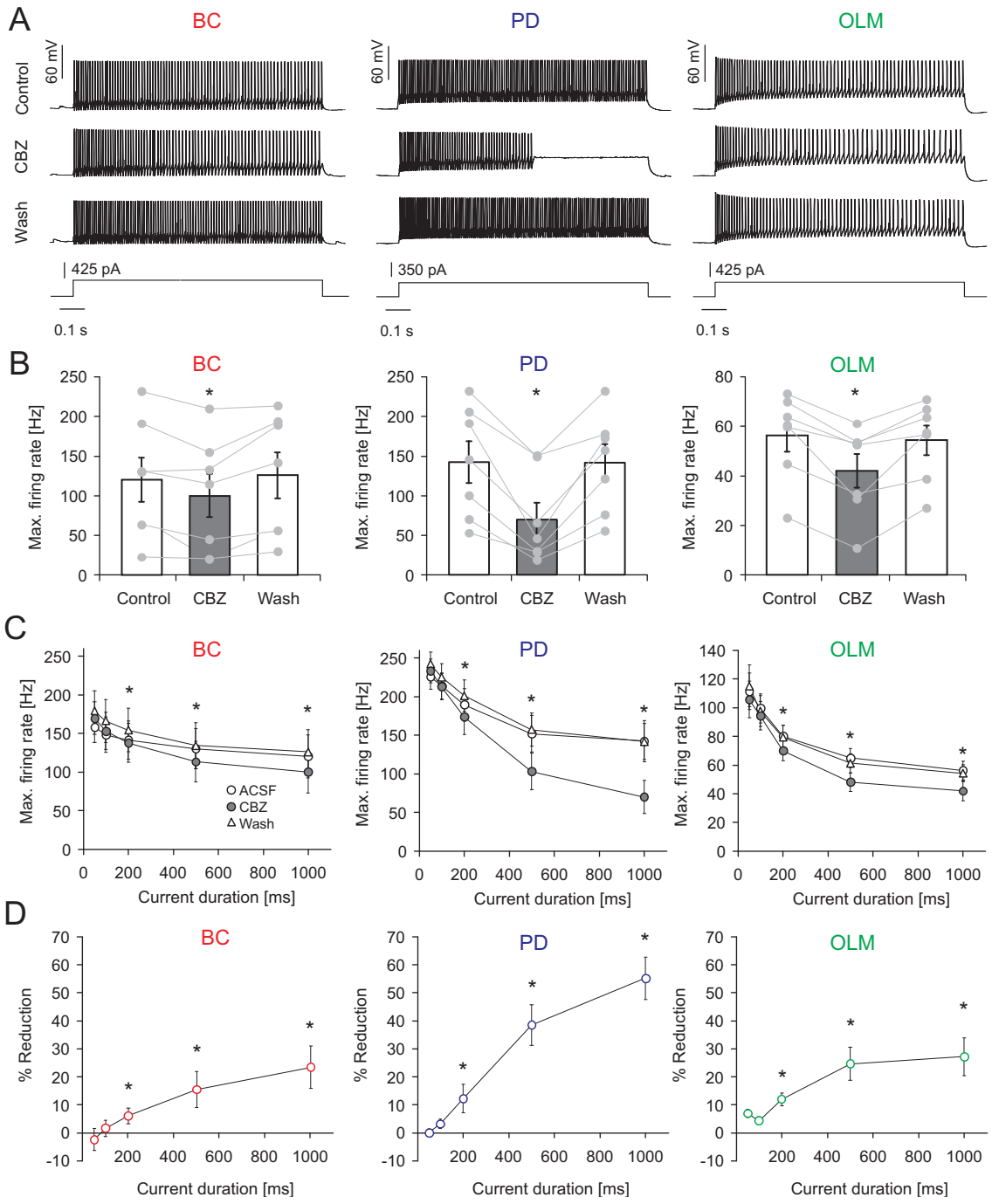

Figure 3.24: Carbamazepine effects on intrinsic firing properties of different types of GABAergic interneurons. **(A)** Effects of 30 µM CBZ on intrinsic firing induced by current injections in a representative basket cell (BC, left panel), a PD cell (middle panel) and an OLM interneuron (right panel). **(B)** Summarized CBZ effect on maximal firing rates of basket cells (BC, left panel), proximal dendritic targeting cells (PD, middle panel) and distal dendritic interneurons (OLM, right panel, * denotes $p < 0.05$) during 1s current injections. **(C)** CBZ effects for different current injection durations measured from the onset of the current injection. **(D)** % reduction in the maximal firing rate for the different time intervals from panel C.

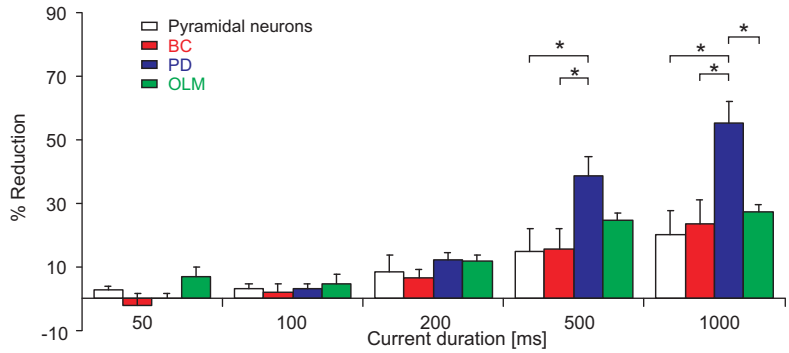

Figure 3.25: Comparison of CBZ effects on interneurons and pyramidal cells during different current durations. At the longest current injection durations (500 and 1000 ms), PD interneurons are affected significantly more compared to other types of neurons. * denotes $p < 0.05$, ANOVA with post-hoc Tukey test.

	Mean ACSF/Wash		CBZ		
	Mean ± SEM		Mean ± SEM		p
Pyramidal neurons					
R_{in} (MΩ)	70.37	4.93	64.70	5.65	0.195
τ (ms)	27.08	1.89	24.485	1.94	0.156
C (nF)	0.38	0.02	0.384	0.03	0.938
Basket cells					
R_{in} (MΩ)	180.46	51.60	185.87	49.13	0.688
τ (ms)	14.59	2.66	13.95	2.52	0.297
C (nF)	0.10	0.02	0.09	0.01	0.078
PD cells					
R_{in} (MΩ)	161.85	31.47	166.89	33.64	0.469
τ (ms)	14.46	2.43	14.11	1.55	0.938
C (nF)	0.10	0.01	0.10	0.02	1.063
OLM cells					
R_{in} (MΩ)	217.21	31.30	194.75	32.39	0.297
τ (ms)	31.84	4.40	27.45	4.03	* 0.031
C (nF)	0.17	0.01	0.16	0.01	0.688

Table 3.1: Effects of CBZ on passive cell properties of different neuronal cell types. Input resistance was calculated from small voltage deflections induced by current injections ranging from -50 to +50 pA with a linear fit. τ was estimated using negative current injections and a standard exponential fit. Cell capacity was calculated from R_{in} and τ. Statistically significant p-values are indicated with asterisks (Wilcoxon signed rank test).

neurons, lower panels show the firing probability during the stimulation train). This temporal pattern of synaptically induced firing can be explained by the different short-term dynamics of excitatory inputs onto interneuron subtypes that were investigated in the first part of this thesis (see Section **3.1.2**): In OLM cells feed-back EPSPs show a pronounced frequency-dependent facilitation, whereas this input to basket- and PD neurons shows a strong depression.

Surprisingly, CBZ failed to affect synaptically driven firing in any of the interneuron subtypes during a 200 ms stimulus train (**Fig. 3.26 C**, n=7, 7 and 6 for BCs, PD cells and OLM cells), even though firing elicited with prolonged current injections was affected

	First AP (0-50 ms), % Control			Late AP (300-500 ms), % Control		
	Mean ± SEM		p	Mean ± SEM		p
Pyramidal neurons						
AP Threshold (mV)	97.72	0.71	0.023 *	84.22	3.93	0.008 **
Max. slope (mV/ms)	96.66	2.94	0.250	72.94	4.68	0.008 **
AP Half width (ms)	99.80	1.20	0.843	106.47	2.17	0.039 *
AP Amplitude (mV)	97.28	1.50	0.078	86.14	3.60	0.008 **
fAHP (mV)	92.60	9.50	0.148	136.42	12.97	0.008 **
Basket cells						
AP Threshold (mV)	98.60	1.06	0.156	95.80	2.13	0.109
Max. slope (mV/ms)	87.13	4.59	0.047 *	86.06	5.91	0.071
AP Half width (ms)	106.17	2.08	0.031 *	105.83	2.47	0.047 *
AP Amplitude (mV)	90.94	3.70	0.047 *	91.07	4.71	0.109
fAHP (mV)	98.27	2.81	0.688	100.03	2.51	0.938
PD cells						
AP Threshold (mV)	98.46	2.08	0.813	90.76	2.23	0.031 *
Max. slope (mV/ms)	101.16	5.98	0.900	87.94	2.76	0.063
AP Half width (ms)	100.14	2.36	0.430	99.88	1.59	0.844
AP Amplitude (mV)	98.11	4.31	0.570	88.98	2.44	0.031 *
fAHP (mV)	101.90	2.75	0.810	110.88	2.64	0.031 *
OLM cells						
AP Threshold (mV)	91.68	5.30	0.046 *	89.36	2.20	0.016 *
Max. slope (mV/ms)	89.24	7.45	0.219	87.62	7.68	0.109
AP Half width (ms)	103.09	3.66	0.469	105.32	4.58	0.469
AP Amplitude (mV)	92.89	5.31	0.219	91.66	4.67	0.109
fAHP (mV)	109.19	5.69	0.219	107.16	2.51	0.015 *

Table 3.2: Effects of CBZ on active properties of different neuronal cell types. For analysis, both, APs at the beginning of the current injection (0-50 ms after onset of the current injection, left column) as well as later in the action potential train (300-500 ms following onset of the current injection, right column) were selected (see Methods for details). Values for fast afterhyperpolarizations (fAHP) are given relative to action potential threshold. Statistically significant p-values are indicated with asterisks (Wilcoxon signed rank test).

in all three classes of interneurons (compare **Fig. 3.24 C,D**). Likewise, CBZ also failed to affect synaptically driven firing during 100 Hz stimulation trains, mimicking high-frequency activation typically present during physiological ripples and epileptogenic high-frequency oscillations (Bragin et al. 1999; Ibarz et al. 2010, **Fig. 3.26 D**, n-numbers as for the 50 Hz stimulation). This was most likely due to the strong depression of afferent synapses that caused PD interneurons as well as basket cells to fire only briefly at the onset of a stimulus train (total number of action potentials per train: BCs: 3.4 ± 0.5 for 50 Hz and 1.7 ± 0.3 for 100 Hz stimulation frequencies, PDs: 3.6 ± 0.4 for 50 Hz and 1.3 ± 0.1 for 100 Hz stimulation frequencies; see insets in **Fig. 3.26 D** left and middle panel). The period of rapid firing is therefore probably to short for the development of a use-dependent block. Indeed, when examining firing within the first 50 or 100 ms after onset of current injection, the discharge frequency of none of the interneuron types was altered by CBZ (see **Fig. 3.24 C,D**). Thus, even in PD interneurons that are in principle very sensitive to CBZ, a use-dependent Na^+ channel block cannot develop, due to the strongly depressing nature of interneuron firing when synaptically recruited.

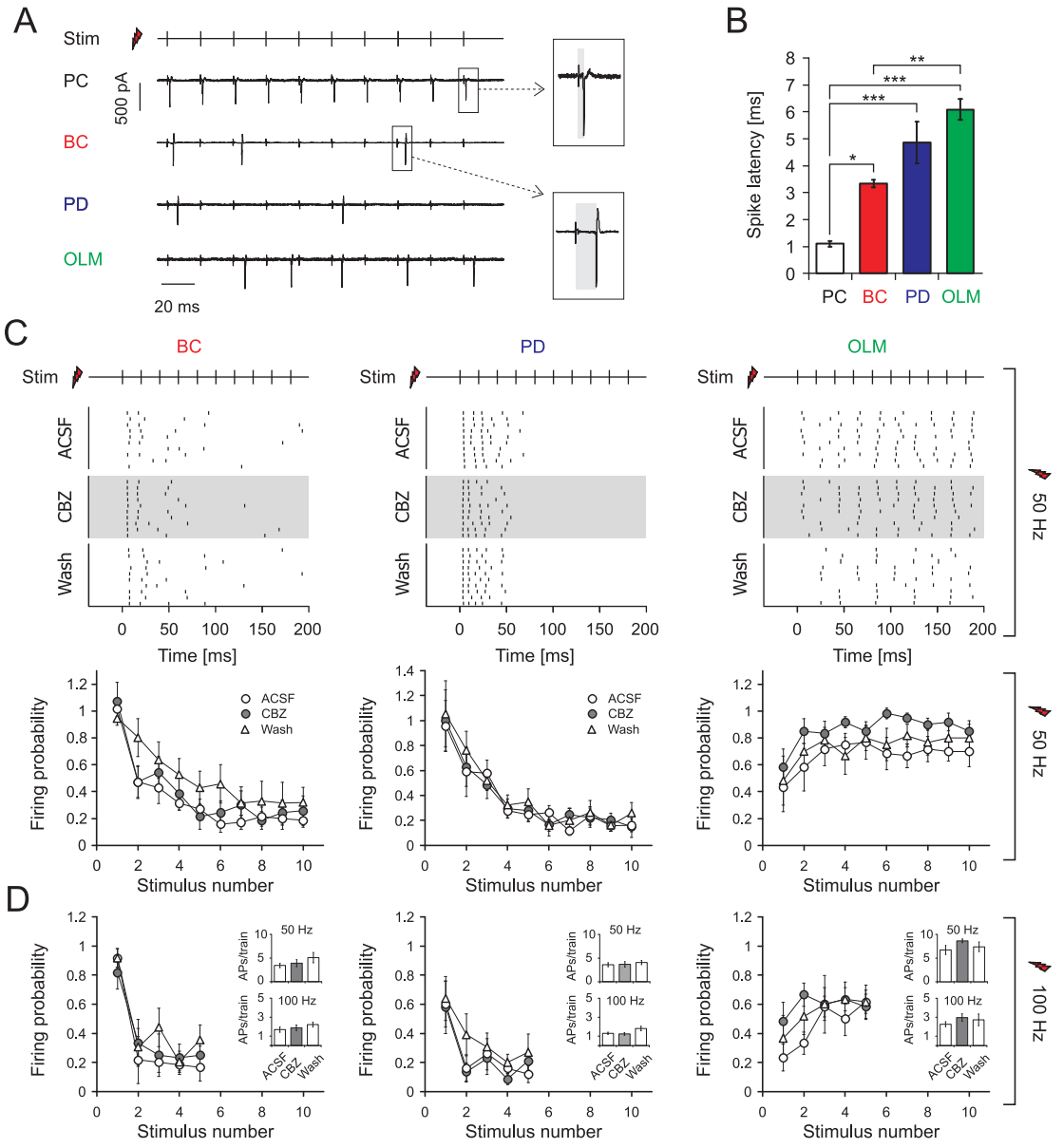

Figure 3.26: Carbamazepine effects on synaptically induced firing of interneurons. **(A)** Cell attached recordings of a pyramidal cell (PC), a basket cell (BC), a bistratified cell (PD) and an OLM interneuron. Stimulation was conducted as in Fig. 3.4 A. **(B)** The latency of antidromic spikes in PCs is significantly shorter than those observed in interneurons as estimated with an ANOVA and a subsequent Tukey's post-hoc test. *, ** and *** indicate $p < 0.05$, 0.01 or 0.001, respectively. **(C)** Synaptically induced firing of interneurons is not affected by CBZ during a 200 ms stimulus train at 50 Hz (Upper panels: Raster plots of action potential firing, 50 Hz stimulus train, lower panels: Average firing probability during trains of 10 stimuli @ 50 Hz). **(D)** Synaptically induced firing of interneurons by stimulation trains composed of 5 stimuli @ 100 Hz. Insets depict the total number of action potentials induced during stimulus trains.

In contrast, OLM cells are reliably recruited during synaptic stimulation trains (**Fig. 3.26A** and **Fig. 3.26 C,D**, rightmost panels) and are able to follow synaptic stimulation over a longer period of time. Nevertheless, this did not translate into a reduction of

synaptically driven firing during 50 or 100 Hz stimulation trains (**Fig. 3.26 C,D** rightmost panels) although in somatic current injections a duration of 200 ms was sufficient to reveal a reduction in firing rate. Because OLM cells faithfully follow synaptic stimulation over a longer period (unlike basket or PD cells), I also tested longer trains of synaptic stimulation to exclude that effects might materialize only during prolonged recruitment (as seen for pyramidal cells, compare **Fig. 3.22 C** and **D**). During these experiments, stimulus strength was set to elicit the maximal number of action potentials over the train. Indeed, when maximal stimulation was carried out with 25 stimuli at 50 Hz firing rate of OLM cells decreased only little over the stimulus train (**Fig. 3.27 A,B**, n=7). Nevertheless, the firing frequency over the stimulus train was largely unaffected by CBZ (**Fig. 3.27 A-C**, Wilcoxon signed-rank test, n=7) with an average reduction in APs per train of 9.78 ± 5.8% (see inset in **Fig. 3.27 B**, Wilcoxon signed-rank test, p=0.03).

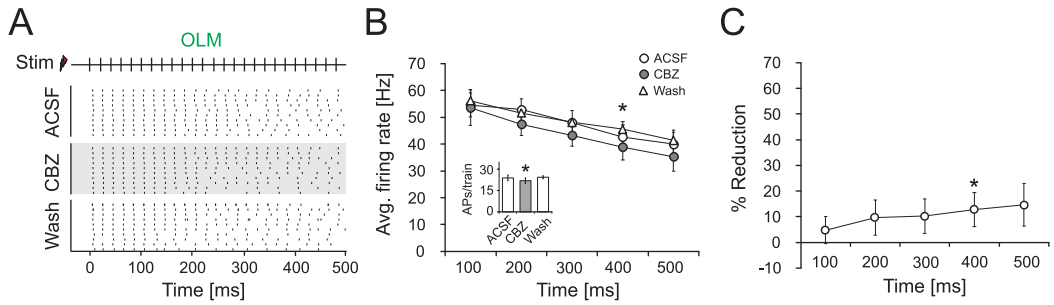

Figure 3.27: Carbamazepine effects on OLM interneuron firing during prolonged synaptic activation. (A) Raster plots of synaptically induced firing of OLM cells with longer stimulation trains of 500 ms at 50 Hz under control conditions, during application of CBZ and after washout. Stimulus strength was adjusted to elicit the maximal number of action potentials over the train. **(B)** Average firing frequency binned over 100 ms periods of stimulation. Inset shows effects on the number of action potentials over the whole stimulus train. **(C)** Percent reduction of firing for the different time intervals. These experiments reveal a minor effect on synaptically driven OLM cell firing (* indicates $p < 0.05$).

The interpretation of drug effects in the alveus stimulation experiments relies on the assumption that the CA1 pyramidal cell recruitment is not affected by the presence of CBZ. I examined CBZ effects on antidromic firing of pyramidal cells during alveus stimulation using cell-attached recordings (**Fig. 3.28**, see panel **A** for recording configuration). To exclude modulation of pyramidal cell firing by feed-back inhibition via CA1 interneurons, experiments were conducted in presence of gabazine (10 µM). Antidromically activated cells were identified based on the spike latency (Compare **Fig. 3.26 A,B**. Average latency: 1.1 ± 0.1 ms, n=5). The firing of pyramidal cells was not affected by CBZ during 500 ms stimulation trains at 50 Hz (**Fig. 3.28 B-D**, n=5), suggesting that CBZ effects on inhibitory micronetworks are not contaminated by changes in CA1 pyramidal cell recruitment.

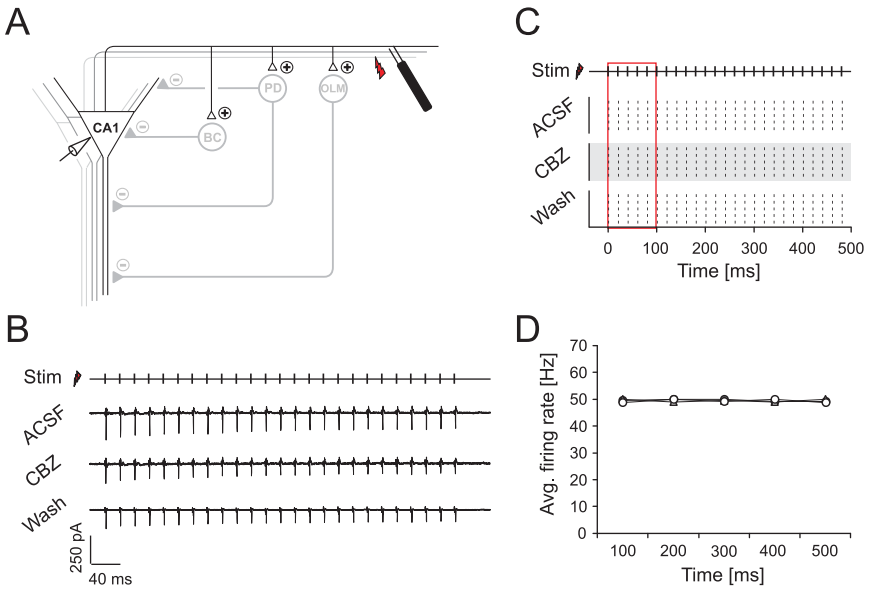

Figure 3.28: Firing of CA1 neurons during alveus stimulation is undisturbed by CBZ. (A) Stimulation of CA1 pyramidal cell axons was carried out in the presence of 10 µM gabazine and antidromically elicited action potentials were recorded in the cell attached configuration. **(B-C)** Representative recording **(B)** and corresponding raster plots **(C)** of antidromic spikes in a CA1 pyramidal cell (25 stimuli @ 50 Hz). **(D)** Average firing frequency during direct stimulation of pyramidal cell axons remains unaffected by CBZ.

3.2.3 Impact of CBZ on feed-back inhibition of pyramidal cells

The interneurons I focused on in this study represent only part of all interneuron subgroups that are present within CA1. However, CA1 pyramidal neurons are the main target of the local inhibitory interneurons. Hence, inhibition impinging on CA1 pyramidal neurons will reflect the summed activity of CA1 interneurons. Any potential effects of CBZ on interneuron firing would therefore manifest in a changed inhibition of principle cells. As a next step in this microcircuit I therefore studied whether feed-back inhibition recorded in CA1 pyramidal cells is altered by CBZ. For this, I stimulated the alveus with 50 or 100 Hz stimulation trains, causing synaptic activation of feed-back microcircuits (see **Fig. 3.29 A** for recording configuration). The stimulation induced pyramidal cell IPSCs were then isolated by subtraction of traces obtained in the presence of gabazine (10 µM, **Fig. 3.29 B,C**). There was no significant effect of CBZ (30 µM) on the peak amplitude of consecutive IPSCs over the stimulus train at either 50 (n=6, **Fig. 3.29 B**) or 100 Hz stimulation frequencies (n=7, **Fig. 3.29 C**, summary in **Fig. 3.29 D**). Similarly, the charge transfer over the stimulus train was not affected (Data not shown; n=6, p=0.156 and n=7 p=0.821 for 50 and 100 Hz respectively, Wilcoxon signed-rank test).

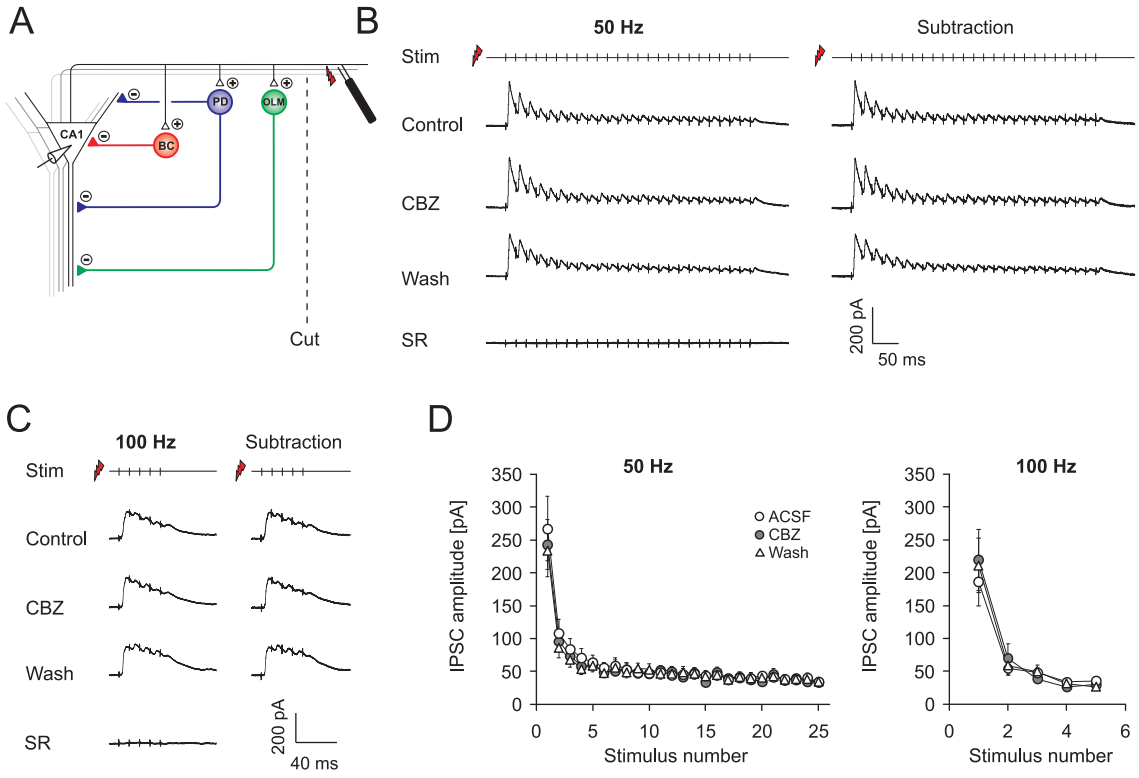

Figure 3.29: Carbamazepine effects on GABAergic feed-back inhibition. (A) Recording configuration used to elicit feed-back inhibition. **(B, C)** Representative recordings of feed-back PSCs with sequential application of 30 µM CBZ, washout of CBZ and application of 10 µM gabazine (left traces). Feed-back IPSCs were isolated by subtracting traces in the presence of gabazine from all other traces (right traces, panel B, 50 Hz, panel C, 100 Hz stimulation). **(D)** Quantification of the peak IPSCs for 50 and 100 Hz stimulation under control conditions, in the presence of CBZ and after washout. IPSC amplitude was measured as in Fig. 3.17.

3.2.4 Impact of CBZ on feed-forward inhibition of CA1 pyramidal cells

The second major excitatory input to CA1 interneurons is from CA3 pyramidal cell axons in a feed-forward manner. I therefore studied the impact of CBZ on feed-forward inhibition by stimulating CA3 pyramidal cells with a stimulation electrode placed into stratum pyramidale of CA3 while recording pyramidal cells in CA1 (**Fig. 3.30 A**). In these experiments, the cut separating CA3 from CA1 was omitted (see Methods, Section 2.7). This stimulation gave rise to large feed-forward IPSCs, with a small EPSC component (**Fig. 3.30 B**). In these experiments, due to the maintained connection with CA3, application of gabazine often resulted in the induction of network events within the CA3 region that propagated to CA1. Subtraction of traces recorded in the presence of gabazine was therefore not feasible in most experiments. However, as shown in **Fig. 3.23**, Schaffer collateral EPSCs are not affected by CBZ. Therefore an analysis of feed-forward inhibition will not be contaminated by CBZ effects on the underlying EPSC component. Similar to feed-back inhibition, measurement of the positive peak of consecutive postsynaptic currents

(PSCs) showed that feed-forward inhibition was unaffected by CBZ at both 50 and 100 Hz (**Fig. 3.30 B**, summary in Fig. **3.30 C** (n=5) and **D** (n=7), Wilcoxon signed-rank test). The charge transfer over the stimulus train was also unaffected (n=6, p=0.156 and n=7 p=0.821 for 50 and 100 Hz respectively, Wilcoxon signed-rank test, data not shown).

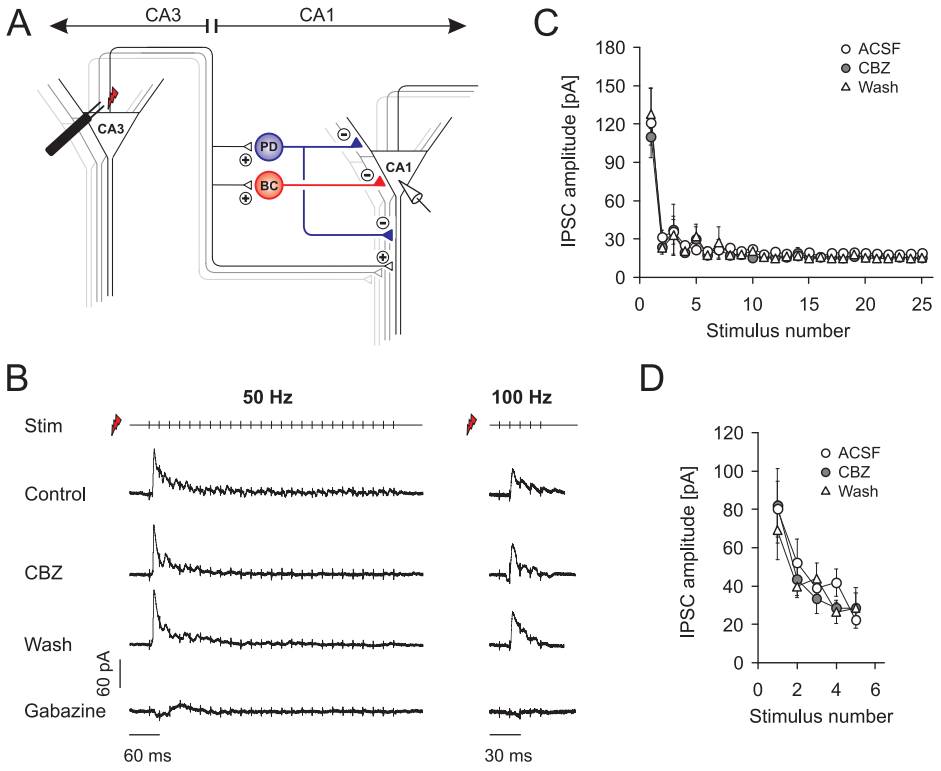

Figure 3.30: Carbamazepine effects on GABAergic feed-forward inhibition. **(A)** Recording configuration to elicit feed-forward inhibition. **(B)** Representative recordings of feed-forward IPSCs under control conditions, after application and washout of CBZ and the subsequent application of 10 µM gabazine during 50 (left traces) and 100 Hz (right traces) stimulus trains. **(C,D)** Quantification of the peak IPSCs elicited with 50 Hz **(C)** and 100 Hz **(D)** stimulation.

3.2.5 Effects of additional anticonvulsants on inhibitory microcircuits

The data so far suggest, that due to temporal dynamics inside of CA1 microcircuits, feed-back and feed-forward inhibition are undisturbed by CBZ. To examine if this is also true for other anticonvulsants with Na^+ channel blocking activity, I examined two additional classical anticonvulsant, phenytoin (PHT, 50 µM) and lamotrigine (LTG, 25 µM, see Section 1.4). As a control experiment I started with current injection experiments in pyramidal cells analogous to the experiments with CBZ (see **Fig. 3.21**).

Both, LTG and PHT caused a significant inhibition of pyramidal cell firing with a reduction in maximal discharge frequency of 25.2 ± 2.4 % and 48.1 ± 4.9 % for LTG and PHT, respectively (**Fig. 3.31 A,B**, n=6, p =0.03 for both, LTG and PHT).

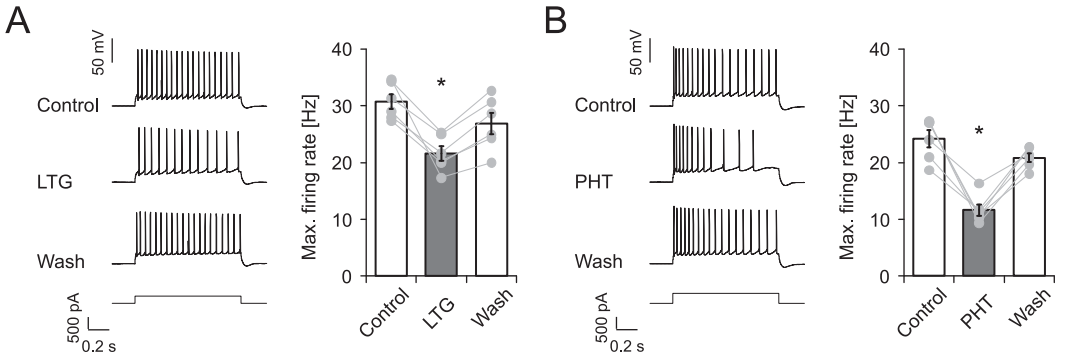

Figure 3.31: Effects of lamotrigine and phenytoin on pyramidal cell firing. (A) Left panel: Representative recordings before, during application and after washout of LTG (25 µM). Right panel: LTG (n=7) reduces maximal average firing rate of pyramidal cells by 25.2 %. Asterisks indicate $p < 0.05$. **(B)** PHT (50 µM) reduces maximal firing rate of pyramidal cells by 48.1 % (n=6, summary plot in right panel).

Following these experiments, effects of both anticonvulsants on feed-back inhibition were analyzed. Despite the blocking effect on pyramidal neuron firing, no effects on the peak amplitude of IPSCs during feed-back stimulation could be observed for LTG (**Fig. 3.32 A**) for neither 50 nor 100 Hz stimulation (**Fig. 3.32 C,D**, left panels, n=6, Wilcoxon signed-rank test). PHT exhibited minimal effects on the peak IPSCs, with only a single individual data point during the 100 Hz stimulation train reaching the level of statistical significance (**Fig. 3.32 B**, summary in **Fig. 3.32 C,D**, right panels. 50 Hz: n=6; 100 Hz: n=7, Wilcoxon signed-rank test). However, neither LTG nor PHT had any significant effect on the charge transfer at both 50 and 100 Hz stimulus trains (LTG: n=7, p=0.56 and n=6, p=1.0 for 50 and 100 Hz respectively; PHT: n=6, p=0.68 and n=7, p=0.68 for 50 and 100 Hz respectively, Wilcoxon signed-rank test). These data suggest that – in addition to CBZ – other Na^+ channel acting anticonvulsants also leave inhibition intact.

3.2.6 Anticonvulsant drug action in the epileptic hippocampus

The results so far suggest that the temporal dynamics of interneuron recruitment are one key parameter rendering inhibition resistant to sodium channel blocking anticonvulsants. However, in the first part of my study I was able to show that the temporal dynamics of interneuron recruitment are altered in chronic epilepsy. The epilepsy associated shift to facilitation in both basket and PD cells is likely to alter their firing patterns during periods of CA1 pyramidal cell activity. CBZ effects on interneuron firing, however, depend on the duration of this firing, as shown in the current injection experiments (see **Fig. 3.24**). Epilepsy associated changes in the synaptic recruitment of interneurons might therefore increase the impact of anticonvulsants on synaptically induced firing of interneurons. Furthermore, the pharmacological properties of interneuron subgroups might change in epilepsy, as has been reported for excitatory neurons in TLE (Remy et al., 2003; Schaub

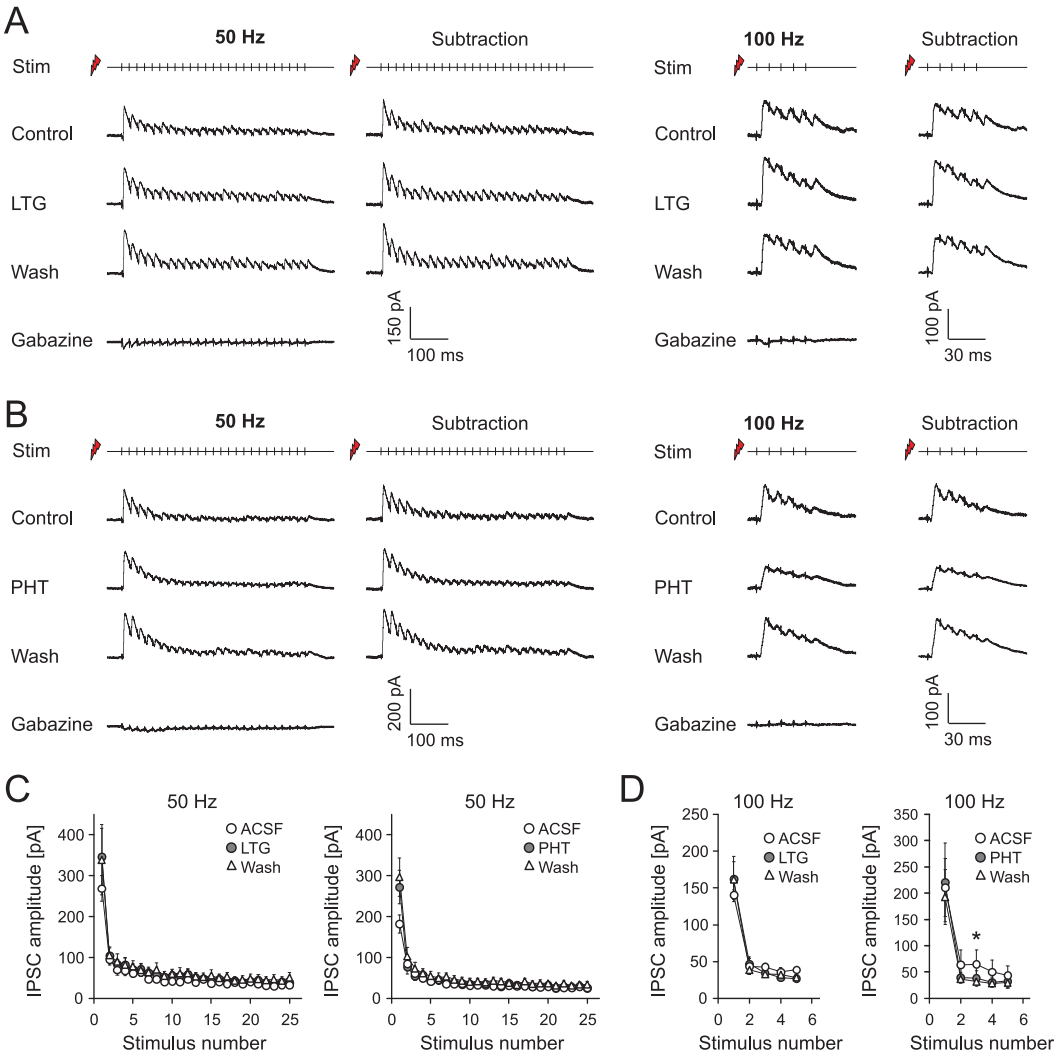

Figure 3.32: Effects of additional anticonvulsants on GABAergic inhibition. (A,B) Effects of LTG (panel A, 25 µM) and PHT (panel B, 50 µM) on feed-back inhibition measured as in panel A-C of Fig. 3.29. **(C,D)** Quantification of the peak IPSCs for 50 Hz (C) and 100 Hz (D) stimulation under control conditions, in the presence of CBZ and after washout. Asterisk indicates $p < 0.05$, Wilcoxon signed-rank test.

et al., 2007). Epilepsy associated alterations in interneurons could therefore further change the response of GABAergic inhibition to anticonvulsant drugs. To test whether the responsiveness of inhibitory microcircuits is changed in epilepsy, I thus went on to study the effects of CBZ in pilocarpine treated, chronically epileptic rats.

I first assessed the effects of CBZ on repetitive firing of pyramidal neurons induced with current injections in epileptic rats. These experiments were conducted exactly as described previously for control animals (**Fig. 3.21**). After application of CBZ, consistent decreases in the firing rate were observed (**Fig. 3.33 A,B**; n=9). The effects were use-dependent, increasing with the duration of the current injection (**Fig. 3.33 C**, black symbols; gray

symbols are values from control animals shown for the sake of comparison). The differences between the CBZ effects in control and epileptic animals were not significant.

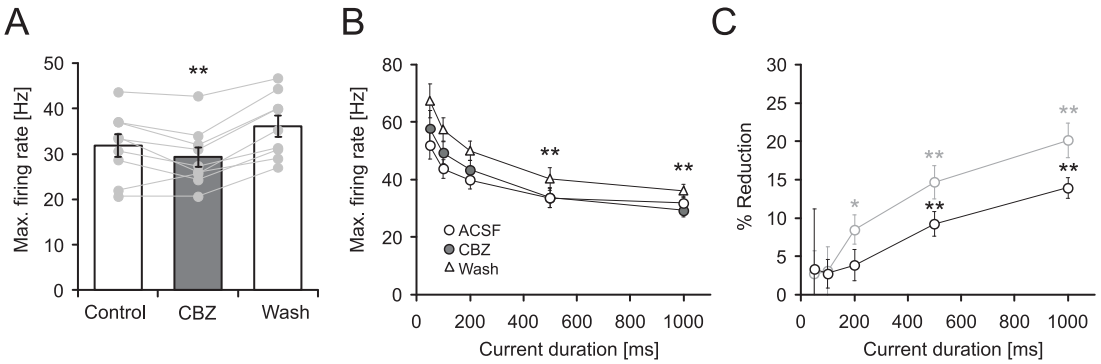

Figure 3.33: Effects of CBZ on pyramidal neurons in the chronically epileptic hippocampus. **(A)** Effects of 30 µM CBZ on the maximal discharge frequency measured during 1 s current injections in pilocarpine-treated rats. **(B)** CBZ effects on the maximal firing rate measured during the first 50, 100, 200, 500, and 1000 ms of current duration (see Fig. 3.21). **(C)** Percent reduction in firing frequency by CBZ within the different time intervals shown in **B**. For comparison, data from control animals (see Fig. 3.21) are indicated in gray. * depicts $p < 0.05$ and ** depicts $p < 0.01$, Wilcoxon signed-rank test.

Inhibition impinging on pyramidal cells are the result of firing of all interneuronal subtypes. Any effect of CBZ on interneuron firing would therefore result in a reduction of feed-back inhibition. CBZ effects of GABAergic inhibition in epileptic rats were therefore tested by means of feed-back inhibition recorded in CA1 pyramidal neurons. Experiments were performed as shown for control animals (**Fig. 3.34 A**). Pyramidal cell IPSCs were isolated by subtraction of traces obtained in the presence of gabazine (10 µM; **Fig. 3.34 B,C**). There was no significant effect of CBZ (30 µM) on the peak amplitude of consecutive IPSCs over the 50 and 100 Hz stimulus trains (**Fig. 3.34 D**; 50 Hz, n=7; 100 Hz, n=10; n.s., Wilcoxon signed rank test). Similarly, the charge transfer over the stimulus train was not affected (data not shown; n=7, p=0.93 and n=10, p=0.92 for 50 and 100 Hz, respectively; Wilcoxon signed rank test). These data suggest that in the chronically altered epileptic hippocampus inhibition remains unaffected by application of the sodium channel blocker carbamazepine.

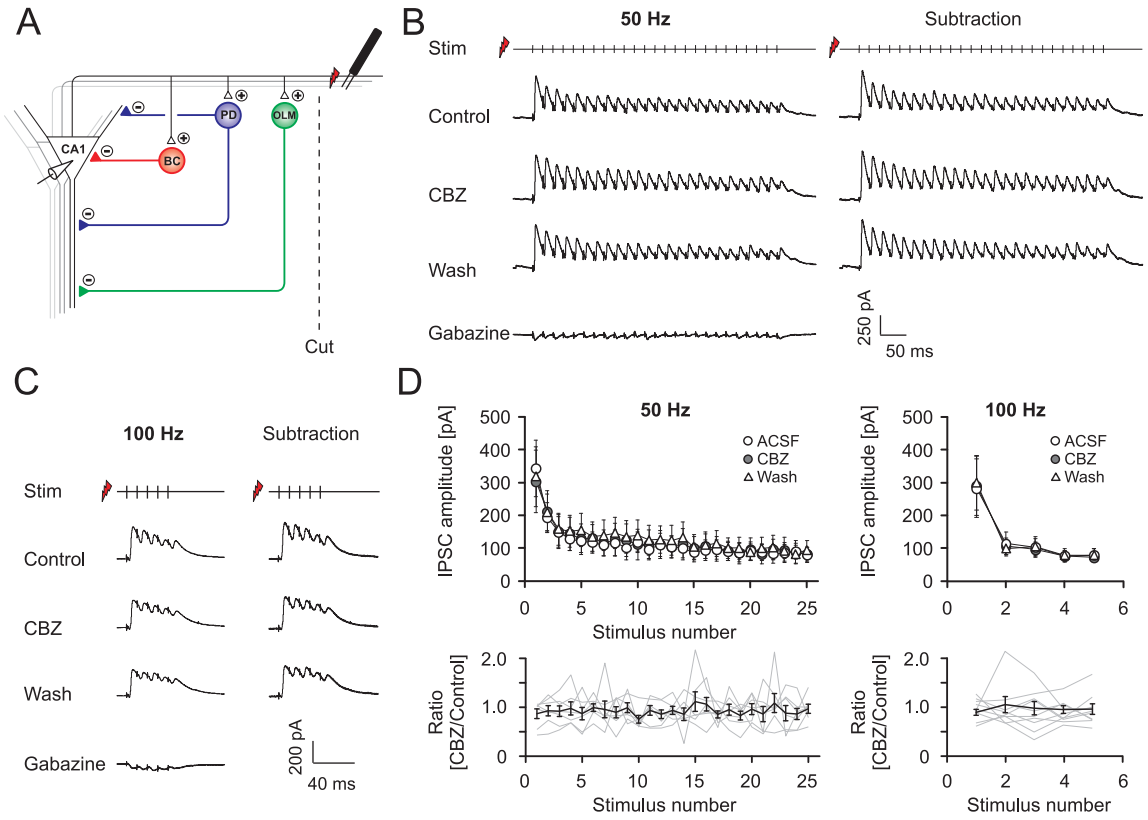

Figure 3.34: Effects of CBZ on feed-back inhibition in the chronically epileptic hippocampus. **(A)** Recording configuration used to elicit feed-back inhibition. **(B, C)** Representative recordings of feed-back PSCs with sequential application of 30 µM CBZ, washout of CBZ, and application of 10 µM gabazine (leftmost traces). Feed-back IPSCs were isolated by subtracting traces recorded in the presence of gabazine (rightmost traces; **B**, 50 Hz stimulation; **C**, 100 Hz stimulation). **(D)** Quantification of the CBZ effect on peak IPSCs during 50 and 100 Hz stimulation. Bottom, Peak IPSCs after CBZ application normalized to the mean of control and washout. Gray traces correspond to individual cells; the black trace shows average ± SEM.

4 Discussion

4.1 Changes of inhibitory microcircuits in epilepsy

In the first part of this thesis I investigated epilepsy associated alterations in the spatio-temporal pattern of feed-back inhibition in the CA1 area of the hippocampus. In control animals, I observed differences in the temporal pattern of excitatory inputs depending on the postsynaptic interneuron subtype. Perisomatically targeting basket cells and proximal dendritic targeting PD interneurons initially received strong excitatory inputs followed by synaptic depression. In contrast, inputs to distally innervating OLM interneurons facilitated during prolonged repetitive activation. In chronic epileptic animals these temporal dynamics onto perisomatic cells were changed. Excitatory inputs from CA1 to both, basket and PD cells shifted from a depressing to a facilitating phenotype. Concomitantly, feed-back inhibition onto CA1 pyramidal cells was no longer depressing but showed short-term facilitation. Furthermore, initial feed-back inhibition during short bursts of activity was reduced. These changes were accompanied by an overall decrease in the inhibitory charge transfer during periods of prolonged activation. Thus, both the spatio-temporal pattern of feed-back inhibition and its amplitude were changed in epilepsy. In the following, I will first review the role of short-term dynamics within the healthy brain and then discuss potential implications of their changes in epilepsy.

4.1.1 Short-term dynamics of inhibitory microcircuits in the healthy brain

Methodological considerations: Stimulus patterns and alveus stimulation

The excitatory inputs from CA1 pyramidal cells onto CA1 interneurons critically depend on the temporal activity pattern of these pyramidal cells. This firing pattern itself is modulated by the several network oscillations that are present during different states of the brain (Klausberger and Somogyi, 2008). The stimulus paradigms I used in this study were chosen to mimic the temporal activity patterns that pyramidal cells exhibit during certain hippocampal network oscillations.

The hippocampal theta rhythm is a field potential oscillation in a frequency band of 5-10 Hz. It is characteristic of exploratory behavior and REM sleep (Vanderwolf, 1969; Buzsaki, 2002). During exploratory behavior, the firing of individual pyramidal cells is linked to specific locations within an environment (O'Keefe and Dostrovsky, 1971; O'Keefe, 1976). These cells are called 'place cells' and their encoded spatial areas are referred to as

their respective 'place fields' (O'Keefe, 1976, 1979). While active, the firing of place cells is phase locked to the theta rhythm (Buzsáki et al., 1983; Kamondi et al., 1998; Csicsvari et al., 1999; Buzsaki, 2002). A second form of hippocampal oscillations are gamma oscillations within a frequency band of 30-85 Hz. They are associated with a number of cognitive functions including sensory processes, selective attention and memory (Colgin and Moser, 2010; Yamamoto et al., 2014). During exploratory behavior they occur nested within theta oscillations where they play a role in encoding and retrieval of memory (Hájos and Paulsen, 2009). Oscillations with an even higher frequency of 140–200 Hz (High frequency oscillations, or "ripples", O'Keefe and Nadel, 1978; Buzsáki, 1986; Buzsáki et al., 1992; Stark et al., 2014) are associated with sharp waves, the electrophysiological manifestation of convergent inputs from CA3 to CA1. Sharp waves and the associated ripples occur during slow-wave sleep and consummatory behaviors and are thought to be relevant during memory consolidation. Within the hippocampus, they represent the oscillation with the highest level of synchronization (Buzsáki, 1986; Buzsáki and da Silva, 2012). During these short episodes, pyramidal cell firing is synchronized into population bursts. Within these bursts, both the firing probability and the firing frequency of individual pyramidal cells is increased (Buzsáki, 1986; Buzsáki and da Silva, 2012). Individual pyramidal cells will fire complex bursts with a frequency of up to 200 Hz (Csicsvari et al., 1999). Importantly, these high frequency oscillations are related to fast ripples, pathological high frequency oscillations in a frequency band of 250-600 Hz that are associated with epilepsy (Bragin et al., 1999; Engel et al., 2009; Köhling and Staley, 2011). These fast ripples have been proposed to play a role in seizure initiation (Khosravani et al., 2005; Jirsch et al., 2006).

The theta burst protocol I used in this study imitates the activity pattern of pyramidal neurons during exploratory behavior (see Fig. 3.5A; Buzsaki, 2002): When a rat enters the place field of a given pyramidal cell, this place cell starts to fire single or bursts of action potentials. This firing reoccurs rhythmically in the theta frequency band and prevails as long as the animal moves within the place field (Buzsaki, 2002; Harvey et al., 2009). The first burst within this stimulus protocol mimics the activity of pyramidal cells while the rat enters a place field. Consecutive stimulus bursts represent the theta modulated firing while the rat keeps moving through the field. Additionally, the short 100 Hz stimulation within the initial theta burst yields information about interneuron recruitment during highly synchronous bursts of pyramidal cell activity. These highly synchronous bursts resemble the pyramidal cell activity during high frequency oscillations such as sharp wave-ripples. Finally, gamma like pyramidal cell activity was produced with a second stimulus protocol consisting of 10 stimuli at 50 Hz.

It is important to keep in mind, that we look at the isolated impact of CA1 feed-back input onto CA1 interneurons. This simplified approach ensures that any changes observed can be assigned to one synaptic connection. However, *in vivo*, the picture is certainly more complex. Together with the input from CA1 pyramidal cells, interneurons will

receive temporally intermingled input from CA3, the entorhinal cortex and the septum, depending on the respective type of oscillation. Additionally, they receive modulatory as well as inhibitory input from various sources.

Target specific short-term synaptic plasticity and its mechanisms

Application of these stimulation protocols revealed that subtypes of feed-back interneurons differ regarding the short-term plasticity of their excitatory inputs (see **Fig. 3.4** and **3.5**). Target cell specific differences in short-term dynamics have been reported before, both in the hippocampus (Ali et al., 1998; Ali and Thomson, 1998; Losonczy et al., 2002) and the cortex (Reyes et al., 1998; Markram et al., 1998). My results are consistent with previous studies in the hippocampus, reporting that perisomatically targeting basket-cells are recruited by strong excitatory inputs that depress rapidly upon repetitive stimulation (Ali et al., 1998). Furthermore, oriens-lacunosum interneurons in the hippocampus and SST positive interneurons in the cortex are reported to receive facilitating excitatory input (Ali and Thomson, 1998; Reyes et al., 1998). Depending on the stimulus pattern and the stimulus duration, I observed additional differences in the short-term dynamics between PD and basket cells: Both PD and basket cells showed depression over consecutive theta cycles. However, within the first theta burst PD interneurons showed facilitation while BCs receive depressing input. Combined facilitating-depressing inputs to interneurons in the hippocampus have been reported previously (Losonczy et al., 2002). In the study of Losonczy et al. (2002) a minority of basket cells and a majority of bistratified cells showed combined facilitating-depressing inputs.

What are the mechanisms underlying these different forms of short-term plasticity? Facilitation and depression can be caused by both pre- and postsynaptic mechanisms (Zucker, 1989; Zucker and Regehr, 2002). One key feature determining the temporal dynamics of a synaptic connection is the presynaptic basal probability of neurotransmitter release (Sun et al., 2005). This probability of release depends both on the size of the ready releasable pool of vesicles and the individual probability of these vesicles to fuse with the membrane (Atwood and Karunanithi, 2002; Dobrunz, 2002; Sun et al., 2005). The fusion probability for a single vesicle is strongly related to the presynaptic Ca^{2+} dynamics. It therefore depends on the number and properties of Ca^{2+} channels, their proximity to the vesicles and the concentration and properties of Ca^{2+} buffers present. Additionally, the basal release probability is modulated by adjoining astrocytes (Perea and Araque, 2007; Bonansco et al., 2011). Glutamate released by these cells can activate presynaptic group I mGluRs and thus increase the presynaptic Ca^{2+} concentration (Schwartz and Alford, 2000).

Depression is often associated with a high initial probability of release (Atwood and Karunanithi, 2002). In these synapses, Ca^{2+} influx readily induces vesicle fusion and a concomitant depletion of the ready releasable pool. Subsequent action potentials are

therefore no longer able to elicit transmitter release and synaptic depression is observed. The time constant of depression and recovery hereby will depend on the rate with which the pool is replenished (Wu and Borst, 1999; Neher and Sakaba, 2008). Further (presynaptic) mechanisms of synaptic depression are the inactivation of presynaptic Ca^{2+} channels and the autoinhibition of transmitter release via presynaptic metabotrobic glutamate receptors (Scanziani et al., 1997; Xu and Wu, 2005).

Facilitation on the other hand can be caused by a low initial probability of transmitter release that increases upon repetitive stimulation (Burnashev and Rozov, 2005; Blatow et al., 2003). This rise in release probability is caused by an activity dependent increase in the presynaptic Ca^{2+} concentration, generated by an accumulation of residual Ca^{2+} or a saturation of the Ca^{2+} buffer capacitance (Fioravante and Regehr, 2011). Another mechanism potentiating the release probability is based on presynaptic kainate or NMDA receptors that respond to increases in the extracellular glutamate concentration during prolonged synaptic activity (Sun and Dobrunz, 2006; Buchanan et al., 2012). Several postsynaptic mechanisms of facilitation have also been described: In the cortex, multipolar interneurons express AMPA receptors that under normal conditions can be blocked by intracellular polyamines. High frequency stimulation promotes dissociation of the polyamines and a concomitant potentiation of the EPSC (Rozov and Burnashev, 1999). Additionally, activation of postsynaptic NMDA receptors during high frequency stimulation can contribute to postsynaptic forms of facilitation (Zhao et al., 2014).

The basal release probability of a synaptic connection can be estimated with paired recordings of synaptically connected neurons. In a connected pair with a low release probability the proportion of synaptic failures following single action potentials is high. Conversely, if probability of transmitter release is high, the failure rate is low. For CA1 paired recordings of pyramidal cells and interneurons have shown that pyramidal-to-basket cell connections are characterized by a low failure rate, whereas in pyramidal-to-OLM interneurons, the initial failure rate is high (Ali et al., 1998; Ali and Thomson, 1998). These results indicate that differences in short-term dynamics between basket and OLM interneurons are of presynaptic origin and are at least partly caused by differences in the basal release probability. My paired pulse experiments reveal that both basket and PD cells have a significantly lower paired pulse ratio than OLM interneurons (see **Fig. 3.13**, Sham animals) and are therefore in accordance with this assumption. The differences between basket and PD interneurons observed in the theta burst protocol may be due to differences in the size of the ready releasable pool (Neher and Sakaba, 2008).

The work of Pouille and Scanziani (2004) suggests that short-term dynamics in CA1 interneurons are supported by disynaptic inhibition. However, I could not confirm this finding. One explanation for this deviation are differences in the preservation of axonal connections during slicing.

If short-term dynamics of CA1 interneurons depend on the release probability of the

presynaptic axon, then two scenarios are conceivable: 1) Interneurons receiving facilitating inputs and interneurons receiving depressing inputs are innervated by two different populations of pyramidal cells that differ in their axonal properties or 2) One type of pyramidal cell innervates both depressing and facilitating interneurons. The latter scenario implies that one single pyramidal neuron can form both, synapses with a high or a low release probability, depending on the postsynaptic target cell type. In both the cortex and CA3, triple recordings have shown that indeed one individual pyramidal cell targets both depressing and facilitating interneurons (Reyes et al., 1998; Scanziani et al., 1998). In CA1 however, triple recordings between pyramidal cells and different types of interneurons have not been conducted so far and therefore the evidence is inconclusive. Furthermore, it is known that pyramidal cells in that region are not a homogenous group but can be differentiated into different subtypes, both in regard of protein expression as well as axonal projection patterns (Lee et al., 2014; Stark et al., 2014).

In both scenarios, target cell dependent adjustment of the presnyaptic release probability requires that the postsynaptic identity is conveyed to the presynaptic terminal. In a very elegant study, Sylwestrak and Ghosh (2012) realized that the postsynaptic transmembrane protein Elfn1 is selectively expressed in SST positive OLM interneurons. They then showed that this postsynaptic protein is necessary for setting a low initial release probability at presynaptic pyramidal cell inputs. The effector molecules downstream of Elfn1 that are responsible for setting the basal release probability have, however, not been identified so far. More interestingly, expression of this protein in basket cells changed their depressing phenotype into a facilitating one. Elfn1 therefore seems to be a key player in adjusting target cell specific synaptic properties. So far, it is not clear whether a similar signal protein exists for depressing synapses, that is selectively expressed in basket or both basket and PD interneurons. Therefore, it is not clear, whether it is just the absence of Elfn1 or an additional factor that specifically indicates a high release probability to the presynaptic terminal. An interesting candidate protein is the postsynaptically expressed N-cadherin: its loss results in a reduction of the recycling pool as well as the basal release probability of its presynaptic partner neuron (Vitureira et al., 2012). However, differential expression in interneuron subtypes has not been reported so far.

Functions of short-term dynamics in the healthy brain

Before I interpret the changes in short-term dynamics observed in epilepsy, their function within the healthy brain has to be analyzed. The temporal dynamics of synaptic inputs determine how the firing pattern of the presynaptic neuron is translated into the firing pattern of the postsynaptic cell. The different short-term dynamics of interneuron subtypes are therefore one key feature enabling interneurons to fulfill their different tasks. During sustained firing of CA1 pyramidal cells, depression and facilitation lead to a temporally distinct recruitment of different interneuron subtypes. Importantly, these

interneuron subtypes also differ morphologically and innervate different layers and compartments of pyramidal cells. The firing pattern of presynaptic CA1 pyramidal cells is therefore translated into a spatially and temporally differentiated pattern of feed-back inhibition.

The high release probability at synapses onto basket cells ensures that these cells are efficiently recruited by single or short bursts of action potentials. During prolonged activation, however, synaptic depression rapidly terminates their firing (see **Fig. 3.26**). Consequently, these cell types are strongly recruited by inputs of low frequencies or short bursts, while sustained activation with higher frequencies will not be translated into action potential firing (Ariel and Ryan, 2012). This behavior is further strengthened by post-synaptic cell properties such as fast EPSC decay kinetics and small values for both cell capacitance and membrane time constant **(Fig. 3.3** and Pouille and Scanziani, 2004, but see Morin et al., 1996). As a result, the temporal summation of synaptic inputs is reduced to a minimum and these neurons are most efficiently recruited by temporally coinciding inputs (Tsodyks and Markram, 1997). In combination with the high initial release probability and the strong synaptic depression, these properties ensure a temporally precise recruitment of somatic targeting basket cells (Geiger et al., 1997; Pouille and Scanziani, 2004; Nörenberg et al., 2010; Bartos et al., 2011). Accordingly, the temporal jitter of synaptically induced firing is minimal. Both, the preferred response to temporally synchronous input and the temporally precise output are important for the ability of basket cells to synchronize large populations of pyramidal cells and to act as rhythm generators (Cobb et al., 1995; Pouille and Scanziani, 2004; Stark et al., 2014).

Unlike basket cells that depress readily during short bursts of inputs, interneurons targeting the proximal dendrites in SO and SR receive excitatory inputs that facilitate initially (**Fig. 3.5** and Losonczy et al., 2002). This differences in short-term dynamics of basket and PD cells might contribute to differences in phase preference during brain rhythms such as theta (Silberberg et al., 2004; Somogyi and Klausberger, 2005; Klausberger et al., 2003; Klausberger and Somogyi, 2008; Somogyi et al., 2014). Nevertheless, the initial failure rate within this connection is low, thereby ensuring reliable recruitment of this cell population by single and short bursts of presynaptic action potentials (Ali et al., 1998). During repetitive stimulation, synaptic depression also predominates in this connection. Prolonged activity of CA1 pyramidal cells therefore recruits PD cells only at the beginning of pyramidal cell firing. The resulting firing pattern of PD cells is similar to the firing pattern observed in basket cells (see **Fig. 3.26**). During short bursts of pyramidal cell activity the strong dendritic inhibition provided by PD cells is able to control excitatory Schaffer collateral inputs within stratum radiatum and stratum oriens. PD cells thereby can prevent the generation of dendritic spikes and burst firing of CA1 pyramidal cells induced by CA3 (Lovett-Barron et al., 2012; Müller et al., 2012). However, during prolonged activation of CA1 pyramidal cells, PD cells cease to fire and the

inhibitory control of excitatory inputs from CA3 is decreases. Accordingly, the impact of excitatory Schaffer collateral inputs increases.

The firing pattern observed in OLM interneurons strongly deviates from that of basket cells and PD interneurons. The high initial failure rate of transmitter release prevents the recruitment of OLM cells with single spikes or short bursts form pyramidal cells (see **Fig. 3.26**). Synaptic facilitation however enables them to follow high frequency activation over a prolonged input periods, such as theta. OLM cells are therefore most efficiently recruited with repetitive action potential trains above a minimum frequency necessary for facilitation (Pouille and Scanziani, 2004). In addition, the large membrane time constant and slow decay kinetics of EPSCs observed in OLM interneurons favor a large time window for temporal summation reinforcing the facilitating phenotype (Pouille and Scanziani, 2004, **Fig. 3.3**). During prolonged activation of CA1 pyramidal cells, feed-back inhibition therefore shifts from the soma and the proximal dendritic compartments to the input zone of the entorhinal cortex within the SLM.

In summary, differences in short-term dynamics enable the temporally segregated activation of interneuron subtypes. Together with the different axonal projections this creates a distinct spatio-temporal pattern of feed-back inhibition: Depending on the input pattern, either temporally precise proximal inhibition is activated, whereas during prolonged activity, inhibition is shifted to the distal dendrites in stratum lacunosum moleculare. Hence, feed-back inhibitory microcircuits selectively control dendritic compartments to favor either excitatory inputs from CA3 or the entorhinal cortex, depending on the temporal activity pattern of CA1 pyramidal cells. My findings are therefore in good agreement with previous studies of CA1 inhibitory microcircuits in the healthy brain (Pouille and Scanziani, 2004; Müller et al., 2012). Note that the differential activation of interneuron subtypes is further strengthened by additional differences in inhibitory, excitatory and modulatory inputs from other sources (Lovett-Barron et al., 2014).

4.1.2 Changes of inhibitory microcircuits in the epileptic hippocampus

Alterations in feed-back inhibitory microcircuits and its potential mechanisms

My experiments in epileptic animals revealed a shift in the temporal recruitment of perisomatic and proximal dendritic interneurons to a facilitating phenotype during prolonged stimulation. Both, synaptic depression and synaptic facilitation are strongly associated with the presynaptic probability of transmitter release. One candidate mechanism for the shift from depression to facilitation is therefore a reduction in the initial release probability. A commonly applied method to test for alterations in release probability are paired pulse experiments. In these experiments, two consecutive synaptic events are triggered with a short delay and the amplitude ratio of the postsynaptic event is calculated. Alterations in the paired pulse ratio are a strong indicator for a change in the presynaptic release

probability. In this study, paired pulse experiments in basket cells indeed revealed a significant increase in the paired pulse ratio (see **Fig. 3.13**). These data therefore strongly suggest that the facilitation observed in basket cells is caused by a reduction in the release probability of CA1 pyramidal cell inputs in epileptic animals.

In PD interneurons no significant change in the paired pulse ratio was observed. It is therefore unlikely, that the change from depression to facilitation seen in PD interneurons is caused by alterations in the presynaptic release probability. Alternative possibilities include postsynaptic mechanisms of facilitation like polyamine-dependent facilitation or activation of postsynaptic NMDA receptors.

A reduced initial release probability does not only influence the synaptic short term plasticity but also causes a reduction in the net transmitter release upon single presynaptic action potentials or at the beginning of an action potential train. Consequently, excitatory inputs onto interneurons at the beginning of presynaptic action potential firing would be reduced. Accordingly, the absolute amplitude of the first EPSP within a stimulus train was strongly reduced in epileptic animals in both cell types (see **Fig. 3.13 A** and **B**, middle panels). However, the EPSP amplitude is influenced by a number of additional factors. Firstly, the number of stimulated pyramidal cells is unknown. Epilepsy associated alterations in axonal distribution and a pronounced loss of CA1 pyramidal cells can lead to a systematic difference between the number of stimulated axons in control and epileptic animals (Toyoda et al., 2013). Secondly, the number of synaptic contacts between CA1 pyramidal cells and interneurons could be reduced. A direct comparison of the absolute amplitude of the EPSP therefore cannot be interpreted unequivocally.

Importantly, the changes in synaptic properties were accompanied by a reduction in input resistance in all three classes of interneurons (**Fig. 3.14**). This reduction diminished both the voltage deflection evoked by current injections and the number of elicited action potentials (**Fig. 3.14**). Consequently, interneurons in epileptic tissue are less excitable and their activation will require stronger synaptic inputs as compared to control animals.

Any change in the recruitment of feed-back interneurons will ultimately affect the pattern of inhibition of CA1 pyramidal cells. Recordings of feed-back inhibition are therefore sensitive to any changes in the activity pattern of interneurons. My recordings of feed-back inhibition revealed that in addition to changes in the temporal dynamics the amplitude of inhibition was changed (**Fig. 3.17** and **3.18**). The IPSC amplitude at the beginning of a stimulus train, and the overall charge transfer were strongly reduced in epileptic animals. Furthermore, inhibition during prolonged activity was not increased relative to control values, despite the facilitation in the excitatory input of basket and PD interneurons.

Taken together, these experiments indicate profound changes in the inhibitory microcircuitry of CA1 in epileptic animals. They suggest that perisomatic inhibition is recruited less efficiently during sparse pyramidal cell activity, short high frequency bursts and at the beginning of prolonged periods of activity.

Molecular mechanisms underlying changes in the presynaptic release probability

The experiments described above indicate a change in the initial release probability of terminals contacting basket cells. Two potential mechanisms could account for this alteration: either, the signal conveying the postsynaptic identity to the presynapse is changed, or the machinery to follow this signal is disturbed. One interesting candidate protein for a transmembrane signal is Elfn1 which is usually expressed in OLM cells (see Section **4.1.1**). It has been shown that an upregulation of Elfn1 in basket cells is sufficient to induce a facilitating phenotype in this cell class (Sylwestrak and Ghosh, 2012). One important future experiment would therefore be to analyze whether Elfn1 is upregulated in basket cells of chronically epileptic rats. Interestingly, epilepsy associated mutations of this gene were found in patients suffering absence epilepsy and juvenile myoclonic epilepsy (Tomioka et al., 2014). The observed mutations seem, however, to be associated with a loss of function and may therefore rather act by disturbing OLM behavior. A second candidate protein is the postsynaptically expressed N-cadherin that has been shown to affect the release probability of the presynaptic partner neuron (Vitureira et al., 2012). However, detailed information on interneuron subtype specific expression has not been reported.

4.1.3 Functional concequences and predictions

Short-term plasticity determines how the temporal pattern of presynaptic input is translated into postsynaptic firing. The shift in short-term plasticity observed in epilepsy will also affect the temporal pattern of interneuron recruitment. My results therefore raise the question how changes in interneuron recruitment will affect their contribution to network oscillations, their role in dendritic integration of pyramidal cells and their pacemaker activity. I will adress this question in regard of two different patterns of pyramidal cell activity, short bursts of firing as present during sharp wave-ripples and prolonged patterns of activity as they occur during gamma and theta oscillations.

In the healthy brain, both basket and PD interneurons are recruited most efficiently by short high frequency bursts, during sparse low frequency firing patterns or at the onset of prolonged pyramidal cells activity (Fig. 3.26; Losonczy et al., 2002; Ylinen et al., 1995; Stark et al., 2014). Accordingly, feed-back inhibition impinging on the soma and proximal dendrites during these input patterns is strong. My results predict that in epilepsy perisomatic feed-back inhibition is recruited less efficiently during these activity patterns. They therefore suggest that during sharp wave-ripples perisomatic inhibition will be reduced. To test this hypothesis, one experiment would be to elicit sharp wave-ripples *in vitro* in epileptic tissue, while monitoring the firing behavior of perisomatic interneurons.

In epilepsy, a pathologically modified form of high frequency oscillations has been described (see Section **4.1.1**). These “fast ripples” resemble the physiological form of

sharp wave-ripples (140-200 Hz), however they occur in a higher frequency band of 250-600 Hz (Köhling and Staley, 2011; Karlócai et al., 2014). In epileptic patients, these pathological fast ripples have been shown to precede seizures (Fisher et al., 1992; Bragin et al., 1999, 2002; Staba et al., 2002, 2004). Furthermore, animal models suggest that fast ripples are involved in seizure initiation (Khosravani et al., 2005; Ibarz et al., 2010). In the healthy brain, both interneurons and pyramidal cells participate in sharp wave ripple complexes (Ylinen et al., 1995; Stark et al., 2014). However, epileptic fast ripples are thought to be generated independent of the firing of inhibitory interneurons (Köhling and Staley, 2011; de la Prida and Trevelyan, 2011) and reflect burst firing of pyramidal cells instead (Köhling and Staley, 2011; Karlócai et al., 2014). Failure in the recruitment of perisomatic interneurons during short bursts might therefore play a role in the conversion of physiological sharp wave-ripples to pathological fast ripples. Interestingly, Rácz et al. (2009) showed that genetically reducing excitatory input onto PV positive interneurons increases burst firing of pyramidal cells during sharp wave-ripples.

The shift to facilitation in basket cells during short bursts of activity is also likely to affect their ability to act as pacemakers. In control conditions, synaptic depression and a short membrane time constant keep temporal summation at a minimum (Pouille and Scanziani, 2004). The shift to facilitation will promote temporal summation and is therefore likely to increase both temporal jitter and spike latency of basket cell firing. Accordingly, the gaps within perisomatic inhibition would enlarge. As a consequence the ability of basket cells to entrain large numbers of pyramidal cells would be decreased (Cobb et al., 1995). A potential experiment to test this hypothesis would be to monitor the temporal jitter of basket cell action potentials elicited with alveus stimulation. Interestingly, experimentally reducing excitatory drive onto PV positive interneurons leads to more imprecise firing of fast spiking interneurons (Fuchs et al., 2007) and optogenetically silencing of PV cells results in a phase shift of pyramidal cell firing within the theta cycle (Royer et al., 2012).

The reduced efficiency of perisomatic inhibition will also affect its control over excitatory inputs from CA3. Under normal conditions, the initial perisomatic inhibition is able to control burst firing in CA1 pyramidal cells elicited by CA3 inputs. One prediction would therefore be that in epileptic tissue, burst firing of CA1 pyramidal cells is increased. In fact, genetically reducing the excitatory drive on PV positive interneurons increases burst firing of pyramidal cells *in vivo* (Rácz et al., 2009). An experiment to test this hypothesis directly is given by the study of Müller et al. (2012): in their experiments they showed that during short bursts of alveus stimulation, perisomatic feed-back inhibition is able to control burst firing of CA1 pyramidal cells. Similar experiments in epileptic animals could reveal whether in epilepsy, the control of CA1 pyramidal cell burst firing is reduced.

Oscillations that are characterized by ongoing pyramidal cell activity such as theta or gamma will be differently affected by the alterations observed in epilepsy. In control

animals, basket and PD cells are not efficiently recruited by prolonged firing of pyramidal cells, owing to the strong synaptic depression. Accordingly, perisomatic inhibition rapidly decreases during these input patterns and inhibition is shifted to the distal dendritic compartments in stratum lacunosum moleculare. Excitatory inputs from CA3 in stratum radiatum and oriens therefore gain strength during these input patterns (Pouille and Scanziani, 2004; Müller et al., 2012). In epilepsy however, synaptic inputs onto basket and PD cells facilitate during theta and gamma patterned stimulation. My experiments on feed-back inhibition in epileptic animals show, however, that inhibition during repetitive activation is not increased relative to control values (**Fig. 3.17** and **3.18**). These experiments therefore suggest that the facilitation observed in basket and PD interneurons does not lead to an increased interneuron activation during prolonged CA1 pyramidal cell activity.

4.2 Anticonvulsant drug action on inhibitory microcircuits

In the second part of the thesis, I investigated how commonly used anticonvulsant drugs act on the level of inhibitory micronetworks. I found that in control animals, pyramidal cell firing is reliably blocked by CBZ. Interneuron subtypes in the hippocampus differed in their responsiveness to CBZ: Interneurons innervating the proximal dendrites of pyramidal cells showed a much stronger decrease in their firing rate compared with OLM interneurons or basket cells. Even though CBZ was capable of reducing the firing of interneurons induced by current injection, both feed-back and feed-forward inhibition remained completely unaffected. Furthermore, feed-back inhibition in the chronically altered hippocampus remained equally unaffected by CBZ.

4.2.1 Circuit analysis of anticonvulsant drug action

In all three classes of interneurons, application of CBZ resulted in a reduction of firing elicited with current injections. These experiments show that interneurons are principally responsive to this anticonvulsant. In all three classes of interneurons, this effect increased with the duration of the current injection and was only visible after a current duration of $\geq$ 200 ms (**Fig. 3.24**). This result can be explained by the use-dependent mechanism of action of CBZ: CBZ binds to a site within the sodium channel pore (Ragsdale et al., 1994, 1996; Yarov-Yarovoy et al., 2001, 2002). This requires the channel to open to allow CBZ to bind (Payandeh et al., 2011). As the proportion of sodium channels in the open/inactivated state increases with depolarization and during prolonged high frequency firing, CBZ blocks sodium channels in a use- and voltage-dependent manner (Willow et al., 1985; McLean and Macdonald, 1986; Schwarz and Grigat, 1989; Kuo et al., 1997).

Even though CBZ was capable of reducing the firing of interneurons induced by current injection, synaptically induced firing was not affected by CBZ. As a consequence,

both feed-back and feed-forward inhibition remained undisturbed. A possible explanation for this discrepancy is given by an analysis of the temporal dynamics of inhibitory microcircuits conducted in the first part of this thesis: Both basket and PD interneurons are recruited by strongly depressing excitatory inputs. Cell attached recordings confirmed that as a consequence, these interneurons fire only briefly when recruited synaptically by CA1 pyramidal cells. A more detailed temporal analysis of the CBZ effects on interneuron firing suggests that these brief episodes of synaptically driven firing are not sufficient for a development of use-dependent Na^+ channel block.

Due to their large number and diversity, I could record only from a subset of CA1 interneurons, and it is conceivable that the findings do not apply to all interneurons. However, inhibition impinging on CA1 pyramidal neurons will reflect the summed activity of all types of interneurons during feed-back and feed-forward activation. My data, therefore, suggest that during feed-forward and feed-back activation, perisomatic CA1 interneurons are not affected by sodium channel blocking anticonvulsants.

For OLM neurons, which reliably follow longer episodes of synaptic recruitment, small effects of CBZ were observed. These effects did not translate into an effect of CBZ onto inhibition measured in CA1 pyramidal cells, most likely because of the dominance of perisomatic inhibition in these recordings. Additionally, in these experiments higher stimulus amplitudes were needed to drive OLM cells sufficiently to fire reliably for 500 ms during every stimulus cycle. Despite the facilitating nature of their excitatory input, individual synapses might not be able to follow stimulation over these prolonged periods but show a subsequent depression (Losonczy et al., 2002). In summary, these results indicate that one principal reason for the efficacy of Na^+channel blockers in epilepsy is not only the use-dependent nature of the blocking action per se, but also a limited efficacy of anticonvulsant drugs on GABAergic inhibition. This limited efficacy is rooted in both intrinsic pharmacological properties of interneurons and in the dynamics of their synaptic recruitment.

A lack of efficacy of CBZ on GABAergic inhibition has been suggested in early experiments using field recording techniques. These experiments have shown that inhibition-related parameters such as paired pulse inhibition of population spikes are CBZ insensitive (Hood et al., 1983; Olpe et al., 1985), even though these experiments have not addressed CBZ effects when inhibitory networks are repetitively recruited at high rates. Other reports suggest a direct allosteric regulatory effect of CBZ on $GABA_A$ receptors in cortical cell culture (Granger et al., 1995). However, my recordings of feed-back and feed-forward inhibition suggest that there are no large direct effects of CBZ on GABA receptors in the CA1 region of native hippocampal slices. It should be noted that this study has focused only on inhibitory circuits inside the hippocampal CA1 region. Therefore, I cannot exclude that anticonvulsant effects on excitation versus inhibition may be different in other brain areas.

The results above show that anticonvulsant drug action strongly depends on the firing pattern of the different neuron types. During electrical stimulation presynaptic pyramidal cells will be activated synchronously, whereas input patterns *in vivo* are likely to be less uniform: some pyramidal cells will start to fire while others are already active or stop firing. This thought is of importance as short-term phenomena take place on the level of individual synapses. Newly participating pyramidal cells will therefore provide strong, not depressed excitatory feed-back input to perisomatic interneurons. Characteristic firing patterns of neuronal subtypes could therefore help to better predict the action of a sodium channel blocking drug within inhibitory microcircuits.

From a biophysical perspective, the differential responses of specific interneuron types and pyramidal neurons are intriguing. Available data suggest that interneuron subtypes may differ in the expression of sodium channel subunits. For instance, $Na_v1.1$ appears to be particularly strongly expressed in parvalbumin-containing interneurons during development (Ogiwara et al., 2007). However, a study by Qiao et al. (2014) revealed that subunit specific differences in the response to CBZ are minimal. A differential expression of sodium channel isoforms is therefore unlikely to be responsible for the differential sensitivity of interneurons to CBZ. An alternative explanation would be that the channel density or gating differs between hippocampal cell types. For instance, the fast Na^+ channel gating and the narrow action potentials observed in some interneurons (Martina and Jonas, 1997) may be associated with a less efficient use-dependent block by CBZ. My data on the action potential properties in the different neuron types do not support such a simple relationship. For instance, the PD neurons, which show the largest CBZ effects, have narrow action potentials (0.37±0.06 ms), whereas basket cells, which show significantly smaller CBZ effects, have broader action potentials (0.47±0.12ms). Alternatively, a higher density of Na^+ channel densities observed in some interneurons might also contribute to a relative insensitivity to Na^+ channel blockers (Hu et al., 2010).

4.2.2 Network effects of CBZ in chronic epilepsy

The experiments in control animals suggest that sparing of inhibitory microcircuits by CBZ strongly depends on the pattern of synaptic recruitment. However, in the first part of my study I was able to show that the temporal dynamics of interneuron recruitment are changed in chronic epilepsy. Epilepsy associated alterations in interneuron recruitment could therefore increase the response of inhibitory microcircuits to antiepileptic drugs. My experiments in chronically epileptic rats now show that alterations in interneuron recruitment are not sufficient to render feed-back inhibition sensitive to CBZ. This suggests that firing of basket and PD interneurons during feed-back recruitment is not sufficiently increased for a use-dependent block to develop. Alternatively, the intrinsic responsiveness of interneurons in the epileptic brain could be reduced. To further explore these two possibilities, both current injection and synaptic stimulation experiments could be repeated

in epileptic animals.

The pilocarpine model of epilepsy reproduces features characteristic for temporal lobe epilepsy. However, epilepsy associated changes in interneurons have been described in other forms of epilepsy as well. In models of Dravet syndrome, a decrease in interneuron Na^+ currents has been proposed as a causative mechanism for seizure generation (Yu et al., 2006; Cheah et al., 2012 but see Liu et al., 2013). In patients with this disorder, treatment with sodium channel blockers can be deleterious. This raises the possibility that in patients with epilepsies associated with sodium channel deficiency in interneurons, the lower density of sodium channels might lead to higher sensitivity of interneuron firing to sodium channel blockers. Additionally, compensatory changes in sodium channel subunit expression might increase sensitivity of interneurons to CBZ as well (Yu et al., 2006). In these cases, CBZ might depress inhibition, even if it does not in other forms of epilepsy. Nevertheless, in most types of epilepsy, blocking excitatory neurons while sparing inhibition appears to be an effective strategy for inhibiting seizure initiation and propagation. As discussed above, interneuron activity is far from being limited to the inhibition of excitatory cells and the contribution of interneurons to oscillatory activity and synchronization has to be kept in mind (for review, see McBain and Fisahn, 2001; Mann and Mody, 2008; Avoli and de Curtis, 2011). Based on *in vitro* models of seizures, a contribution of interneuron firing to pathological network events has been proposed (Kawaguchi, 2001). These results raise the possibility that limiting the excitability of specific types of interneurons may also be a viable strategy to limit excitability.

In summary, my results show that several commonly used anticonvulsants fail to affect GABAergic inhibition while inhibiting firing of principal neurons. These results have implications for drug development, suggesting that novel compounds should be evaluated for their quantitative effects on synaptic inhibition early on in the drug development process.

5 Appendix

5.1 Abbreviations

ACSF: artificial cerebrospinal fluid
AED: antiepileptic drugs
Amg: amygdala
AP: action potential
BC: basket cell
CA1-3: Cornus Ammonis 1-3
CBZ: carbamazepine
CCK: cholecystokinin
CNS: central nervous system
DG: dentate gyrus
EC: entorhinal cortex
EGTA: ethylene glycol tetraacetic acid
EPSC: excitatory postsynaptic current
EPSP: excitatory postsynaptic potential
fAHP: fast after hyperpolarizing potential
FB: feed-back
GABA: γ-amminobutyric acid
$G_{i/o}$-proteins: guanine nucleotide-binding proteins
GIRK channels: G protein-coupled inwardly-rectifying potassium channels
HEPES: 4-(2-hydroxyethyl)-1-piperazineethanesulfonic acid
ILAE: International League Against Epilepsy
I_{NaT}: transient sodium current
ISI: interneurons selective interneuron
IPSC: inhibitory postsynaptic current
IPSP: inhibitory postsynaptic potential
KCC2: potassium-chloride transporter member 5
LTG: lamotrigine
mTLE: mesial temporal lobe epilepsy
OLM interneuron: oriens-lacunosum moleculare interneuron
PC: pyramidal cell

PD: proximal dendritic targeting interneuron
PHT: phenytoin
PSC: postsynaptic current
PSP: postsynaptic potential
PV: parvalbumin
R_{in}: input resistance
SE: status epilepticus
SEM: standard error of the mean
SLM: stratum lacunosum moleculare
SO: stratum oriens
SP: stratum pyramidale
SR: stratum radiatum
SUB: subiculum
SST: somatostatin
Stim: Stimulus
TLE: temporal lobe epilepsy
TH: thalamus
VGSC: voltage-gated sodium channel

6 Contributions

Biocytin stainings for morphological reconstruction of interneurons were partially conducted by Olivia Steffan. Special thanks for that!

Bibliography

Acsády, L., Görcs, T. J., Freund, T. F., 1996. Different populations of vasoactive intestinal polypeptide-immunoreactive interneurons are specialized to control pyramidal cells or interneurons in the hippocampus. Neuroscience 73, 317–334.

Ali, A. B., Deuchars, J., Pawelzik, H., Thomson, A. M., 1998. CA1 pyramidal to basket and bistratified cell EPSPs: dual intracellular recordings in rat hippocampal slices. J Physiol 507, 201–217.

Ali, A. B., Thomson, A. M., 1998. Facilitating pyramid to horizontal oriens-alveus interneurone inputs: dual intracellular recordings in slices of rat hippocampus. J Physiol 507, 185–199.

Amaral, D., Lavenex, P., 2007. Hippocampal Neuroanatomy. In: Andersen, P., Morris, R., Amaral, D., Bliss, T., O'Keefe, J. (eds) The hippocampus book. Oxford University Press, New York. p 37-117.

Amaral, D. G., 1993. Emerging principles of intrinsic hippocampal organization. Curr Opin Neurobiol 3, 225–229.

Amaral, D. G., Dolorfo, C., Alvarez-Royo, P., 1991. Organization of CA1 projections to the subiculum: a PHA-L analysis in the rat. Hippocampus 1, 415–435.

Amaral, D. G., Witter, M. P., 1989. The three-dimensional organization of the hippocampal formation: a review of anatomical data. Neuroscience 31, 571–591.

Ang, C. W., Carlson, G. C., Coulter, D. A., 2006. Massive and specific dysregulation of direct cortical input to the hippocampus in temporal lobe epilepsy. J Neurosci 26, 11850–11856.

Ariel, P., Ryan, T. A., 2012. New insights into molecular players involved in neurotransmitter release. Physiology (Bethesda) 27, 15–24.

Ascoli, G. A., Alonso-Nanclares, L., Anderson, S. A., Barrionuevo, G., Benavides-Piccione, R., Burkhalter, A., Buzsáki, G., Cauli, B., Defelipe, J., Fairén, A., Feldmeyer, D., Fishell, G., Fregnac, Y., Freund, T. F., Gardner, D., Gardner, E. P., Goldberg, J. H., Helmstaedter, M., Hestrin, S., Karube, F., Kisvárday, Z. F., Lambolez, B., Lewis, D. A., Marin, O., Markram, H., Muñoz, A., Packer, A., Petersen, C. C. H., Rockland, K. S.,

Rossier, J., Rudy, B., Somogyi, P., Staiger, J. F., Tamas, G., Thomson, A. M., Toledo-Rodriguez, M., Wang, Y., West, D. C., Yuste, R., 2008. Petilla terminology: nomenclature of features of GABAergic interneurons of the cerebral cortex. Nat Rev Neurosci 9, 557–568.

Ashton, D., Willems, R., de Prins, E., Wauquier, A., 1988. Field-potential assay of antiepileptic drugs in the hippocampal slice. Epilepsia 29, 321–329.

Aso, K., Watanabe, K., 2000. Limitations in the medical treatment of cryptogenic or symptomatic localization-related epilepsies of childhood onset. Epilepsia 41 (Suppl 9), 18–20.

Atwood, H. L., Karunanithi, S., 2002. Diversification of synaptic strength: presynaptic elements. Nat Rev Neurosci 3, 497–516.

Avoli, M., de Curtis, M., 2011. GABAergic synchronization in the limbic system and its role in the generation of epileptiform activity. Prog Neurobiol 95, 104–132.

Barbarosie, M., Louvel, J., Kurcewicz, I., Avoli, M., 2000. CA3-released entorhinal seizures disclose dentate gyrus epileptogenicity and unmask a temporoammonic pathway. J Neurophysiol 83, 1115–1124.

Bartos, M., Alle, H., Vida, I., 2011. Role of microcircuit structure and input integration in hippocampal interneuron recruitment and plasticity. Neuropharmacology 60, 730–739.

Baulac, S., Huberfeld, G., Gourfinkel-An, I., Mitropoulou, G., Beranger, A., Prud'homme, J. F., Baulac, M., Brice, A., Bruzzone, R., LeGuern, E., 2001. First genetic evidence of $GABA_A$ receptor dysfunction in epilepsy: a mutation in the γ2-subunit gene. Nat Genet 28, 46–48.

Beck, H., Elger, C. E., 2008. Epilepsy research: a window onto function to and dysfunction of the human brain. Dialogues Clin Neurosci 10, 7–15.

Becker, A. J., Pitsch, J., Sochivko, D., Opitz, T., Staniek, M., Chen, C., Campbell, K. P., Schoch, S., Yaari, Y., Beck, H., 2008. Transcriptional upregulation of $Ca_v3.2$ mediates epileptogenesis in the pilocarpine model of epilepsy. J Neurosci 28, 13341–13353.

Ben-Ari, Y., Holmes, G. L., 2005. The multiple facets of gamma-aminobutyric acid dysfunction in epilepsy. Curr Opin Neurol 18, 141–145.

Benini, R., Avoli, M., 2005. Rat subicular networks gate hippocampal output activity in an in vitro model of limbic seizures. J Physiol 566, 885–900.

Bernard, C., Anderson, A., Becker, A., Poolos, N. P., Beck, H., Johnston, D., 2004. Acquired dendritic channelopathy in temporal lobe epilepsy. Science 305, 532–535.

Bettler, B., Kaupmann, K., Mosbacher, J., Gassmann, M., 2004. Molecular structure and physiological functions of $GABA_A$ receptors. Physiol Rev 84, 835–867.

Blatow, M., Caputi, A., Burnashev, N., Monyer, H., Rozov, A., 2003. Ca^{2+} buffer saturation underlies paired pulse facilitation in calbindin-D28k-containing terminals. Neuron 38, 79–88.

Blümcke, I., Becker, A. J., Klein, C., Scheiwe, C., Lie, A. A., Beck, H., Waha, A., Friedl, M. G., Kuhn, R., Emson, P., Elger, C., Wiestler, O. D., 2000. Temporal lobe epilepsy associated up-regulation of metabotropic glutamate receptors: correlated changes in mGluR1 mRNA and protein expression in experimental animals and human patients. J Neuropathol Exp Neurol 59, 1–10.

Blümcke, I., Thom, M., Aronica, E., Armstrong, D. D., Bartolomei, F., Bernasconi, A., Bernasconi, N., Bien, C. G., Cendes, F., Coras, R., Cross, J. H., Jacques, T. S., Kahane, P., Mathern, G. W., Miyata, H., Moshé, S. L., Oz, B., Özkara C., Perucca, E., Sisodiya, S., Wiebe, S., Spreafico, R., 2013. International consensus classification of hippocampal sclerosis in temporal lobe epilepsy: a Task Force report from the ILAE Commission on Diagnostic Methods. Epilepsia 54, 1315–1329.

Blümcke, I., Thom, M., Wiestler, O. D., 2002. Ammon's horn sclerosis: a maldevelopmental disorder associated with temporal lobe epilepsy. Brain Pathol 12, 199–211.

Bonansco, C., Couve, A., Perea, G., Ferradas, C., Roncagliolo, M., Fuenzalida, M., 2011. Glutamate released spontaneously from astrocytes sets the threshold for synaptic plasticity. Eur J Neurosci 33, 1483–1492.

Bormann, J., Hamill, O. P., Sakmann, B., 1987. Mechanism of anion permeation through channels gated by glycine and gamma-aminobutyric acid in mouse cultured spinal neurones. J Physiol 385, 243–286.

Brackenbury, W. J., Isom, L. L., 2011. Na^+ channel beta subunits: Overachievers of the ion channel family. Front Pharmacol 2, 53.

Brady, R. J., Swann, J. W., 1984. Postsynaptic actions of baclofen associated with its antagonism of bicuculline-induced epileptogenesis in hippocampus. Cell Mol Neurobiol 4, 403–408.

Bragin, A., Engel, J., Wilson, C. L., Fried, I., Mathern, G. W., 1999. Hippocampal and entorhinal cortex high-frequency oscillations (100–500 hz) in human epileptic brain and in kainic acid–treated rats with chronic seizures. Epilepsia 40, 127–137.

Bragin, A., Wilson, C. L., Staba, R. J., Reddick, M., Fried, I., Engel, J., 2002. Interictal high-frequency oscillations (80-500 hz) in the human epileptic brain: entorhinal cortex. Ann Neurol 52, 407–415.

Brickley, S. G., Mody, I., 2012. Extrasynaptic $GABA_A$ receptors: their function in the CNS and implications for disease. Neuron 73, 23–34.

Brickley, S. G., Revilla, V., Cull-Candy, S. G., Wisden, W., Farrant, M., 2001. Adaptive regulation of neuronal excitability by a voltage-independent potassium conductance. Nature 409, 88–92.

Brodie, M. J., 2010. Antiepileptic drug therapy the story so far. Seizure 19, 650–655.

Brodie, M. J., Barry, S. J. E., Bamagous, G. A., Norrie, J. D., Kwan, P., 2012. Patterns of treatment response in newly diagnosed epilepsy. Neurology 78, 1548–1554.

Brooks-Kayal, A. R., Shumate, M., Hong, J., Rikhter, T. Y., Coulter, D. A., 1998. Selective changes in single cell $GABA_A$ receptor subunit expression and function in temporal lobe epilepsy. Nat Med 4, 1166–1172.

Brown, J. H., 1990. Atropine, scopolamine, and related antimuscarinic drugs. In: Goodman, L. S., Gilman, A., Rall, T. W., Nies, A., Taylor P. (eds) The pharmacological basis of therapeutics. Macmillian Pergamon Press, New York, p. 150–156.

Buchanan, K. A., Blackman, A. V., Moreau, A. W., Elgar, D., Costa, R. P., Lalanne, T., Tudor Jones, A. A., Oyrer, J., Sjöström, P. J., 2012. Target-specific expression of presynaptic NMDA receptors in neocortical microcircuits. Neuron 75, 451–466.

Buckmaster, P. S., Jongen-Rêlo, A. L., 1999. Highly specific neuron loss preserves lateral inhibitory circuits in the dentate gyrus of kainate-induced epileptic rats. J Neurosci 19, 9519–9529.

Buhl, E. H., Halasy, K., Somogyi, P., 1994a. Diverse sources of hippocampal unitary inhibitory postsynaptic potentials and the number of synaptic release sites. Nature 368, 823–828.

Buhl, E. H., Han, Z. S., Lörinczi, Z., Stezhka, V. V., Karnup, S. V., Somogyi, P., 1994b. Physiological properties of anatomically identified axo-axonic cells in the rat hippocampus. J Neurophysiol 71, 1289–1307.

Bunsey, M., Eichenbaum, H., 1996. Conservation of hippocampal memory function in rats and humans. Nature 379, 255–257.

Burnashev, N., Rozov, A., 2005. Presynaptic Ca^{2+} dynamics, Ca^{2+} buffers and synaptic efficacy. Cell Calcium 37, 489–495.

Buzsáki, G., 1986. Hippocampal sharp waves: their origin and significance. Brain Res 398, 242–252.

Buzsaki, G., 2002. Theta oscillations in the hippocampus. Neuron 33, 325–340.

Buzsáki, G., Chrobak, J. J., 1995. Temporal structure in spatially organized neuronal ensembles: a role for interneuronal networks. Curr Opin Neurobiol 5, 504–510.

Buzsáki, G., da Silva, F. L., 2012. High frequency oscillations in the intact brain. Prog Neurobiol 98, 241–249.

Buzsáki, G., Horváth, Z., Urioste, R., Hetke, J., Wise, K., 1992. High-frequency network oscillation in the hippocampus. Science 256, 1025–1027.

Buzsáki, G., Leung, L. W., Vanderwolf, C. H., 1983. Cellular bases of hippocampal EEG in the behaving rat. Brain Res 287, 139–171.

Catterall, W. A., 2000. From ionic currents to molecular mechanisms: the structure and function of voltage-gated sodium channels. Neuron 26, 13–25.

Catterall, W. A., Goldin, A. L., Waxman, S. G., 2005. International Union of Pharmacology. XLVII. Nomenclature and structure-function relationships of voltage-gated sodium channels. Pharmacol Rev 57, 397–409.

Cavalheiro, E. A., 1995. The pilocarpine model of epilepsy. Ital J Neurol Sci 16, 33–37.

Cendes, F., Sakamoto, A. C., Spreafico, R., Bingaman, W., Becker, A. J., 2014. Epilepsies associated with hippocampal sclerosis. Acta Neuropathol 128, 21–37.

Cheah, C. S., Yu, F. H., Westenbroek, R. E., Kalume, F. K., Oakley, J. C., Potter, G. B., Rubenstein, J. L., Catterall, W. A., 2012. Specific deletion of NaV1.1 sodium channels in inhibitory interneurons causes seizures and premature death in a mouse model of Dravet syndrome. Proc Natl Acad Sci USA 109, 14646–14651.

Chen, J.-Y., Chauvette, S., Skorheim, S., Timofeev, I., Bazhenov, M., 2012. Interneuron-mediated inhibition synchronizes neuronal activity during slow oscillation. J Physiol 590, 3987–4010.

Chen, K., Aradi, I., Thon, N., Eghbal-Ahmadi, M., Baram, T. Z., Soltesz, I., 2001. Persistently modified h-channels after complex febrile seizures convert the seizure-induced enhancement of inhibition to hyperexcitability. Nat Med 7, 331–337.

Cobb, S. R., Buhl, E. H., Halasy, K., Paulsen, O., Somogyi, P., 1995. Synchronization of neuronal activity in hippocampus by individual GABAergic interneurons. Nature 378, 75–78.

Cobb, S. R., Halasy, K., Vida, I., Nyiri, G., Tamás, G., Buhl, E. H., Somogyi, P., 1997. Synaptic effects of identified interneurons innervating both interneurons and pyramidal cells in the rat hippocampus. Neuroscience 79, 629–648.

Cohen, I., Navarro, V., Clemenceau, S., Baulac, M., Miles, R., 2002. On the origin of interictal activity in human temporal lobe epilepsy in vitro. Science 298, 1418–1421.

Colgin, L. L., Moser, E. I., 2010. Gamma oscillations in the hippocampus. Physiology (Bethesda) 25, 319–329.

Cossart, R., Bernard, C., Ben-Ari, Y., 2005. Multiple facets of GABAergic neurons and synapses: multiple fates of GABA signalling in epilepsies. Trends Neurosci 28, 108–115.

Cossart, R., Dinocourt, C., Hirsch, J. C., Merchan Perez, A., De Felipe, J., Ben-Ari, Y., Esclapez, M., Bernard, C., 2001. Dendritic but not somatic GABAergic inhibition is decreased in experimental epilepsy. Nat Neursci 4, 52–62.

Cossart, R., Esclapez, M., Hirsch, J. C., Bernard, C., Ben-Ari, Y., 1998. GluR5 kainate receptor activation in interneurons increases tonic inhibition of pyramidal cells. Nat Neurosci 1, 470–478.

Csicsvari, J., Hirase, H., Czurkó, A., Mamiya, A., Buzsáki, G., 1999. Oscillatory coupling of hippocampal pyramidal cells and interneurons in the behaving rat. J Neurosci 19, 274–287.

de la Prida, L. M., Trevelyan, A. J., 2011. Cellular mechanisms of high frequency oscillations in epilepsy: on the diverse sources of pathological activities. Epilepsy Res 97, 308–317.

de Lanerolle, N. C., Kim, J. H., Robbins, R. J., Spencer, D. D., 1989. Hippocampal interneuron loss and plasticity in human temporal lobe epilepsy. Brain Research 495, 387–395.

DeFelipe, J., López-Cruz, P. L., Benavides-Piccione, R., Bielza, C., Larrañaga, P., Anderson, S., Burkhalter, A., Cauli, B., Fairén, A., Feldmeyer, D., Fishell, G., Fitzpatrick, D., Freund, T. F., González-Burgos, G., Hestrin, S., Hill, S., Hof, P. R., Huang, J., Jones, E. G., Kawaguchi, Y., Kisvárday, Z., Kubota, Y., Lewis, D. A., Marín, O., Markram, H., McBain, C. J., Meyer, H. S., Monyer, H., Nelson, S. B., Rockland, K., Rossier, J., Rubenstein, J. L. R., Rudy, B., Scanziani, M., Shepherd, G. M., Sherwood, C. C., Staiger, J. F., Tamás, G., Thomson, A., Wang, Y., Yuste, R., Ascoli, G. A., 2013. New insights into the classification and nomenclature of cortical GABAergic interneurons. Nat Rev Neurosci 14, 202–216.

Deuchars, J., Thomson, A. M., 1996. CA1 pyramid-pyramid connections in rat hippocampus in vitro: dual intracellular recordings with biocytin filling. Neuroscience 74, 1009–1018.

Dinocourt, C., Petanjek, Z., Freund, T. F., Ben-Ari, Y., M, E., 2003. Loss of interneurons innervating pyramidal cell dendrites and axon initial segments in the CA1 region of the hippocampus following pilocarpine-induced seizures. J comp neurol 459, 407–425.

Dobrunz, L. E., 2002. Release probability is regulated by the size of the readily releasable vesicle pool at excitatory synapses in hippocampus. Int J Dev Neurosci 20, 225–236.

Elger, C. E., Helmstaedter, C., Kurthen, M., 2004. Chronic epilepsy and cognition. Lancet Neurol 3, 663–672.

Ellender, T. J., Nissen, W., Colgin, L. L., Mann, E. O., Paulsen, O., 2010. Priming of hippocampal population bursts by individual perisomatic-targeting interneurons. J Neurosci 30, 5979–5991.

Engel, J., 1996a. Introduction to temporal lobe epilepsy. Epilepsy Res 26, 141–150.

Engel, J., 1996b. Surgery for seizures. N Engl J Med 334, 647–652.

Engel, J., 2001a. Mesial temporal lobe epilepsy: what have we learned? Neuroscientist 7, 340–352.

Engel, J., 2001b. A proposed diagnostic scheme for people with epileptic seizures and with epilepsy: report of the ILAE Task Force on Classification and Terminology. Epilepsia 42, 796–803.

Engel, J., 2004. The goal of epilepsy therapy: no seizures, no side effects, as soon as possible. CNS Spectr 9, 95–97.

Engel, J., 2006. Report of the ILAE classification core group. Epilepsia 47, 1558–1568.

Engel, J., Bragin, A., Staba, R., Mody, I., 2009. High-frequency oscillations: what is normal and what is not? Epilepsia 50, 598–604.

Engel, J., Pedley, T. A., 2008. Introduction: What is Epilepsy? In: Engel, J. and Pedley, T. A. (eds) Epilepsy: A comprehensive textbook. Lippincott Williams & Wilkins, Philadelphia, p. 1-8.

Engel, J., Williamson, P. D., Berg, A. T., Wolf, P., 2008. Classification of epileptic seizures. In: Engel, J. and Pedley, T. A. (eds) Epilepsy: A comprehensive textbook. Lippincott Williams & Wilkins, Philadelphia, p. 511-519.

Fioravante, D., Regehr, W. G., 2011. Short-term forms of presynaptic plasticity. Curr Opin Neurobiol 21, 269–274.

Fisher, R. S., van Emde, W., Blume, W., Elger, C., Genton, P., Lee, P., Engel, J., 2005. Epileptic seizures and epilepsy: definitions proposed by the International League Against Epilepsy (ILAE) and the International Bureau for Epilepsy (IBE). Epilepsia 46, 470–472.

Fisher, R. S., Webber, W. R., Lesser, R. P., Arroyo, S., Uematsu, S., 1992. High-frequency EEG activity at the start of seizures. J Clin Neurophysiol 9, 441–448.

Freund, T. F., Buzsaki, G., 1996. Interneurons of the hippocampus. Hippocampus 6, 347–470.

Freund, T. F., Katona, I., 2007. Perisomatic inhibition. Neuron 56, 33–42.

Fritschy, J. M., Kiener, T., Bouilleret, V., Loup, F., 1999. GABAergic neurons and $GABA_A$-receptors in temporal lobe epilepsy. Neurochem Int 34, 435–445.

Fuchs, E. C., Zivkovic, A. R., Cunningham, M. O., Middleton, S., Lebeau, F. E. N., Bannerman, D. M., Rozov, A., Whittington, M. A., Traub, R. D., Rawlins, J. N. P., Monyer, H., 2007. Recruitment of parvalbumin-positive interneurons determines hippocampal function and associated behavior. Neuron 53, 591–604.

Geiger, J. R., Lübke, J., Roth, A., Frotscher, M., Jonas, P., 1997. Submillisecond AMPA receptor-mediated signaling at a principal neuron-interneuron synapse. Neuron 18, 1009–1023.

Gibbs, J. W., Shumate, M. D., Coulter, D. A., 1997. Differential epilepsy-associated alterations in postsynaptic $GABA_A$ receptor function in dentate granule and CA1 neurons. J Neurophysiol 77, 1924–1938.

Goldin, A. L., 2003. Mechanisms of sodium channel inactivation. Curr Opin Neurobiol 13, 284–290.

Goldin, A. L., Barchi, R. L., Caldwell, J. H., Hofmann, F., Howe, J. R., Hunter, J. C., Kallen, R. G., Mandel, G., Meisler, M. H., Netter, Y. B., Noda, M., Tamkun, M. M., Waxman, S. G., Wood, J. N., Catterall, W. A., Nov 2000. Nomenclature of voltage-gated sodium channels. Neuron 28 (2), 365–368.

González, M. I., Angel, Y. C. D., Brooks-Kayal, A., 2013. Down-regulation of gephyrin and $GABA_A$ receptor subunits during epileptogenesis in the CA1 region of hippocampus. Epilepsia 54, 616–624.

Granger, P., Biton, B., Faure, C., Vige, X., Depoortere, H., Graham, D., Langer, S. Z., Scatton, B., Avenet, P., 1995. Modulation of the gamma-aminobutyric acid type A receptor by the antiepileptic drugs carbamazepine and phenytoin. Mol Pharmacol 47, 1189–1196.

Gulyás, A. I., Hájos, N., Freund, T. F., 1996. Interneurons containing calretinin are specialized to control other interneurons in the rat hippocampus. J Neurosci 16, 3397–3411.

Gulyás, A. I., Hájos, N., Katona, I., Freund, T. F., 2003. Interneurons are the local targets of hippocampal inhibitory cells which project to the medial septum. Eur J Neurosci 17, 1861–1872.

Halabisky, B., Parada, I., Buckmaster, P. S., Prince, D. A., 2010. Excitatory input onto hilar somatostatin interneurons is increased in a chronic model of epilepsy. J Neurophysiol 104, 2214–2223.

Halasy, K., Buhl, E. H., Lörinczi, Z., Tamás, G., Somogyi, P., 1996. Synaptic target selectivity and input of GABAergic basket and bistratified interneurons in the CA1 area of the rat hippocampus. Hippocampus 6, 306–329.

Hamann, M., Rossi, D. J., Attwell, D., 2002. Tonic and spillover inhibition of granule cells control information flow through cerebellar cortex. Neuron 33, 625–633.

Han, Z. S., Buhl, E. H., Lörinczi, Z., Somogyi, P., 1993. A high degree of spatial selectivity in the axonal and dendritic domains of physiologically identified local-circuit neurons in the dentate gyrus of the rat hippocampus. Eur J Neurosci 5, 395–410.

Harris, K. M., Marshall, P. E., Landis, D. M., 1985. Ultrastructural study of cholecystokinin-immunoreactive cells and processes in area CA1 of the rat hippocampus. J Comp Neurol 233, 147–158.

Harvey, C. D., Collman, F., Dombeck, D. A., Tank, D. W., 2009. Intracellular dynamics of hippocampal place cells during virtual navigation. Nature 461, 941–946.

Hershkowitz, N., Ayala, G. F., 1981. Effects of phenytoin on pyramidal neurons of the rat hippocampus. Brain Res 208, 487–492.

Hájos, N., Mody, I., 1997. Synaptic communication among hippocampal interneurons: properties of spontaneous IPSCs in morphologically identified cells. J Neurosci 17, 8427–8442.

Hájos, N., Paulsen, O., 2009. Network mechanisms of gamma oscillations in the CA3 region of the hippocampus. Neural Netw 22, 1113–1119.

Hood, T. W., Siegfried, J., Haas, H. L., 1983. Analysis of carbamazepine actions in hippocampal slices of the rat. Cell Mol Neurobiol 3, 213–222.

Hu, H., Martina, M., Jonas, P., 2010. Dendritic mechanisms underlying rapid synaptic activation of fast-spiking hippocampal interneurons. Science 327, 52–58.

Huberfeld, G., Wittner, L., Clemenceau, S., Baulac, M., Kaila, K., Miles, R., Rivera, C., 2007. Perturbed chloride homeostasis and GABAergic signaling in human temporal lobe epilepsy. J Neurosci 27, 9866–9873.

Ibarz, J. M., Foffani, G., Cid, E., Inostroza, M., de la Prida, L. M., 2010. Emergent dynamics of fast ripples in the epileptic hippocampus. J Neurosci 30, 16249–16261.

Jeong, S.-W., Lee, S. K., Hong, K.-S., Kim, K.-K., Chung, C.-K., Kim, H., 2005. Prognostic factors for the surgery for mesial temporal lobe epilepsy: longitudinal analysis. Epilepsia 46, 1273–1279.

Jinno, S., Klausberger, T., Marton, L. F., Dalezios, Y., Roberts, J. D. B., Fuentealba, P., Bushong, E. A., Henze, D., Buzsáki, G., Somogyi, P., 2007. Neuronal diversity in GABAergic long-range projections from the hippocampus. J Neurosci 27, 8790–8804.

Jirsch, J. D., Urrestarazu, E., LeVan, P., Olivier, A., Dubeau, F., Gotman, J., 2006. High-frequency oscillations during human focal seizures. Brain 129, 1593–1608.

Johnson, M. R., Sander, J. W., 2001. The clinical impact of epilepsy genetics. J Neurol Neurosurg Psychiatry 70, 428–430.

Kamondi, A., Acsády, L., Wang, X. J., Buzsáki, G., 1998. Theta oscillations in somata and dendrites of hippocampal pyramidal cells in vivo: activity-dependent phase-precession of action potentials. Hippocampus 8, 244–261.

Kandratavicius, L., Balista, P. A., Lopes-Aguiar, C., Ruggiero, R. N., Umeoka, E. H., Garcia-Cairasco, N., Bueno-Junior, L. S., Leite, J. P., 2014. Animal models of epilepsy: use and limitations. Neuropsychiatr Dis Treat 10, 1693–1705.

Karlócai, M. R., Kohus, Z., Káli, S., Ulbert, I., Szabó, G., Máté, Z., Freund, T. F., Gulyás, A. I., 2014. Physiological sharp wave-ripples and interictal events in vitro: what's the difference? Brain 137, 463–485.

Kasperaviciute, D., Catarino, C. B., Matarin, M., Leu, C., Novy, J., Tostevin, A., Leal, B., Hessel, E. V. S., Hallmann, K., Hildebrand, M. S., Dahl, H.-H. M., Ryten, M., Trabzuni, D., Ramasamy, A., Alhusaini, S., Doherty, C. P., Dorn, T., Hansen, J., Krämer, G., Steinhoff, B. J., Zumsteg, D., Duncan, S., Kälviäinen, R. K., Eriksson, K. J., Kantanen, A.-M., Pandolfo, M., Gruber-Sedlmayr, U., Schlachter, K., Reinthaler, E. M., Stogmann, E., Zimprich, F., Théâtre, E., Smith, C., O'Brien, T. J., Tan, K. M., Petrovski, S., Robbiano, A., Paravidino, R., Zara, F., Striano, P., Sperling, M. R., Buono, R. J., Hakonarson, H., Chaves, J., Costa, P. P., Silva, B. M., da Silva, A. M., de Graan, P. N. E., Koeleman, B. P. C., Becker, A., Schoch, S., von Lehe, M., Reif, P. S., Rosenow, F., Becker, F., Weber, Y., Lerche, H., Rössler, K., Buchfelder, M., Hamer, H. M., Kobow, K., Coras, R., Blumcke, I., Scheffer, I. E., Berkovic, S. F., Weale, M. E., Consortium, U. K. B. E., Delanty, N., Depondt, C., Cavalleri, G. L., Kunz, W. S., Sisodiya, S. M., 2013. Epilepsy, hippocampal sclerosis and febrile seizures linked by common genetic variation around SCN1A. Brain 136, 3140–3150.

Kawaguchi, Y., 2001. Distinct firing patterns of neuronal subtypes in cortical synchronized activities. J Neurosci 21, 7261–7272.

Kemppainen, S., Jolkkonen, E., Pitkänen, A., 2002. Projections from the posterior cortical nucleus of the amygdala to the hippocampal formation and parahippocampal region in rat. Hippocampus 12, 735–755.

Kerr, M. P., 2012. The impact of epilepsy on patients' lives. Acta Neurol Scand Suppl 126, 1–9.

Köhling, R., Staley, K., 2011. Network mechanisms for fast ripple activity in epileptic tissue. Epilepsy Res 97, 318–323.

Khosravani, H., Pinnegar, C. R., Mitchell, J. R., Bardakjian, B. L., Federico, P., Carlen, P. L., 2005. Increased high-frequency oscillations precede in vitro low-Mg seizures. Epilepsia 46, 1188–1197.

Klausberger, T., 2009. GABAergic interneurons targeting dendrites of pyramidal cells in the CA1 area of the hippocampus. Eur J Neurosci 30, 947–957.

Klausberger, T., Magill, P. J., Márton, L. F., Roberts, J. D. B., Cobden, P. M., Buzsáki, G., Somogyi, P., 2003. Brain-state- and cell-type-specific firing of hippocampal interneurons in vivo. Nature 421, 844–848.

Klausberger, T., Marton, L. F., O'Neill, J., Huck, J. H. J., Dalezios, Y., Fuentealba, P., Suen, W. Y., Papp, E., Kaneko, T., Watanabe, M., Csicsvari, J., Somogyi, P., 2005. Complementary roles of cholecystokinin- and parvalbumin-expressing GABAergic neurons in hippocampal network oscillations. J Neurosci 25, 9782–9793.

Klausberger, T., Somogyi, P., 2008. Neuronal diversity and temporal dynamics: the unity of hippocampal circuit operations. Science 321, 53–57.

Knowles, W. D., Schwartzkroin, P. A., 1981. Axonal ramifications of hippocampal CA1 pyramidal cells. J Neurosci 1, 1236–1241.

Koch, C., Poggio, T., Torre, V., 1983. Nonlinear interactions in a dendritic tree: localization, timing, and role in information processing. Proc Natl Acad Sci USA 80, 2799–2802.

Kosaka, T., Katsumaru, H., Hama, K., Wu, J. Y., Heizmann, C. W., 1987. GABAergic neurons containing the Ca^{2+}-binding protein parvalbumin in the rat hippocampus and dentate gyrus. Brain Res 419, 119–130.

Kuo, C. C., 1998. A common anticonvulsant binding site for phenytoin, carbamazepine, and lamotrigine in neuronal Na^{+} channels. Mol Pharmacol 54, 712–721.

Kuo, C. C., Chen, R. S., Lu, L., Chen, R. C., 1997. Carbamazepine inhibition of neuronal Na^+ currents: quantitative distinction from phenytoin and possible therapeutic implications. Mol Pharmacol 51, 1077–1083.

Kwan, P., Arzimanoglou, A., Berg, A. T., Brodie, M. J., Hauser, W. A., Mathern, G., Moshé, S. L., Perucca, E., Wiebe, S., French, J., 2010. Definition of drug resistant epilepsy: consensus proposal by the ad hoc Task Force of the ILAE Commission on Therapeutic Strategies. Epilepsia 51, 1069–1077.

Kwan, P., Brodie, M. J., 2000. Early identification of refractory epilepsy. N Engl J Med 342, 314–319.

Kwan, P., Sander, J. W., 2004. The natural history of epilepsy: an epidemiological view. J Neurol Neurosurg Psychiatry 75, 1376–1381.

Lee, S.-H., Marchionni, I., Bezaire, M., Varga, C., Danielson, N., Lovett-Barron, M., Losonczy, A., Soltesz, I., 2014. Parvalbumin-positive basket cells differentiate among hippocampal pyramidal cells. Neuron 82, 1129–1144.

Lee, V., Maguire, J., 2013. Impact of inhibitory constraint of interneurons on neuronal excitability. J Neurophysiol 110, 2520–2535.

Liotta, A., Caliskan, G., ul Haq, R., Hollnagel, J. O., Rösler, A., Heinemann, U., Behrens, C. J., 2011. Partial disinhibition is required for transition of stimulus-induced sharp wave-ripple complexes into recurrent epileptiform discharges in rat hippocampal slices. J Neurophysiol 105, 172–187.

Lipkind, G. M., Fozzard, H. A., 2010. Molecular model of anticonvulsant drug binding to the voltage-gated sodium channel inner pore. Mol Pharmacol 78, 631–638.

Liu, Y., Lopez-Santiago, L. F., Yuan, Y., Jones, J. M., Zhang, H., O'Malley, H. A., Patino, G. A., O'Brien, J. E., Rusconi, R., Gupta, A., Thompson, R. C., Natowicz, M. R., Meisler, M. H., Isom, L. L., Parent, J. M., 2013. Dravet syndrome patient-derived neurons suggest a novel epilepsy mechanism. Ann Neurol 74, 128–139.

Losonczy, A., Zemelman, B. V., Vaziri, A., Magee, J. C., 2010. Network mechanisms of theta related neuronal activity in hippocampal CA1 pyramidal neurons. Nat Neurosci 13, 967–972.

Losonczy, A., Zhang, L., Shigemoto, R., Somogyi, P., Nusser, Z., 2002. Cell type dependence and variability in the short-term plasticity of EPSCs in identified mouse hippocampal interneurones. J Physiol 542, 193–210.

Loup, F., Wieser, H. G., Yonekawa, Y., Aguzzi, A., Fritschy, J. M., 2000. Selective alterations in $GABA_A$ receptor subtypes in human temporal lobe epilepsy. J Neurosci 20, 5401–5419.

Lovett-Barron, M., Kaifosh, P., Kheirbek, M. A., Danielson, N., Zaremba, J. D., Reardon, T. R., Turi, G. F., Hen, R., Zemelman, B. V., Losonczy, A., 2014. Dendritic inhibition in the hippocampus supports fear learning. Science 343, 857–863.

Lovett-Barron, M., Turi, G. F., Kaifosh, P., Lee, P. H., Bolze, F., Sun, X.-H., Nicoud, J.-F., Zemelman, B. V., Sternson, S. M., Losonczy, A., 2012. Regulation of neuronal input transformations by tunable dendritic inhibition. Nat Neurosci 15, 423–30, S1–3.

Maccaferri, G., Lacaille, J.-C., 2003. Interneuron diversity series: Hippocampal interneuron classifications–making things as simple as possible, not simpler. Trends Neurosci 26, 564–571.

Maccaferri, G., Roberts, J. D., Szucs, P., Cottingham, C. A., Somogyi, P., 2000. Cell surface domain specific postsynaptic currents evoked by identified GABAergic neurones in rat hippocampus in vitro. J Physiol 524, 91–116.

Maglóczky, Z., Freund, T. F., 2005. Impaired and repaired inhibitory circuits in the epileptic human hippocampus. Trends Neurosci 28, 334–340.

Mann, E. O., Mody, I., 2008. The multifaceted role of inhibition in epilepsy: seizure-genesis through excessive GABAergic inhibition in autosomal dominant nocturnal frontal lobe epilepsy. Curr Opin Neurol 21, 155–160.

Mann, E. O., Paulsen, O., 2007. Role of GABAergic inhibition in hippocampal network oscillations. Trends Neurosci 30, 343–349.

Margerison, J. H., Corsellis, J. A., 1966. Epilepsy and the temporal lobes. a clinical, electroencephalographic and neuropathological study of the brain in epilepsy, with particular reference to the temporal lobes. Brain 89, 499–530.

Markram, H., Wang, Y., Tsodyks, M., 1998. Differential signaling via the same axon of neocortical pyramidal neurons. Proc Natl Acad Sci USA 95, 5323–5328.

Martina, M., Jonas, P., 1997. Functional differences in na^+ channel gating between fast-spiking interneurones and principal neurones of rat hippocampus. J Physiol 505 (Pt 3), 593–603.

Martínez-Delgado, G., Estrada-Mondragón, A., Miledi, R., Martínez-Torres, A., 2010. An update on $GABA_\rho$ receptors. Curr Neuropharmacol 8, 422–433.

Mathern, G. W., Babb, T. L., Vickrey, B. G., Melendez, M., Pretorius, J. K., 1995. The clinical-pathogenic mechanisms of hippocampal neuron loss and surgical outcomes in temporal lobe epilepsy. Brain 118, 105–118.

McBain, C. J., DiChiara, T. J., Kauer, J. A., 1994. Activation of metabotropic glutamate receptors differentially affects two classes of hippocampal interneurons and potentiates excitatory synaptic transmission. J Neurosci 14, 4433–4445.

McBain, C. J., Fisahn, A., 2001. Interneurons unbound. Nat Rev Neurosci 2, 11–23.

McLean, M. J., Macdonald, R. L., 1986. Carbamazepine and 10,11-epoxycarbamazepine produce use- and voltage-dependent limitation of rapidly firing action potentials of mouse central neurons in cell culture. J Pharmacol Exp Ther 238, 727–738.

Meldrum, B. S., 1975. Epilepsy and gamma-aminobutyric acid-mediated inhibition. Int Rev Neurobiol 17, 1–36.

Meldrum, B. S., Horton, R. W., 1971. Convulsive effects of 4-deoxypyridoxine and of bicuculline in photosensitive baboons (*Papio papio*) and in rhesus monkeys (*Macaca mulatta*). Brain Res 35, 419–436.

Meyer, A. H., Katona, I., Blatow, M., Rozov, A., Monyer, H., 2002. *In vivo* labeling of parvalbumin-positive interneurons and analysis of electrical coupling in identified neurons. J Neurosci 22, 7055–7064.

Miles, R., Toth, K., Gulyas, A., Hajos, N., Freund, T. F., 1996. Differences between somatic and dendritic inhibition in the hippocampus. Neuron 16, 815–823.

Miles, R., Wong, R. K., 1983. Single neurones can initiate synchronized population discharge in the hippocampus. Nature 306, 371–373.

Mittmann, W., Chadderton, P., Häusser, M., 2004. Neuronal microcircuits: frequency-dependent flow of inhibition. Curr Biol 14, R837–R839.

Müller, C., Beck, H., Coulter, D., Remy, S., 2012. Inhibitory control of linear and supralinear dendritic excitation in ca1 pyramidal neurons. Neuron 75, 851–864.

Mohanraj, R., Brodie, M. J., 2006. Diagnosing refractory epilepsy: response to sequential treatment schedules. Eur J Neurol 13, 277–282.

Morin, F., Beaulieu, C., Lacaille, J. C., 1996. Membrane properties and synaptic currents evoked in CA1 interneuron subtypes in rat hippocampal slices. J Neurophysiol 76, 1–16.

Moser, E. I., Kropff, E., Moser, M.-B., 2008. Place cells, grid cells, and the brain's spatial representation system. Annu Rev Neurosci 31, 69–89.

Neher, E., Sakaba, T., 2008. Multiple roles of calcium ions in the regulation of neurotransmitter release. Neuron 59, 861–872.

Nörenberg, A., Hu, H., Vida, I., Bartos, M., Jonas, P., 2010. Distinct nonuniform cable properties optimize rapid and efficient activation of fast-spiking GABAergic interneurons. Proc Natl Acad Sci U S A 107, 894–899.

Nunzi, M. G., Gorio, A., Milan, F., Freund, T. F., Somogyi, P., Smith, A. D., 1985. Cholecystokinin-immunoreactive cells form symmetrical synaptic contacts with pyramidal and nonpyramidal neurons in the hippocampus. J Comp Neurol 237, 485–505.

Nusser, Z., Hájos, N., Somogyi, P., Mody, I., 1998. Increased number of synaptic $GABA_A$ receptors underlies potentiation at hippocampal inhibitory synapses. Nature 395, 172–177.

Ogiwara, I., Miyamoto, H., Morita, N., Atapour, N., Mazaki, E., Inoue, I., Takeuchi, T., shigeyoshi, I., Yanagawa, Y., Obata, K., Furuichi, T., Hensch, T. K., Yamakawa, K., 2007. $Na_v1.1$ localizes to axons of parvalbumin-positive inhibitory interneurons: A circuit basis for epileptic seizures in mice carrying an Scn1a gene mutation. J Neurosci 27, 5903–5914.

O'Keefe, J., 1976. Place units in the hippocampus of the freely moving rat. Exp Neurol 51, 78–109.

O'Keefe, J., 1979. A review of the hippocampal place cells. Prog Neurobiol 13, 419–439.

O'Keefe, J., Dostrovsky, J., 1971. The hippocampus as a spatial map. Preliminary evidence from unit activity in the freely-moving rat. Brain Res 34, 171–175.

O'Keefe, J., Nadel, L., 1978. The hippocampus as a cognitive map. Vol. 3. Clarendon Press Oxford.

Oliva, M., Berkovic, S. F., Petrou, S., 2012. Sodium channels and the neurobiology of epilepsy. Epilepsia 53, 1849–1859.

Olpe, H. R., Baudry, M., Jones, R. S., 1985. Electrophysiological and neurochemical investigations on the action of carbamazepine on the rat hippocampus. Eur J Pharmacol 110, 71–80.

Olsen, R. W., Sieghart, W., 2008. International Union of Pharmacology. LXX. Subtypes of gamma-aminobutyric acid(A) receptors: classification on the basis of subunit composition, pharmacology, and function. Update. Pharmacol Rev 60, 243–260.

Orman, R., Gizycki, H. V., Lytton, W. W., Stewart, M., 2008. Local axon collaterals of area CA1 support spread of epileptiform discharges within CA1, but propagation is unidirectional. Hippocampus 18, 1021–1033.

Pathak, H. R., Weissinger, F., Terunuma, M., Carlson, G. C., Hsu, F.-C., Moss, S. J., Coulter, D. A., 2007. Disrupted dentate granule cell chloride regulation enhances synaptic excitability during development of temporal lobe epilepsy. J Neurosci 27, 14012–14022.

Pawelzik, H., Hughes, D. I., Thomson, A. M., 2002. Physiological and morphological diversity of immunocytochemically defined parvalbumin- and cholecystokinin-positive interneurones in CA1 of the adult rat hippocampus. J Comp Neurol 443, 346–367.

Pawelzik, H., Hughes, D. I., Thomson, A. M., 2003. Modulation of inhibitory autapses and synapses on rat CA1 interneurones by $GABA_A$ receptor ligands. J Physiol 546, 701–716.

Payandeh, J., Scheuer, T., Zheng, N., Catterall, W. A., 2011. The crystal structure of a voltage-gated sodium channel. Nature 475, 353–358.

Peng, Z., Zhang, N., Wei, W., Huang, C. S., Cetina, Y., Otis, T. S., Houser, C. R., 2013. A reorganized GABAergic circuit in a model of epilepsy: evidence from optogenetic labeling and stimulation of somatostatin interneurons. J Neurosci 33, 14392–14405.

Perea, G., Araque, A., 2007. Astrocytes potentiate transmitter release at single hippocampal synapses. Science 317, 1083–1086.

Peroutka, S. J., Snyder, S. H., 1982. Antiemetics: neurotransmitter receptor binding predicts therapeutic actions. Lancet 1, 658–659.

Picot, M.-C., Baldy-Moulinier, M., Daurès, J.-P., Dujols, P., Crespel, A., 2008. The prevalence of epilepsy and pharmacoresistant epilepsy in adults: a population-based study in a western european country. Epilepsia 49, 1230–1238.

Pikkarainen, M., Rönkkö, S., Savander, V., Insausti, R., Pitkänen, A., 1999. Projections from the lateral, basal, and accessory basal nuclei of the amygdala to the hippocampal formation in rat. J Comp Neurol 403, 229–260.

Pitkänen, A., Lukasiuk, K., 2011. Mechanisms of epileptogenesis and potential treatment targets. Lancet Neurol 10, 173–186.

Pouille, F., Scanziani, M., 2001. Enforcement of temporal fidelity in pyramidal cells by somatic feed-forward inhibition. Science 293, 1159–1163.

Pouille, F., Scanziani, M., 2004. Routing of spike series by dynamic circuits in the hippocampus. Nature 429, 717–723.

Qiao, X., Sun, G., Clare, J. J., Werkman, T. R., Wadman, W. J., 2014. Properties of human brain sodium channel alpha-subunits expressed in HEK293 cells and their modulation by carbamazepine, phenytoin and lamotrigine. Br J Pharmacol 171, 1054–1067.

Ragsdale, D. S., Avoli, M., 1998. Sodium channels as molecular targets for antiepileptic drugs. Brain Res Brain Res Rev 26, 16–28.

Ragsdale, D. S., McPhee, J. C., Scheuer, T., Catterall, W. A., 1994. Molecular determinants of state-dependent block of Na^+ channels by local anesthetics. Science 265, 1724–1728.

Ragsdale, D. S., McPhee, J. C., Scheuer, T., Catterall, W. A., 1996. Common molecular determinants of local anesthetic, antiarrhythmic, and anticonvulsant block of voltage-gated Na^+ channels. Proc Natl Acad Sci USA 93, 9270–9275.

Rambeck, B., Jürgens, U. H., May, T. W., Pannek, H. W., Behne, F., Ebner, A., Gorji, A., Straub, H., Speckmann, E.-J., Pohlmann-Eden, B., Löscher, W., 2006. Comparison of brain extracellular fluid, brain tissue, cerebrospinal fluid, and serum concentrations of antiepileptic drugs measured intraoperatively in patients with intractable epilepsy. Epilepsia 47, 681–694.

Rácz, A., Ponomarenko, A. A., Fuchs, E. C., Monyer, H., 2009. Augmented hippocampal ripple oscillations in mice with reduced fast excitation onto parvalbumin-positive cells. J Neurosci 29, 2563–2568.

Remy, S., Urban, B. W., Elger, C. E., Beck, H., 2003. Anticonvulsant pharmacology of voltage-gated Na^+ channels in hippocampal neurons of control and chronically epileptic rats. Eur J Neurosci 17, 2648–2658.

Reyes, A., Lujan, R., Rozov, A., Burnashev, N., Somogyi, P., Sakmann, B., 1998. Target-cell-specific facilitation and depression in neocortical circuits. Nat Neursci 1, 279–285.

Rogawski, M. A., Löscher, W., 2004. The neurobiology of antiepileptic drugs. Nat Rev Neurosci 5, 553–564.

Royer, S., Zemelman, B. V., Losonczy, A., Kim, J., Chance, F., Magee, J. C., Buzsáki, G., 2012. Control of timing, rate and bursts of hippocampal place cells by dendritic and somatic inhibition. Nat Neurosci 15, 769–775.

Rozov, A., Burnashev, B., 1999. Polyamine-dependent facilitation of postsynaptic AMPA receptors counteracts paired-pulse depression. Nature 401, 594–598.

Sari, P., Kerr, D. S., 2001. Domoic acid-induced hippocampal CA1 hyperexcitability independent of region CA3 activity. Epilepsy Res 47, 65–76.

Scanziani, M., Gähwiler, B. H., Charpak, S., 1998. Target cell-specific modulation of transmitter release at terminals from a single axon. Proc Natl Acad Sci USA 95, 12004–12009.

Scanziani, M., Salin, P. A., Vogt, K. E., Malenka, R. C., Nicoll, R. A., 1997. Use-dependent increases in glutamate concentration activate presynaptic metabotropic glutamate receptors. Nature 385, 630–634.

Schaub, C., Uebachs, M., Beck, H., 2007. Diminished response of CA1 neurons to antiepileptic drugs in chronic epilepsy. Epilepsia 48, 1339–1350.

Schevon, C. A., Weiss, S. A., McKhann, G., Goodman, R. R., Yuste, R., Emerson, R. G., Trevelyan, A. J., 2012. Evidence of an inhibitory restraint of seizure activity in humans. Nat Commun 3, 1060.

Schmidt, D., Löscher, W., 2005. Drug resistance in epilepsy: putative neurobiologic and clinical mechanisms. Epilepsia 46, 858–877.

Schwartz, N. E., Alford, S., 2000. Physiological activation of presynaptic metabotropic glutamate receptors increases intracellular calcium and glutamate release. J Neurophysiol 84, 415–427.

Schwarz, J. R., Grigat, G., 1989. Phenytoin and carbamazepine: potential- and frequency-dependent block of Na currents in mammalian myelinated nerve fibers. Epilepsia 30, 286–294.

Sendrowski, K., Sobaniec, W., 2013. Hippocampus, hippocampal sclerosis and epilepsy. Pharmacol Rep 65, 555–565.

Shneker, B. F., Fountain, N. B., 2003. Epilepsy. Dis Mon 49, 426–478.

Sik, A., Penttonen, M., Ylinen, A., Buzsáki, G., 1995. Hippocampal CA1 interneurons: an *in vivo* intracellular labeling study. J Neurosci 15, 6651–6665.

Silberberg, G., Wu, C., Markram, H., 2004. Synaptic dynamics control the timing of neuronal excitation in the activated neocortical microcircuit. J Physiol 556, 19–27.

Sillanpää, M., 2004. Learning disability: occurrence and long-term consequences in childhood-onset epilepsy. Epilepsy Behav 5, 937–944.

Sisdosiya, S. M., Beck, H anad Löscher, W., Vezzani, A., 2008. Mechanisms of drug resistance. In: Engle, J. and Pedley, T. A. (eds) Epilepsy: A comprehensive textbook. Lippincott Williams & Wilkins, Philadelphia, p. 1279-1289.

Sitges, M., Guarneros, A., Nekrassov, V., 2007. Effects of carbamazepine, phenytoin, valproic acid, oxcarbazepine, lamotrigine, topiramate and vinpocetine on the presynaptic Ca^{2+} channel-mediated release of [^{3}H]glutamate: comparison with the Na^+ channel-mediated release. Neuropharmacology 53, 854–862.

Somogyi, P., Katona, L., Klausberger, T., Lasztóczi, B., Viney, T. J., 2014. Temporal redistribution of inhibition over neuronal subcellular domains underlies state-dependent rhythmic change of excitability in the hippocampus. Philos Trans R Soc Lond B Biol Sci 369, 20120518.

Somogyi, P., Klausberger, T., 2005. Defined types of cortical interneurone structure space and spike timing in the hippocampus. J Physiol 562, 9–26.

Somogyi, P., Nunzi, M. G., Gorio, A., Smith, A. D., 1983. A new type of specific interneuron in the monkey hippocampus forming synapses exclusively with the axon initial segments of pyramidal cells. Brain Res 259, 137–142.

Squire, L. R., 1992. Memory and the hippocampus: a synthesis from findings with rats, monkeys, and humans. Psychol Rev 99, 195–231.

Squire, L. R., Nov 2004. Memory systems of the brain: a brief history and current perspective. Neurobiol Learn Mem 82 (3), 171–177.

Squire, L. R., Stark, C. E. L., Clark, R. E., 2004. The medial temporal lobe. Annu Rev Neurosci 27, 279–306.

Staba, R. J., Wilson, C. L., Bragin, A., Fried, I., Engel, Jr, J., 2002. Quantitative analysis of high-frequency oscillations (80-500 Hz) recorded in human epileptic hippocampus and entorhinal cortex. J Neurophysiol 88, 1743–1752.

Staba, R. J., Wilson, C. L., Bragin, A., Jhung, D., Fried, I., Engel, Jr, J., 2004. High-frequency oscillations recorded in human medial temporal lobe during sleep. Ann Neurol 56, 108–115.

Staley, K. J., Mody, I., 1992. Shunting of excitatory input to dentate gyrus granule cells by a depolarizing $GABA_A$ receptor-mediated postsynaptic conductance. J Neurophysiol 68, 197–212.

Staley, K. J., Soldo, B. L., Proctor, W. R., 1995. Ionic mechanisms of neuronal excitation by inhibitory $GABA_A$ receptors. Science 269, 977–981.

Stanfield, B. B., Cowan, W. M., 1979. The morphology of the hippocampus and dentate gyrus in normal and reeler mice. J Comp Neurol 185, 393–422.

Stark, E., Roux, L., Eichler, R., Senzai, Y., Royer, S., Buzsáki, G., 2014. Pyramidal cell-interneuron interactions underlie hippocampal ripple oscillations. Neuron 83, 467–480.

Steward, O., 1976. Topographic organization of the projections from the entorhinal area to the hippocampal formation of the rat. J Comp Neurol 167, 285–314.

Steward, O., Scoville, S. A., 1976. Cells of origin of entorhinal cortical afferents to the hippocampus and fascia dentata of the rat. J Comp Neurol 169, 347–370.

Stuart, G., Schiller, J., Sakmann, B., 1997. Action potential initiation and propagation in rat neocortical pyramidal neurons. J Physiol 505, 617–632.

Sun, H. Y., Dobrunz, L. E., 2006. Presynaptic kainate receptor activation is a novel mechanism for target cell-specific short-term facilitation at schaffer collateral synapses. J Neurosci 26, 10796–10807.

Sun, H. Y., Lyons, A. A., Dobrunz, L. E., 2005. Mechanisms of target-cell specific short-term plasticity at Schaffer collateral synapses onto interneurones versus pyramidal cells in juvenile rats. J Physiol 568, 815–840.

Sun, Y., Nguyen, A. Q., Nguyen, J. P., Le, L., Saur, D., Choi, J., Callaway, E. M., Xu, X., 2014. Cell-type-specific circuit connectivity of hippocampal CA1 revealed through Cre-dependent rabies tracing. Cell Rep 7, 269–280.

Swartzwelder, H. S., Anderson, W. W., Wilson, W. A., 1988. Mechanism of electrographic seizure generation in the hippocampal slice in Mg^{2+}-free medium: the role of $GABA_A$ inhibition. Epilepsy Res 2, 239–245.

Sylwestrak, E. L., Ghosh, A., 2012. Elfn1 regulates target-specific release probability at CA1-interneuron synapses. Science 338, 536–540.

Takacs, V. T., Klausberger, T., Somogyi, P., Freund, T. F., Gulyas, 2012. Extrinsic and local glutamatergic inputs of the rat hippocampal CA1 area differentially innervate pyramidal cells and interneurons. Hippocampus 22, 1379–1391.

Tamás, G., Buhl, E. H., Lörincz, A., Somogyi, P., 2000. Proximally targeted GABAergic synapses and gap junctions synchronize cortical interneurons. Nat Neurosci 3, 366–371.

Thome, C., Kelly, T., Yanez, A., Schultz, C., Engelhardt, M., Cambridge, S. B., Both, M., Draguhn, A., Beck, H., Egorov, A. V., 2014. Axon-carrying dendrites convey privileged synaptic input in hippocampal neurons. Neuron 83, 1418–1430.

Tomioka, N. H., Yasuda, H., Miyamoto, H., Hatayama, M., Morimura, N., Matsumoto, Y., Suzuki, T., Odagawa, M., Odaka, Y. S., Iwayama, Y., Um, J. W., Ko, J., Inoue, Y., Kaneko, S., Hirose, S., Yamada, K., Yoshikawa, T., Yamakawa, K., Aruga, J., 2014. Elfn1 recruits presynaptic mGluR7 in trans and its loss results in seizures. Nat Commun 5, 4501.

Toyoda, I., Bower, M. R., Leyva, F., Buckmaster, P. S., 2013. Early activation of ventral hippocampus and subiculum during spontaneous seizures in a rat model of temporal lobe epilepsy. J Neurosci 33, 11100–11115.

Treiman, D. M., 2001. GABAergic mechanisms in epilepsy. Epilepsia 42 Suppl 3, 8–12.

Trevelyan, A. J., Sussillo, D., Watson, B. O., Yuste, R., 2006. Modular propagation of epileptiform activity: evidence for an inhibitory veto in neocortex. J Neurosci 26, 12447–12455.

Trevelyan, A. J., Sussillo, D., Yuste, R., 2007. Feedforward inhibition contributes to the control of epileptiform propagation speed. J Neurosci 27, 3383–3387.

Trimmer, J. S., Rhodes, K. J., 2004. Localization of voltage-gated ion channels in mammalian brain. Annu Rev Physiol 66, 477–519.

Tsodyks, M. V., Markram, H., 1997. The neural code between neocortical pyramidal neurons depends on neurotransmitter release probability. Proc Natl Acad Sci USA 94, 719–723.

Turski, W. A., Cavalheiro, E. A., Schwarz, M., Czuczwar, S. J., Kleinrok, Z., Turski, L., 1983. Limbic seizures produced by pilocarpine in rats: behavioural, electroencephalographic and neuropathological study. Behav Brain Res 9, 315–335.

Uebachs, M., Opitz, T., Royeck, M., Dickhof, G., Horstmann, M., Isom, L. L., Beck, H., 2010. Efficacy loss of the anticonvulsant carbamazepine in mice lacking sodium channel beta subunits via paradoxical effects on persistent sodium currents. J Neurosci 30, 8489–8501.

Ulbricht, W., 2005. Sodium channel inactivation: molecular determinants and modulation. Physiol Rev 85, 1271–1301.

Vandecasteele, M., Varga, V., Berényi, A., Papp, E., Barthó, P., Venance, L., Freund, T. F., Buzsáki, G., 2014. Optogenetic activation of septal cholinergic neurons suppresses sharp wave ripples and enhances theta oscillations in the hippocampus. Proc Natl Acad Sci USA 111, 13535–13540.

Vanderwolf, C. H., 1969. Hippocampal electrical activity and voluntary movement in the rat. Electroencephalogr Clin Neurophysiol 26, 407–418.

Vida, I., Halasy, K., Szinyei, C., Somogyi, P., Buhl, E. H., 1998. Unitary IPSPs evoked by interneurons at the stratum radiatum-stratum lacunosum-moleculare border in the CA1 area of the rat hippocampus in vitro. J Physiol 506, 755–773.

Vitureira, N., Letellier, M., White, I. J., Goda, Y., 2012. Differential control of presynaptic efficacy by postsynaptic N-cadherin and β-catenin. Nat Neurosci 15, 81–89.

Walker, M., Chan, D., Thom, M., 2007. Hippocampus and Human Disease. In: Andersen, P., Morris, R., Amaral, D., Bliss, T., O'Keefe, J. (eds) The hippocampus book. Oxford University Press, New York. p. 769–812.

Walker, M. C., White, H. S., Sander, J. W. A. S., 2002. Disease modification in partial epilepsy. Brain 125 (m), 1937–1950.

Wallace, R. H., Marini, C., Petrou, S., Harkin, L. A., Bowser, D. N., Panchal, R. G., Williams, D. A., Sutherland, G. R., Mulley, J. C., Scheffer, I. E., Berkovic, S. F., 2001. Mutant $GABA_A$ receptor γ2-subunit in childhood absence epilepsy and febrile seizures. Nat Genet 28, 49–52.

Whatley, A. D., DiIorio, C. K., Yeager, K., 2010. Examining the relationships of depressive symptoms, stigma, social support and regimen-specific support on quality of life in adult patients with epilepsy. Health Educ Res 25, 575–584.

Wieser, H.-G., 2004. ILAE Commission Report. Mesial temporal lobe epilepsy with hippocampal sclerosis. Epilepsia 45, 695–714.

Willow, M., Gonoi, T., Catterall, W. A., 1985. Voltage clamp analysis of the inhibitory actions of diphenylhydantoin and carbamazepine on voltage-sensitive sodium channels in neuroblastoma cells. Mol Pharmacol 27, 549–558.

Witter, M. P., 1993. Organization of the entorhinal-hippocampal system: a review of current anatomical data. Hippocampus 3 (S1), 33–44.

Witter, M. P., Groenewegen, H. J., da Silva, F. H. L., Lohman, A. H., 1989. Functional organization of the extrinsic and intrinsic circuitry of the parahippocampal region. Prog Neurobiol 33, 161–253.

Wittner, L., Eross, L., Czirják, S., Halász, P., Freund, T. F., Maglóczky, Z., 2005. Surviving CA1 pyramidal cells receive intact perisomatic inhibitory input in the human epileptic hippocampus. Brain 128, 138–152.

World Health Organization, 2012. Epilepsy Fact sheet N°999., http://www.who.int/mediacentre/factsheets/fs999/en/.

Wouterlood, F. G., Saldana, E., Witter, M. P., 1990. Projection from the nucleus reuniens thalami to the hippocampal region: light and electron microscopic tracing study in the rat with the anterograde tracer phaseolus vulgaris-leucoagglutinin. J Comp Neurol 296, 179–203.

Wozny, C., Gabriel, S., Jandova, K., Schulze, K., Heinemann, U., Behr, J., 2005. Entorhinal cortex entrains epileptiform activity in CA1 in pilocarpine-treated rats. Neurobiol Dis 19, 451–460.

Wu, L. G., Borst, J. G., 1999. The reduced release probability of releasable vesicles during recovery from short-term synaptic depression. Neuron 23, 821–832.

Wyeth, M. S., Zhang, N., Mody, I., Houser, C. R., 2010. Selective reduction of cholecystokinin-positive basket cell innervation in a model of temporal lobe epilepsy. J. Neurosci. 30, 8993–9006.

Xu, J., Wu, L.-G., 2005. The decrease in the presynaptic calcium current is a major cause of short-term depression at a calyx-type synapse. Neuron 46, 633–645.

Yamamoto, J., Suh, J., Takeuchi, D., Tonegawa, S., 2014. Successful execution of working memory linked to synchronized high-frequency gamma oscillations. Cell 157, 845–857.

Yarov-Yarovoy, V., Brown, J., Sharp, E. M., Clare, J. J., Scheuer, T., Catterall, W. A., 2001. Molecular determinants of voltage-dependent gating and binding of pore-blocking drugs in transmembrane segment IIIS6 of the Na^+ channel alpha subunit. J Biol Chem 276, 20–27.

Yarov-Yarovoy, V., McPhee, J. C., Idsvoog, D., Pate, C., Scheuer, T., Catterall, W. A., 2002. Role of amino acid residues in transmembrane segments IS6 and IIS6 of the Na_+ channel alpha subunit in voltage-dependent gating and drug block. J Biol Chem 277, 35393–35401.

Ylinen, A., Soltész, I., Bragin, A., Penttonen, M., Sik, A., Buzsáki, G., 1995. Intracellular correlates of hippocampal theta rhythm in identified pyramidal cells, granule cells, and basket cells. Hippocampus 5, 78–90.

Yu, F. H., Mantegazza, M., Westenbroek, R. E., Robbins, C. A., Kalume, F., Burton, K. A., Spain, W. J., McKnight, G. S., Scheuer, T., Catterall, W. A., 2006. Reduced sodium current in GABAergic interneurons in a mouse model of severe myoclonic epilepsy in infancy. Nat Neurosci 9, 1142–1149.

Zhang, W., Yamawaki, R., Wen, X., Uhl, J., Diaz, J., Prince, D. A., Buckmaster, P. S., 2009. Surviving hilar somatostatin interneurons enlarge, sprout axons, and form new synapses with granule cells in a mouse model of temporal lobe epilepsy. J Neurosci 29, 14247–14256.

Zhao, H., Peters, J. H., Zhu, M., Page, S. J., Ritter, R. C., Appleyard, S. M., 2014. Frequency-dependent facilitation of synaptic throughput via postsynaptic nmda receptors in the nucleus of the solitary tract. J Physiol [Epub ahead of print]. doi: 10.1113/jphysiol.2013.258103.

Zucker, R. S., 1989. Short-term synaptic plasticity. Annu Rev Neurosci 12, 13–31.

Zucker, R. S., Regehr, W. G., 2002. Short-term synaptic plasticity. Annu. Rev. Physiol. 64, 355–405.